Dissertation zur Erlangung des Doktorgrades

der Universität Potsdam

Factors modifying the aggregation of atrophin-1 acting in *cis* and in *trans*

Justyna Hinz
aus
Katowice, Polen

2012

Published online at the
Institutional Repository of the University of Potsdam:
URL http://opus.kobv.de/ubp/volltexte/2012/6038/
URN urn:nbn:de:kobv:517-opus-60385
http://nbn-resolving.de/urn:nbn:de:kobv:517-opus-60385

Acknowledgements

I express my sincere gratitude and appreciation to my advisor Prof. Dr. Zoya Ignatova for her supervision and valuable suggestions, which helped me to shape this thesis. I thank her for her patience, support and encouragement during this work.

I am grateful to Dr. Martin Vabulas and Dr. Peter Breuer for reviewing my thesis.

I thank to my group members for their helpful advices. My special thanks go to Prof. Zhang Gong, Dr. Tejas Borwankar, Dr. Hannah Girstmair and Christoph Röthlein for sharing their expertise and for inspiring scientific discussions.

I am grateful to Prof. Ralph Gräf, Prof. Otto Baumann and Prof. Bernd Walz for their constructive comments and help with the confocal microscope.

I thank to Silke Zakrzewski for her contribution to the *in vivo* cross-seeding experiments. I am also grateful to Dr. Lothar Lehnhard for his invaluable help with the 2D-gel experiments and Dr. Jörg Fettke for helping with the mass spectrometry analysis.

I acknowledge PoGS program for their financial support.

Thanks to all my family and friends whose encouragement and faith helped me to accomplish this work. I particularly thank to my sister, my parents and my infinitely patient husband Heiko for supporting me unfailingly during this memorable journey.

Summary

In the complex cellular environment aggregation and toxicity of mutant polyglutamine (polyQ) proteins is affected by both the sequences of the corresponding disease protein and the cellular environment. Additionally, the nucleus has been suggested to be the primary site of toxicity in the polyQ-based neurodegeneration.

In this study, the dynamics and structure of nuclear and cytoplasmic inclusions were examined to determine the intrinsic and extrinsic factors influencing the cellular aggregation of atrophin-1, a protein implicated in the pathology of dentatorubral-pallidoluysian atrophy, a polyQ-based disease with complex clinical features. Dynamic imaging, combined with biochemical and biophysical approaches revealed a large heterogeneity in the dynamics of atrophin-1 within the nuclear inclusions compared with the compact and immobile cytoplasmic aggregates. At least two types of inclusions of polyQ-expanded atrophin-1 with different mobility of the molecular species and ability to exchange with the surrounding monomer pool coexist in the nucleus of the model cell system, neuroblastoma N2a cells. The enrichment of nuclear inclusions with slow dynamics coincided with the change in their solubility. Furthermore, our novel cross-seeding approach which allows for monitoring of the architecture of the aggregate core directly in the cell revealed an evolution of the aggregate core of the expanded ATN1 from one composed of the sequences flanking the polyQ domain at early aggregation phases to one dominated by the polyQ stretch in the later aggregation phase. Intriguingly, these changes in the aggregate core architecture of nuclear and cytoplasmic inclusions mirrored the changes in the protein dynamics and physico-chemical properties of the aggregates in the aggregation time course. 2D-gel analyses followed by MALDI-TOF MS were used to detect alterations in the interaction partners of the pathological ATN1 variant compared to the non-pathological ATN1. Based on these results, we propose that the observed complexity in the dynamics of the nuclear inclusions provides a molecular explanation for the enhanced cellular toxicity of the nuclear aggregates in polyQ-based neurodegeneration.

Contents

1. Introduction

1.1 Neurodegenerative amyloid diseases

Accumulation of macroscopically discernible, intra- or extracellular abnormal protein deposits is the unifying histopathological feature of many age-related neurodegenerative diseases, including Alzheimer's disease (AD), Parkinson's disease (PD), amyotrophic lateral sclerosis (ALS), and polyglutamine (polyQ) diseases (Caughey and Lansbury 2003; Kato, et al. 2000; Liberski 2004; Selkoe 2003; Zoghbi and Orr 2000). Formation of such protein deposits, containing fibrillar polymers is a result of misfolding and aggregation of the structurally destabilized disease proteins. Despite different native folds accessible to monomeric disease proteins, such aggregate species, collectively referred to as amyloid fibrils share some morphological, structural and staining characteristics (Soto 2003).
The aggregation of almost all amyloidogenic proteins is, however, a complex process involving multiple routes and structurally diverse aggregate species with a different relevance to the cytotoxicity (Luheshi, et al. 2008; Walsh and Selkoe 2004). The amyloid fibrils might represent the end-stage of a multi-step assembly (Caughey and Lansbury 2003; Ding, et al. 2002; Ellisdon, et al. 2006; Lashuel, et al. 2002; Poirier, et al. 2002; Walsh and Selkoe 2004).

1.1.1 DRPLA and other polyglutamine (polyQ) disorders

Polyglutamine (polyQ) diseases constitute a class of genetically distinct, late-onset, progressive, neurodegenerative diseases resulting from expansion of the unstable CAG repeat in the respective disease genes over the pathological threshold (Orr and Zoghbi 2007). In each of these diseases the CAG repeat is translated to a homopolymeric polyglutamine stretch (Bulone, et al. 2006; Scherzinger, et al. 1999; Yamada, et al. 2008). They include dentatorubral-pallidoluysian atrophy (DRPLA), Huntington's disease (HD), spino-bulbar muscular atrophy (SBMA) and spino-cerebellar ataxias (SCAs) type 1, 2, 3 (known also as MJD, Machado-Joseph

disease), 6, 7, 12, and 17 (Bulone, et al. 2006; Cholfin, et al. 2001; Scherzinger, et al. 1999; Yamada, et al. 2008). PolyQ disorders are characterized by autosomal-dominant mode of inheritance that is supported by the fact that homozygous and heterozygous patients show similar clinical features (Durr, et al. 1999; Goldfarb, et al. 1996; Mallik and Lakhotia 2010; Matsumura, et al. 1997; Narain, et al. 1999; Sato, et al. 1995; Sobue, et al. 1996). Only SBMA shows X-linked inheritance (Fischbeck, et al. 1999). With the exception of SCA6, polyQ diseases manifest themselves when the CAG expansion, exceeds 36-40 repeats (Andrew, et al. 1997; Gatchel and Zoghbi 2005). There are, however, disease-specific variations in the pathological threshold of the polyQ expansion (Table 1-1). The long uninterrupted CAG repeats in the disease genes show both somatic and germ-line instability resulting in their further expansion in successive transmissions from one generation to the next (Cummings and Zoghbi 2000; Zoghbi and Orr 2000). The larger the expansion beyond the threshold, the more prone it is to such dynamic mutations (Cummings and Zoghbi 2000; Goldberg, et al. 1993; Licht and Lynch 2002). The abnormal expansion of polyQ domain has been shown to alter protein conformation invariably leading to its aggregation and formation of the intraneuronal inclusion bodies (IBs) in disease-specific regions of central nervous system (CNS) (Gatchel and Zoghbi 2005; Soto 2003). The expanded polyglutamine stretch is the only common molecular feature of the disease proteins that otherwise do not share any sequence or functional similarity. Thus, the aggregation has been proposed to be polyQ driven (Bulone, et al. 2006; Chen, et al. 2002b; Hands and Wyttenbach 2010). The expanded polyQ stretch when added to a protein normally not associated with any polyQ disorder causes neuropathological phenotype in mice (Ordway, et al. 1997), thus indicating that polyQ tract may confer toxic properties on the host protein. In addition, the dependence of the aggregation propensity of polyQ peptides on the polyQ-repeat length mirrors the repeat-length dependence of disease onset and severity, linking the aggregation and aggregate formation with the pathogenesis of polyQ diseases (Chen, et al. 2002b; Scherzinger, et al. 1997; Scherzinger, et al. 1999). The pathogenic role of the extended polyQ stretch is further supported by the genetic anticipation phenomenon accompanying the increase in the length of the polyQ tract during intergenerational transmissions of polyQ disorders, i.e. an earlier age of onset

and increasing severity of symptoms in the subsequent generations of the affected families (Zoghbi and Orr 2000).

DRPLA is a hereditary, autosomal dominant disease, which similar of the other polyQ diseases is caused by the expansion of the CAG repeat. The CAG repeat is located in the fifth exon of the gene encoding a 1185 amino acid protein atrophin-1 (ATN1), on chromosome 12p31.13 (Onodera, et al. 1995).

Table 1-1: Comparison of the pathological thresholds of glutamine repeats number in the polyQ disease genes. *In a few wild-type proteins the CAG repeats contain *CAA or ** 1 to 3 CAT (histidine encoding) interruptions, whereas the mutated polyglutamine stretches are encoded by pure CAG repeats. TBP – TATA box binding protein (Adapted from (Andrew, et al. 1997; Cholfin, et al. 2001; Gatchel and Zoghbi 2005).*

polyQ disorder	**Gen (protein)**	**$(CAG)_n$ (wild-type)**	**$(CAG)_n$ (pathogenic)**
DRPLA	ATN1 (atrophin-1)	7-34	49-88
HD	huntingtin (Htt)	6-36*	40-121
SBMA	AR (androgen receptor)	9-36	38-62
SCA1	SCA1 (ataxin-1)	6-39**	40-82
SCA2	SCA2 (ataxin-2)	14-32*	34-200
SCA3 (MJD)	SCA3 (ataxin-3)	12-40	61-86
SCA6	CACNA1A (calcium channel α1A subunit)	4-19	20-30
SCA7	SCA7 (ataxin-7)	4-35	37-306
SCA12	PPP2R2 (brain-specific regulatory subunit of protein phosphatase 2A)	7-28	66-78
SCA17	SCA17 (TBP)	25-42	47-63

ATN1 is a nucleo-cytoplasmatic protein containing N-terminal NLS (nuclear localization signal) and C-terminally located NES (nuclear export signal) found to be functional in transient cell transfection experiments (Nucifora, et al. 2003).

ATN1 contains also in its C-terminus two RE-repeats consisting of Arg-Glu (RE), Lys-Glu (KE), Arg-Asp (RD) and Lys Asp (KD) repeats, the protein-protein interaction motif responsible for binding of ATN1 to atrophin-2 (ATN2-L). ATN2-L, also called RERE, is a 1559 amino acids-long protein, identified as transcriptional repressor that

mediates histone deacetylation and methylation (Wang, et al. 2008; Yanagisawa, et al. 2000). The function of ATN1 is not well understood, however, human ATN1 has been shown to act together with a component of the nuclear transcriptional co-repressor complex, ETO/MTG8, in a cell culture model (Wood, et al. 2000). ATN1 protein has been also suggested to be involved in a signal transduction pathway coupled with insulin/insulin-like growth factor-I (Okamura-Oho, et al. 1999).

DRPLA disease is prevalent in Japanese population and rare in Caucasians (Kanazawa 1999). The length of CAG repeats in normal chromosomes ranges from 7 to 34, while in the DRPLA patients it expands from 49 to 88 (Ikeda, et al. 1996; Komure, et al. 1995; Nagafuchi, et al. 1994).

DRPLA patients show various symptoms. The cardinal clinical features are strongly correlated with the length of the CAG repeat and the age of onset (Ikeuchi, et al. 1995; Komure, et al. 1995). The juvenile type of DRPLA (age of onset below 20 years old) exhibits progressive myoclonus, epilepsy and mental retardation, whereas patients with the late disease onset (over the age of 40 years) predominantly show cerebellar ataxia and dementia with no myoclonus or epileptic seizures (late adult type) (Kanazawa 1999). These symptoms are in parallel with a characteristic neurodegeneration pattern. Generally, pallidoluysian degeneration is more severe than that of the dentatorubral systems in the juvenile type and the reverse situation is observed in the late adult type DRPLA (Yamada, et al. 2008).

Although the disease-causing proteins are widely expressed throughout the central nervous system (CNS) and other tissues (Bauer, et al. 1995; Bauer and Nukina 2009; Gusella and MacDonald 2000), only specific subsets of neurons are vulnerable in each disease, resulting in disease-specific patterns of neurodegeneration and clinical features (Table 1-2) (Hands and Wyttenbach 2010; Mallik and Lakhotia 2010).

The expression of polyQ peptides with 108 consecutive glutamines, however, has been shown to lead to the indiscriminate neurodegeneration in different subsets of neurons and non-neuronal tissues of *Drosophila* model (Marsh, et al. 2000), suggesting that the selective vulnerability of different populations of neurons in each disease is rather influenced by the cellular environment or sequences outside the polyQ stretch.

Table 1-2: Clinical and pathological features of polyQ disorders. *(Adapted from (Hands and Wyttenbach 2010; Mallik and Lakhotia 2010)*

Disease	Protein	Main clinical features	Affected regions of the brain
DRPLA	ATN1	ataxia, mental retardation, seizures, dementia	cerebellum, cerebellar cortex, basal ganglia, Luys body
HD	Htt	chorea, dystonia, psychiatric, motor and cognitive deficits	striatum, cerebellar cortex
SBMA	AR	muscular atrophy, motor and endocrine abnormalities	anterior horn, bulbar neurons, dorsal root ganglia
SCA1	SCA1	ataxia, slurred speech, spasticity, cognitive deficits	cerebellar Purkinje cells, dentate nucleus, brainstem
SCA2	SCA2	ataxia, rigidity, muscular atrophy, mental deterioration	cerebellar Purkinje cells, brain stem, fronto-temporal lobes
SCA3	SCA3	ataxia, parkinsonism, severe spasticity	cerebellar dentate neurons, basal ganglia, brainstem, spinal cord
SCA6	CACNA1A	ataxia, oculomotor disorders, peripherial neuropathy	cerebellar Purkinje cells, dentate nucleus, inferior olive
SCA7	SCA7	ataxia, blindness, cardiac failure in infantile variant	cerebellum, brainstem, macula, visual cortex
SCA12	PPP2R2	ataxia, seizures	cerebellum, cerebellar cortex
SCA17	TBP	ataxia, dementia, epilepsy	cerebellum, basal ganglia

1.2 Amyloids and amyloid aggregates

Intraneuronal nuclear and, more rarely, cytoplasmatic inclusion bodies (IBs) are often observed in or near the affected brain regions in humans and animal models (DiFiglia, et al. 1997). The inclusion bodies deposited in disease-specific subsets of neurons usually are highly ubiquitinated (Becher, et al. 1998; DiFiglia, et al. 1997; Holmberg, et al. 1998). In addition to full-length and proteolytic fragments of the mutant polyQ proteins, IBs may contain cellular proteins, including proteins from the ubiquitin-proteasome system and molecular chaperones, or transcription factors (Goti, et al. 2004; Kayed, et al. 2003; Nucifora, et al. 2003; Poirier, et al. 2002; Ross and Poirier 2004).

IBs with similar molecular structure to those formed by polyQ proteins have been observed in a number of other misfolding diseases. These include not only neurodegenerative disorders, but also non-neuropathic localized amyloidoses, in which aggregation occurs in single type of tissue other than brain, like type II

diabetes, medullary carcinoma of the thyroid, cataract or non-neuropathic systemic amyloidoses, where aggregation occurs in multiple tissues, f.e. AA, AL, lysosyme and fibrinogen amyloidoses, senile amyloidosis (reviewed in Chiti and Dobson 2006). Amyloid aggregation phenomenon is not limited to disease-associated deposits. Various peptides and proteins, e.g., fibronectin type III-module, SH3-domain of phosphatidylinositol-3-kinase or myoglobin, with no link to protein deposition diseases can form amyloid fibrils *in vitro* under suitable destabilizing conditions (Chiti, et al. 2001; Fandrich, et al. 2001; Guijarro, et al. 1998; Litvinovich, et al. 1998; Rochet and Lansbury 2000). In contrast, several proteins, including *E. coli* curlin, *S. coelicolor* chaplins and intralumenal domain of mammalian membrane protein Pmel17 in melanosomes, natively form filamentous structures closely resembling the amyloid fibrils (Berson, et al. 2003; Chapman, et al. 2002; Claessen, et al. 2003). This has led to a notion that the capacity to aggregate is an intrinsic feature of any polypeptide chain (Ferreira, et al. 2006).

The term “amyloid” results from early observation and initial misidentification of the deposits causing neuropathological phenotype as composed of starch. Presently, after determining their proteinaceous character the “amyloid fibrils” are defined as highly ordered protein aggregates, based on the common structural and biophysical properties exhibited by amyloid deposits of different proteins despite the dissimilarities in sequence and native folds of the soluble monomers (Sipe and Cohen 2000). Amyloid fibrils have been characterized *in vitro* by transmission electron microscopy (TEM) and atomic force microscopy (AFM) as filamentous aggregates, generally unbranched, typically consisting of 2-6 protofilaments, twisted together to form rope-like fibrils with diameters 2-20 nm wide (Serpell, et al. 2000; Sunde and Blake 1997) or associated laterally in long ribbons (Bauer, et al. 1995; Pedersen, et al. 2006). In circular dichroism (CD) experiments amyloid fibrils have been shown to be rich in ß-sheet structure (Bauer, et al. 1995; Serpell, et al. 2000; Sunde and Blake 1997). In each individual protofilament the polypeptide chain regions contributing to the core of the fibril are arranged in ß-strands stacked on each other, running perpendicular to the long fibre axis, a structure known as cross-ß-structure and are stabilized by hydrogen bonds which are parallel to the long axis (Sunde and Blake 1997). Amyloid is also generally relatively resistant to proteolysis and denaturation, including SDS-insolubility and shows yellow-green birefringence

after binding of Congo red and intense fluorescence upon thioflavin T binding (Groenning, et al. 2007; Nilsson 2004; Scherzinger, et al. 1997).

High resolution structure of polyQ fibrils is missing, however based on the X-ray diffraction data it has been proposed that $D_2Q_{15}K_2$ aggregates were water-filled nanotubes, formed by circular parallel β-helix with 20 residues per turn and side chains pointing alternately into or out of the cylinder (Perutz, et al. 2002). The reanalysis of this data suggests a cross-β structure consisting of antiparallel β-sheets, with high-density intersheet compaction due to side chain-side chain hydrogen bonding (Sikorski and Atkins 2005).

Helical structure has been also proposed by a molecular dynamics simulation study, however, the authors suggested that it collapses into a triangular β-helix with flat single β-sheet segments linked by planar bends, with water excluded from the center of the fibril (Khare, et al. 2005). Similarly a recent solid-state NMR study of peptides with non-pathological (Q15) and pathological (Q38-54) Q-length has revealed fibrils with a dry core (Schneider, et al. 2011). Thereby, Q15 peptides form single extended β-strands, whereas longer constructs have been organized in higher order structures consisting of more than one sheet, stabilized by the tight interdigitation of Gln side chains from different sheets, with antiparallel arrangement of β-strands contributed by individual molecules within the β-sheet (Schneider, et al. 2011). These structural differences may result from different experimental conditions used in each of the studies and are consistent with the observation that variations in the environment and growth conditions can evoke polymorphism in the molecular structure and morphology of fibrils formed by the same amyloidogenic protein (Paravastu, et al. 2006; Petkova, et al. 2005).

1.3 PolyQ aggregation pathways

Although differences in neurodegeneration patterns and symptoms of polyQ diseases implicate the involvement of other factors, the expanded polyQ stretch appears to be a strong determinant of aggregation and pathology (Orr and Zoghbi 2007; Zoghbi and Orr 2000). Therefore, in many studies synthetic polyQ peptides have been used

as a model to study the polyQ aggregation pathway (Chen, et al. 2002a; Chen, et al. 2001; Chen, et al. 2002b; Perutz, et al. 2002; Sharma, et al. 1999).

Monomeric, soluble polyQ peptides occur to be unstructured (Chen, et al. 2001), with a propensity to form collapsed structures (Crick, et al. 2006). Similarly to other amyloidogenic proteins (Collins, et al. 2004; Lomakin, et al. 1996; Wood, et al. 1999), the aggregation of simple polyQ peptides *in vitro* has been shown to follow nucleated growth polymerization (Chen, et al. 2002b). Characteristic of this mechanism is that preformed fibrils (seeds) can bypass the initiating energetically unfavorable nucleation event (Chen, et al. 2001; Chen, et al. 2002b). The efficiency of the nucleation increases with the length of the polyQ stretch, the steady-state concentration of the nucleus and the concentration of bulk phase monomer available for its elongation (Slepko, et al. 2006). Aggregation kinetics analyses of Q_{28}-Q_{47} peptides from Wetzel's lab have shown that the nucleus, which is the least stable species on the polyQ aggregation pathway is monomeric (Chen, et al. 2002b).

Introducing in the polyQ peptides Pro-Gly substitutions in regular intervals Thakur and colleagues have proposed that the monomeric nucleus formation is an extremely unfavorable structural transition to an elongation-competent species, containing β-sheet elements in common with the final fibril structure (Bhattacharyya, et al. 2005). The structured monomer serves in this model as a binding site for another unstructured monomer (docking) that in result acquires β-structure (locking) thus providing a new elongation site (Bhattacharyya, et al. 2005; Thakur and Wetzel 2002)(Fig. 1-1).

A closer look to the aggregation kinetics of shorter polyQ peptides has revealed an abrupt change in the nucleus size from monomeric for the peptides with repeat length Q_{26}, through dimeric for Q_{25}, to tetrameric for repeat length range Q_{18}-Q_{23} (Kar, et al. 2011). However, Wetzel and colleagues have observed that shorter polyQ peptides still aggregate via two-state nucleated growth polymerization and they propose that larger nuclei also are β-structured. Extrapolation of the nucleation kinetics data to a concentration range likely for the cellular environment has suggested an explanation for the relationship between pathological threshold of the polyQ repeat length and the age of disease onset. Whereas *in vitro* incubation at 1 nM of Q37 would result in fibrillisation within 10-100 years, Q23 aggregation is expected to begin in 10-100 billion years (Kar, et al. 2011).

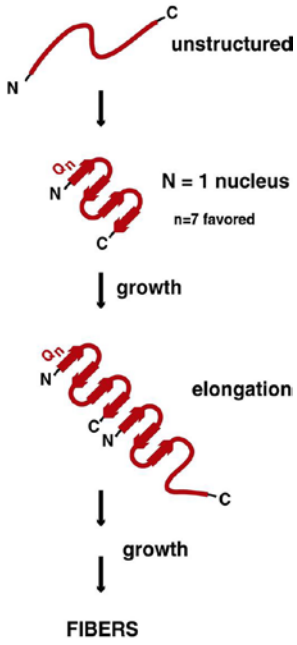

Fig. 1-1: "Dock-and-lock" model of aggregation of simple polyQ peptides. *The rate-limiting nucleation step involves a rearrangement of an unstructured monomer to a β-sheet conformation. The structured monomer acts as a nucleus for binding a second unstructured monomer (docking). When bound to the ordered monomer the new disordered monomer also acquires a β-structure (locking). (Adapted from(Ross, et al. 2003)*

Simple dock-and-lock model is however insufficient to explain aggregation mechanism of full-length polyQ proteins. Although nucleation-dependent aggregation kinetics with a monomeric nucleus formation has been also described for polyQ-expanded ataxin-3 and CRABP1-huntingtin exon 1chimera (Ellisdon, et al. 2007; Ignatova and Gierasch 2006), generally the mechanism of full-length polyQ proteins aggregation occures to be much more complicated than that of polyQ peptides and remains still poorly understood. Many different intermediates between monomeric and fibrillar states of mutant Htt-exon1 (huntingtin exon 1) and SCA3 (ataxin-3) have been identified *in vitro.* Based on the AFM studies of aggregates of the Htt-exon1 with 53Q, Muchowski and colleagues observed prefibrillar aggregates with diverse morphologies: small spherical structures which evolved with time, annular structures of approximately 100 nm, composed of smaller annular and spherical structures,

larger amorphous assemblies and protofibrils, defined as species with a fibril-like morphology that may assemble into protofilaments and finally into fibrils (Wacker, et al. 2004). The distribution, appearance and stability of these distinct intermediates depend on the initial protein concentration and polyQ length (Legleiter, et al. 2010). *In situ* AFM experiments, tracking the fates of individual prefibrillar aggregates have suggested two parallel ways of fibril formation. In one fibrils are built directly, without formation of oligomers. Or, spherical and annular oligomers transiently precede the fibril formation (Legleiter, et al. 2010; Wacker, et al. 2004).

In another *in vitro* study a purified mutant Htt-exon 1 aggregates through a multistep pathway and forms globular oligomers, followed by protofibrils, finally these SDS-soluble species are followed by insoluble fibrillar aggregates (Poirier, et al. 2002). Similar SDS-labile spherical oligomers and curvilinear protofibrils have been shown to precede *in vitro* accumulation of SCA3 fibrils (Ellisdon, et al. 2006; Gales, et al. 2005). Prefibrillar polyQ species strongly resemble in morphology, size and solubility characteristics the spheroid oligomers of Aβ (amyloid β) (Harper, et al. 1997; Lambert, et al. 1998) and the globular, ring-like and curvilinear structures observed in the α-synuclein aggeragtion pathway (Lashuel, et al. 2002; Volles, et al. 2001). This strongly supports the idea of a common aggregation mechanism of the polyQ proteins and other amyloidogenic proteins.

Visualisation of oligomeric species directly *in vivo* is extremely challenging due to their transient character, however Htt-exon 1 assemblies, isolated from cultured cells or HD mouse models, has also been shown to form a number of oligomeric, protofibrillar and fibrillar structures (Mukai, et al. 2005; Sathasivam, et al. 2010).

Taken together these results suggest an aggregation model for polyQ proteins in which conformational change of the monomer leads either to elongation-competent nucleus or morphologically distinct oligomeric and protofibrillar intermediates. Amyloid fibrils might be formed by the linear addition of monomers, without intermediate species or through intermediate oligomeric and protofibrillar assemblies each of which might be “off” the pathway to the fibril formation (Ross and Poirier 2005; Wacker, et al. 2004) (Fig.1-2). Hence, multiple aggregate species could be intermediates of a sequential or parallel multistep assembly pathway(s) (Legleiter, et al. 2010; Ross and Poirier 2005; Wacker, et al. 2004). Additionally, different intra-

and intermolecular factors can also modify the morphology, structure and toxic properties of polyQ aggregates, as described in the following chapters.

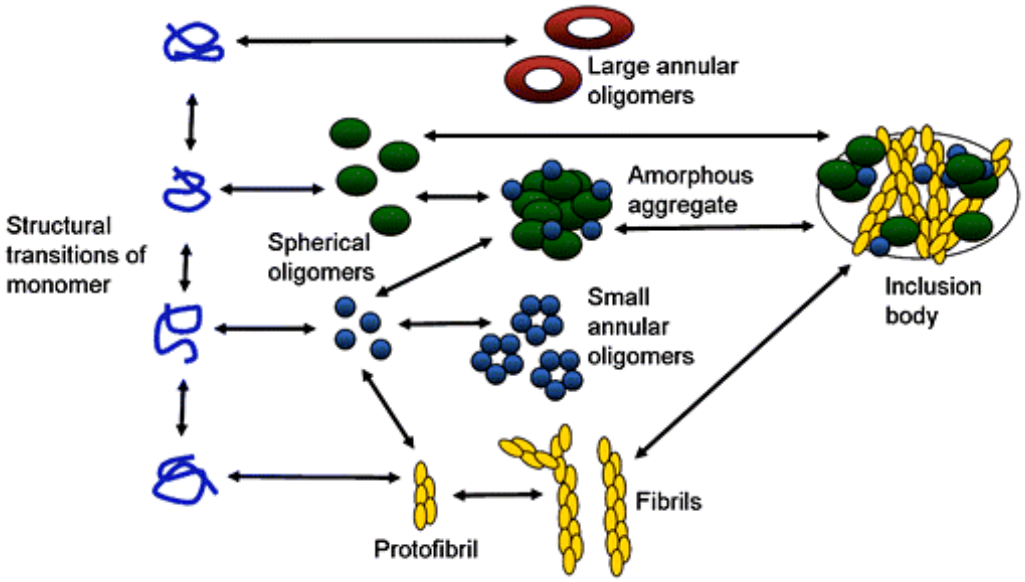

Fig 1-2: Model of aggregation of the full-length polyQ proteins. *Conformational change within a monomer, may give rise to several abnormal conformations forming morphologically distinct intermediates. Amyloid fibrils might be formed by the linear addition of monomers or through assembling intermediate oligomeric and protofibrillar assemblies (Adapted from (Hands and Wyttenbach 2010).*

1.4 Factors modifying polyQ aggregation in *cis*

Similar threshold of the glutamine repeats number in the most of polyQ proteins and formation of the intracellular aggregates with similar molecular characteristics suggest a common aggregation mechanism for the polyQ disorders. On the other hand, the disease proteins differ vastly in the sequence context flanking the pathogenic repeat, domain architecture, proposed function and cellular localization (Orr and Zoghbi 2007; Saunders and Bottomley 2009). Together with disease-specific neuronal vulnerability to damage (Gusella and MacDonald 2000), this implicates that aggregation and toxicity of misfolded polyQ proteins may be

modulated by different sequences and/or domains of the corresponding disease protein which are collectively named in *cis*–acting factors.

Several algorithms have been developed to predict amyloid propensity based on the primary sequence characteristics. Generally, increased hydrophobicity, low charge and intrinsic disorder (or destabilized globular structure), are common sequence features in the amyloid-prone domains (Chiti, et al. 2003; Olzscha, et al. 2011; Toombs, et al. 2010). Differing rates of aggregation of the fusion proteins comprising the polyQ stretch of the same pathological length placed in the context of eight N-terminal and nine C-terminal amino acids from SCA2, SCA3, Htt-exon1 and ATN1 have demonstrated importance of flanking sequences in the polyQ aggregation (Nozaki, et al. 2001). Consistently with the lower polyQ repeat thresholds SCA2 and Htt-exon1 variants exhibit a higher aggregation propensity. However, mutating four hydrophobic residues in the N-terminal flanking sequence of SCA2 to charged ones have decreased the aggregation rate, underscoring the modulatory effect of the protein context on polyQ aggregation propensity (Nozaki, et al. 2001).

Polyproline (polyP) sequence C-terminal to the expanded polyQ stretch slows down the aggregation and decreases the stability of aggregates compared with the Q_{40} peptide alone, whereas when placed N-terminally to the polyQ, polyP had no impact on aggregation (Bhattacharyya, et al. 2006). This effect is likely to be physiologically relevant, since the polyQ tract in Htt is directly followed by eleven consecutive proline residues. Mechanism of this aggregation inhibition has been explained by intrinsic propensity of the polyP to form PPII (polyproline type II) helix, that induces a PPII-like structure in the polyQ tract, opposing acquisition of the aggregation-prone β-sheet conformation by this region (Darnell, et al. 2007). It appears to be an evolutionarily conserved protective mechanism since aggregation-prone regions in proteins often are flanked by “gatekeeper” residues (P, K, R, D, E), that have low hydrophobicity and propensity to form β-sheet structure and/or are charged (Rousseau, et al. 2006).

Additionally polyP sequence is able to change the morphology of aggregates and to decrease the toxicity of the polyQ-expanded Htt-exon1 in a yeast model (Duennwald, et al. 2006). Duennwald and colleagues have also shown that negatively charged FLAG tag increases, whereas solubilizing GST domain prevents the toxicity in the same polyQ model (Duennwald, et al. 2006). Wild-type SCA1 protein may contain one to several histidine interruptions within its polyglutamine stretch (Klement, et al.

1998; Zoghbi and Orr 1995). In contrast, in SCA1 protein variants with pathologically expanded polyQ region these histidine insertions are absent (Matsuyama, et al. 1999; Zoghbi and Orr 1995). In the studies of polyQ peptides the histidine disruptions mimicking those in SCA1 have been shown to decrease the aggregation rates, although the nucleated growth polymerization mechanism with a critical nucleus of one and without non-fibrillar intermediates remains intact (Jayaraman, et al. 2009; Sen, et al. 2003; Sharma, et al. 1999). Interestingly, the polyQ stretch of DRPLA protein is flanked by an N-terminal pentahistidine sequence and one C-terminal histidine residue (Nagafuchi, et al. 1994), however the effect of these residues on ATN1 aggregation is yet to be determined.

In globular proteins amyloidogenic motifs are buried in a stable fold thus preventing conformational fluctuations and sampling for an aggregation-competent conformation (Chiti and Dobson 2006; Soto 2003). This leads to a hypothesis that local or global destabilization of the folded structure should precede the aggregation (Tartaglia, et al. 2008).

Recently, structured flanking domains have been shown to participate in the aggregation of a few polyQ proteins and to influence the type of aggregates formed.

The two-stage aggregation pathway of SCA3 has been described *in vitro* (Ellisdon, et al. 2007; Ellisdon, et al. 2006). In this model the first step is mediated by the intermolecular interactions of globular N-terminal Josephin domain, resulting in the formation of SDS-soluble, β-structured aggregates (Ellisdon, et al. 2006; Gales, et al. 2005). PolyQ region is not directly involved in this first step, as demonstrated by QBP1 peptide binding, however, the aggregation kinetics have increased with the polyQ length. Moreover, the isolated Josephin domain has been found to have an intrinsic ability to aggregate *in vitro* forming small curvilinear, soluble aggregates, similar to these observed for full-length protein (Chow, et al. 2004b; Masino, et al. 2004). The second step depends on the interactions of polyQ stretch, since only polyQ-expanded SCA3 is able to form SDS-resistant fibrillar aggregates (Ellisdon, et al. 2006).

Seeding is a highly discriminating ability of the aggregates to recruit new monomers based on sequence or structure similarity (Chien and Weissman 2001; O'Nuallain, et al. 2004). As suggested by differences in their morphology and solubility, SCA3 variants with a polyQ stretch in normal and pathological range form structurally

distinct end-stage aggregates (Ellisdon, et al. 2006; Gales, et al. 2005). The ability of these end-stage aggregates of non-pathological and mutant SCA3 variants to cross-seed each other suggests that the aggregation of both follows the same aggregation pathway (Ellisdon, et al. 2006). Similarly, C-terminal AXH domain of SCA1 can spontaneously aggregate *in vitro* and *in vivo* when isolated. The pro-aggregation effect of the AXH domain in the context of ataxin-1 has been evidenced by the decrease in formation of the nuclear inclusions in a cell model upon deletion or replacement of AXH with homologous non-aggregation-prone sequence (de Chiara, et al. 2005a; de Chiara, et al. 2005b). Hence, although the analysis of *in vitro* kinetics and aggregate evolution are lacking experimental evidence thus far suggests the multistage aggregation mechanism of SCA1.

The first 17 amino acids of Htt (HTT^{NT}) N-terminally upstream of the polyQ stretch form an amphipatic α-helical membrane domain found to be a key intrinsic modulator of Htt aggregation (Atwal, et al. 2007; Kim, et al. 2009; Rockabrand, et al. 2007; Tam, et al. 2009; Thakur, et al. 2009). HTT^{NT} has been shown to act as an aggregation enhancer *in vitro* that is able to dominate over the suppressing polyP effect in $HTT^{NT}Q_{30}P_6$ and $HTT^{NT}Q_{37}P_{10}$ peptides (Thakur, et al. 2009) and in Q51 Htt-exon1 (Tam, et al. 2009). Similarly, disruption of HTT^{NT} domain decreases or abolishes the aggregation and increases the toxicity of Htt-exon1 (Atwal, et al. 2007; Kim, et al. 2009; Rockabrand, et al. 2007). HTT^{NT} has been found to interact with itself and with the polyQ tract within Htt-exon1 suggesting an explanation of its pro-aggregation effect. Homotypic HTT^{NT} interactions have been proposed to facilitate self-association of Htt molecules into oligomers or fibrils, whereas interaction with a polyQ stretch has been suggested to stabilize its amyloidogenic conformation (Tam, et al. 2009). Thakur and colleagues have recently proposed a multi-domain misfolding mechanism for Htt-exon1 *in vitro* (Thakur, et al. 2009). They have shown that the isolated HTT^{NT} peptide has an aggregation-resistant compact conformation. The fusion of polyQ to this sequence induces in HTT^{NT} a more extended conformation in a polyQ length-dependant manner (Thakur, et al. 2009). In this extended state the HTT^{NT} segment becomes susceptible to formation of metastable, micelle-like aggregates with the HTT^{NT} involved in the loosely packed core and with the polyQ region exposed (Fig. 1-3). A kinetic analysis of this initial aggregation step suggests that formation of these first oligomeric species follows non-nucleated “downhill”

aggregation mechanism (Thakur, et al. 2009). The next step is rate-limiting and is proposed to involve a conformational rearrangement into β-sheet-rich amyloid fibril structure, followed by rapid fibril elongation via recruiting monomers or other oligomers (Fig. 1-3). The aggregate core in the end-stage fibrils comprises both HTT^{NT} and polyQ. (Thakur, et al. 2009) (Fig.1-3)

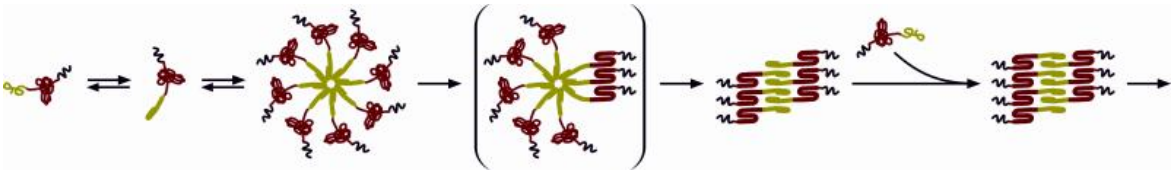

Fig. 1-3: Mechanism of HTT^{NT} mediated exon1 aggregation. *The HTT^{NT} domain (yellow) unfolds in a polyQ repeat-length dependent manner and is highly prone to self-association without a nucleation barrier. The core of the oligomers comprises only HTT^{NT} sequences. The final aggregates are fibrillar and rich in β-sheet and involve both HTT^{NT} and polyQ sequences (red) (Adapted from (Thakur, et al. 2009).*

Similar evolution of the aggregate core has been reported for CRABP1-Htt-exon1 fusion protein comprising the abnormally expanded polyQ tract (Ignatova, et al. 2007). Analogically to SCA1 and SCA3, CRABP1 domain which is stably folded domain gets destabilized in a polyQ-length dependent manner (Ignatova and Gierasch 2006). The destabilized CRABP1 domain establishes first interations thus forming spherical amorphous, detergent-labile aggergates (Ignatova and Gierasch 2006; Ignatova, et al. 2007). In the second stage, the core of the aggregates evolves into polyQ-dominated accompanied also by a structuring of the aggregates and changes in their physico-chemical properties (Ignatova and Gierasch 2006; Ignatova, et al. 2007).

PolyQ tracts in most of disease proteins are located outside of structured domains and regions in the closest vicinity of a polyQ stretch are known to be unstructured or are topologically undefined (Faux, et al. 2005).

The aggregation of Josephin, AXH and HTT^{NT} increases upon fusion of a polyQ and is dependent on the length of the expansion (de Chiara, et al. 2005a; de Chiara, et al. 2005b; Ellisdon, et al. 2006; Thakur, et al. 2009). The polyQ stretch in the pathological but not in the normal range destabilizes CRABP1 when fused to the Htt-exon1 (Ignatova and Gierasch 2006). On the other hand pathological and non-pathological polyQ lengths have a similar effect on the thermodynamic stability of SCA3 however the expanded polyQ stretch has been still suggested to change a conformational dynamics of Josephin domain (Chow, et al. 2004a; Masino, et al. 2004). Conversely, the pathological polyQ expansion has no effect on the structural stability of a juxtaposed α-helical domain in a model protein (Robertson, et al. 2008). Although the pathological polyQ expansion influences the architecture of amyloidogenic flanking domains the interplay between flanking domains and the polyQ tract appears to be highly sequence-specific, thus further investigation of polyQ effects upon dynamics and local stability of flanking sequences is necessary to understand the early aggregation events.

1.5 Factors modifying polyQ aggregation acting in *trans*

Various post-translational modifications may change conformation, aggregation propensity, stability, localization and turnover of mutated polyQ proteins, thus influencing their ability to interact with cellular proteins and their toxic properties (Bauer and Nukina 2009). On the other hand the alterations in the interaction networks may be associated with the sequence context of the disease polyQ proteins. Flanking sequences and thus the ability to interact with cellular proteins varies among the aggregates composed of different disease proteins (Chai, et al. 2002). Fluorescent techniques with high time resolution (i.e., fluorescent recovery after photobleaching (FRAP) and fluorescence loss in photobleaching (FLIP)) have revealed that cellular aggregates of ataxin-1 and Htt-exon 1 are highly heterogeneous with different mobility of the monomers inside them (Chai, et al. 2002; Kim, et al. 2002; Stenoien, et al. 2002). These various aggregate types may expose different parts of the primary protein sequences thus providing different surfaces for aberrant biophysical interactions with the cellular proteins. In turn, these interactions

and in general the whole cellular environment, collectively termed as extrinsic factors or factors acting in *trans*, also are likely to modify aggregation and toxicity of polyQ disease proteins.

The abnormal expansion in the polyQ region may allow either new, non-native protein-protein interactions or loss of the physiological ones. The strength of some interactions of polyQ proteins has occurred to be sensitive to the length of the polyQ tract. For example, the pathological elongation of the Htt-exon1 polyQ results in tighter binding with Htt-associated protein 1 (HAP1) and disruption of the axonal transport of brain-derived neurotrophic factor (BDNF) (Gauthier, et al. 2004; Li, et al. 1995). Conversely, Htt-interacting protein 1 (HIP1) binds weaker to mutated Htt-exon1 than to the wild-type, non-expanded protein and this alteration interferes with a clathrin-mediated endocytosis (Kalchman, et al. 1997).

SCA1 is involved in the protein complexes with both RNA-binding protein RBM17 and transcription factor Capicua (CIC) proteins (Lim, et al. 2008). An abnormal elongation of the polyQ region perturbs the balance of the formation of these complexes. The enhancement of interaction of the mutant SCA1 with RBM17, concomitant with the impaired interaction with CIC leads to an increase of the formation of the neurotoxic RBM17-SCA1complex in parallel to a decrease in the formation of the neuroprotective CIC-SCA1 complex. These alterations might be relevant for the ataxia type 1 pathology, since reduced levels of RBM17 and increased expression of CIC ameliorate the SCA-1 toxicity in a fly model (Lam, et al. 2006; Lim, et al. 2008).

Wild-type ATN1 dimerizes with RERE (ATN2-L) via RE-repeats, located at the C-termini of both proteins and pathological polyQ expansion in ATN1 enhances this binding with yet unclear effect (Yanagisawa, et al. 2000). RERE predominantly localizes in nuclei, in sub-nuclear domains PODs (PML oncogenic domains) through binding to an as yet unidentified POD partner (Shen, et al. 2007; Terashima, et al. 2002). PODs are defined by the tight co-localization of the tumor suppressor PML protein (promyelotic leukemia protein). In addition to PML, PODs may contain a set of proteins involved in repression of transcription, growth regulation and apoptosis, depending on the cellular context (Hodges, et al. 1998; Lamond and Earnshaw 1998; Seeler and Dejean 1999). A histopathological study of brains of DRPLA patients suggests that nuclear inclusions of mutant ATN1 rearrange the intranuclear distribution of PODs from multiple small speckle-like assemblies to one large

inclusion that co-localizes with the ATN1-aggregates, thus implicating involvement of PODs in the DRPLA pathology (Yamada, et al. 2001).

A multi-domain misfolding may lead to building aggregate species with an exposed, flexible polyQ domain (Ignatova, et al. 2007; Thakur, et al. 2009), thus facilitating non-native interactions with other proteins harboring accessible polyQ segments. Transcription factors, including TATA-binding protein (TBP), CREB-binding protein (CBP), TAFII130, Sp1 and p53 constituting an important class of polyQ-containing proteins have been shown to bind to some polyQ disease proteins and some of these associations might be triggered by specific interactions (McCampbell, et al. 2000; Shimohata, et al. 2000a; Steffan, et al. 2000; Strom and Sjogren 2005; Yamada, et al. 2000). Mutant Htt has been found to interact with the transcription activator Sp1 interrupting CRE-mediated transcription (CRE, cAMP responsible element) (Shimohata, et al. 2000a). TBP and TAFII130 have been found in IBs in DRPLA, SCA3 and HD brains, whereas CBP is additionally sequestered in SBMA and SCA7 inclusions (McCampbell, et al. 2000; Shimohata, et al. 2000a; Strom and Sjogren 2005; Yamada, et al. 2000). Sequestration in the IBs and thereby decreasing the amount of soluble histone acetyltransferases (HATs), like transcription factor CBP, may interfere with the acetylation and thus leads to cellular dysfunction (Ying, et al. 2006). Acetylation of the histones and transcription factors is a post-transcriptional modification which is necessary for transcriptional activation of specific genes. The toxicity might be due to perturbation of the balance between acetylation by HATs and deacetylation by HDACs (histone deacetylases) as it has been shown in DRPLA cell culture and mouse models, where HDACs inhibitors alleviated the toxicity of polyQ extended ATN1 (Kariya, et al. 2006; Ying, et al. 2006).

In addition to transcriptional factors many other cellular proteins crucial for maintaining the cellular homeostasis, including, molecular chaperones and components of the ubiquitin-proteasome system can be stably or transiently recruited into the aggregates of polyQ proteins (Chai, et al. 2002; Cummings, et al. 1998; Kazantsev, et al. 1999; Kim, et al. 2002; Nucifora, et al. 2001; Rajan, et al. 2001; Steffan, et al. 2000; Stenoien, et al. 2002).

Molecular chaperones play an essential role in recognizing and refolding of misfolded proteins (Sakahira, et al. 2002). Variable effects of the interplay between sequences of the host polyQ protein undergoing multi-domain aggregation may also account for

the context-dependent differences of chaperone recognition and interactions with polyQ proteins. For instance a Hsp70/Hsp40 chaperone complex has been suggested to decrease formation of spherical and annular oligomeric species of mutated Htt-exon1 by facilitating the refolding of a misfolded monomeric conformation to the native state or by enhancing fibril formation, following the structural rearrangement within the oligomers (Wacker, et al. 2004). In contrast, Hsp70 and HDJ-1, a member of Hsp40 chaperone family, acting separately or in cooperation have been shown to interfere with aggregation of a mutant AR by promoting formation of SDS-soluble aggregates and facilitating degradation of the misfolded protein by the ubiquitin-proteasome system (Bailey, et al. 2002).

Since the ability of molecular chaperones to rescue the misfolded proteins is limited other quality-control mechanisms are employed to avoid accumulation of aggregated proteins in cells. Proteasome is a multimeric enzyme complex that degrades abnormally folded proteins from cytoplasm and nuclei (Hershko and Ciechanover 1998; Schubert, et al. 2000). Similarly to chaperones a context-dependent character of interactions of polyQ-expanded proteins with proteasomal subunits has been described. Different proteasomal components can be stably recruited into Htt-exon1 aggregates, whereas their interaction with SCA1 is transient (Chai, et al. 2002; Stenoien, et al. 2002).

Poly-ubiquitination is a signal for protein degradation via ubiquitin-proteasome system and accumulation of highly ubiquitinated IBs in the majority of polyQ disorders suggests their inefficient proteasomal degradation (DiFiglia, et al. 1997). Additionally sequestration of the ubiquitin in the IBs may lead to the decrease of its concentration in the cellular pool and perturb the targeting of polyQ and other misfolded cellular proteins to the proteasomal degradation (Waelter, et al. 2001).

The misfolding and aggregation have also a potential to alter the pattern of other post-translational modifications of polyQ disease proteins which in consequence influences their toxic properties and aggregation behavior (Atwal, et al. 2011; Bauer and Nukina 2009). Aberrant phosphorylation of mutant polyQ proteins may affect protein cleavage, conformation, turnover and nuclear transport (Warby, et al. 2009).

For example serines 13 and 16 (S13 and S16) within the first 17 amino acids of Htt (N17 domain) can be phosphorylated in cultured mammalian cells (Aiken, et al. 2009; Thompson, et al. 2009). Introducing the phosphomimetic mutation that substitutes

aspartates for serines, spatially mimicking phospho-serines at positions 13 and 16 have been shown to suppress the toxicity in mouse model of full-length polyQ-expanded huntingtin (Gu, et al. 2009). The N17 domain normally functions as a cytoplasmic retention signal and mediates the association of Htt with membrane structures, such as the endoplasmic reticulum, Golgi or mitochondria (Atwal, et al. 2007; Slepko, et al. 2006). Atwal and colleagues have recently shown in cellular model that polyQ-expanded mutant huntingtin is hyperphosphorylated within its 17 N-terminal amino acids (N17) and that stress-dependent double-phosphorylation at S13 and S16 affects conformation of the N17 domain and targets full-length huntingtin to the subregions of the nucleus (Atwal, et al. 2011). Similarly, the phosphorylation of Htt at Ser421 by Akt kinase decreases nuclear inclusions formation and reduces toxicity in cell (Humbert, et al. 2002) and mice (Pardo, et al. 2006) HD models. Conversely, the phosphorylation of SCA1 by Akt at Ser 776 increases the interaction with the molecular chaperone 14-3-3, resulting in the protein stabilization and increased formation of IBs (Chen, et al. 2003). The IBs of ATN1 with expanded polyQ tract are also aberrantly phosphorylated in brains of DRPLA patients, however it remains unclear how these modifications affect ATN1 function (Okamura-Oho, et al. 2003).

Increased SUMO-ylation, a post-translational modification by small ubiquitin-related modifier (SUMO), has been shown to enhance toxicity and aggregation of mutant ATN1 (Terashima, et al. 2002), whereas the toxicity of SUMO-ylated mutant Htt-exon1 was enhanced by stabilizing its oligomeric state. SUMO-ylation is also suggested to be involved in transcriptional repression of Htt (Steffan, et al. 2004).

A proteolytic cleavage of the disease proteins generating small fragments comprising the polyQ tract is suggested to be a prerequisite for the disease pathology of HD, SCA3 and SBMA (Lunkes, et al. 2002; Walsh, et al. 2005; Wellington, et al. 1998). Such cleaved small polyQ-containing fragments are more aggregation-prone than the parental protein (Berke, et al. 2004; Cooper, et al. 1998; Haacke, et al. 2006), translocate more readily into the cell nucleus (Hackam, et al. 2000; Igarashi, et al. 1998) and may have an increased cytotoxicity (Colomer Gould, et al. 2007; Graham, et al. 2006; Ikeda, et al. 1996). 120 kDa N-terminal fragment found in brains of DRPLA patients and in DRPLA transgenic mice is relatively large compared to the proteolytic fragments of other polyQ proteins, usually small enough to diffuse even

freely into the nucleus. However, expression of the similar fragment, carrying expanded polyQ stretch and devoid of NES in a cell culture experiment results in increased nuclear localization and toxicity of the fragment (Nucifora, et al. 2003; Schilling, et al. 1999).

Taken together, polyQ-triggered conformational changes in the flanking sequences, which are unique for each disease protein, may expose sequence motifs that are normally buried in the native fold and lead to non-native protein-protein interactions either directly or provide a surface for aberrant post-translational modifications. Thus, studying the individual changes in the interactomes of mutant polyQ proteins is essential for understanding the variety in the clinical features of the different polyQ diseases.

1.6 Mechanisms of polyQ neuronal toxicity

Although the site of the cellular toxicity in the polyQ diseases has been controversial, the nucleus seems to be more sensitive to aggregation and neurotoxicity (Klement, et al. 1998; Nucifora, et al. 2003; Saudou, et al. 1998). Preferential accumulation of mutant polyQ proteins in the nucleus intensifies the disease phenotypes as shown by experimental redirection to nucleus of mutant Htt and ATN1 variants normally partitioning between nucleus and cytoplasm. Similarly, targeting the predominantly nuclear SCA1 to the cytoplasm reduces toxicity and aggregation in the mouse model (Klement, et al. 1998; Nucifora, et al. 2003; Peters, et al. 1999; Schilling, et al. 2004)

When cytoplasmic or shuttling nucleo-cytoplasmic polyQ proteins predominantly aggregate in the nucleus the toxicity is enhanced most likely due to compartment-specific alterations in the interaction partners network or in the availability of protein quality-control systems (Cornett, et al. 2005; Hands and Wyttenbach 2010; Iwata, et al. 2005). Toxic effects might be directly coupled to changes in the native function of the polyQ proteins, resulting from the altered pattern of their interactions. Alternatively, the functions of other cellular proteins involved in the key cellular processes may be compromised after their sequestration into the IBs formed by the mutant polyQ proteins (Hands and Wyttenbach 2010). Both of these mechanisms have been shown to contribute to the impairment of the transcription process in the

polyQ diseases (Lim, et al. 2008; McCampbell, et al. 2000; Shimohata, et al. 2000b; Steffan, et al. 2000; Yamada, et al. 2000), providing an explanation for the effect of the nuclear localization on the toxicity in the polyQ diseases.

A differential efficiency of protein quality-control systems in nucleus and cytoplasm might be another source of the increased polyQ cytotoxicity in the nucleus. Iwata and colleagues have established that autophagy efficiently degrades aggregates of mutant Htt and SCA1 from the cytoplasm but not in the nucleus in cellular model and in brains of transgenic mice; the autophagy markers associate only with the cytoplasmatic aggregates (Iwata, et al. 2005). Similarly, an induced cellular stress response results in inhibition of aggregation and proteasomal degradation of the aggregation prone polyQ-expanded SCA3 fragment that is more efficient in the cytoplasm than in the nuclei in the mammalian cell model (Breuer, et al. 2010).

In addition to depletion of ubiquitin and other components of the proteasome from the cellular pool due to their co-aggregation with the polyQ proteins, an alternative mechanism of proteasomal impairment have been proposed (Bence, et al. 2001; Brignull, et al. 2007; Venkatraman, et al. 2004). In contrast to the flanking sequences, polyQ tracts are degraded inefficiently hence leading to the accumulation of toxic polyQ-containing peptides (Bence, et al. 2001; Jana, et al. 2001; Venkatraman, et al. 2004). Such peptides and expanded polyQ stretches within the disease proteins can block the proteasomal activity, thus resulting in the accumulation of other misfolded proteins in the cell which perturbs in general the cellular homeostasis (Bence, et al. 2001; Brignull, et al. 2007).

It remains unclear whether the toxicity in the polyQ diseases is due to the toxic gain- or loss-of-function of the disease-related proteins. Deletions of the Htt, SCA1 or ATN1 genes failed to evoke the disease phenotype in transgenic mice. In contrast, transgenic mice and flies expressing the polyQ-expanded forms of the genes encoding ataxins-1, -2, -3 or huntingtin develop clinical and histopathological features reminiscent of the corresponding diseases (Ambrose, et al. 1994; Clark, et al. 1997; Davies, et al. 1999; DeMarch, et al. 2008; Huynh, et al. 2000; Ikeda, et al. 1996; Shen, et al. 2007; Yamamoto, et al. 2000). Hence, although the exact functions of most of the polyQ proteins are largely unknown (Gatchel and Zoghbi 2005), the toxic gain-of-function of the misfolded, mutant proteins has been suggested as the primary cause of polyQ disorders. On the other hand, aggregation of mutant Htt-exon1 has

been shown to promote fibrillization of the wild-type protein by recruiting it to IBs and thus loss-of-function may contribute to gain-of-function mechanism of the HD pathology (Busch, et al. 2003). An overexpression of wild-type Htt has been found to reduce markedly the toxicity in HD mice, further supporting the contribution of loss-of-function mechanism to the Htt toxicity (Leavitt, et al. 2001) It might be that the overexpression of the wild-type protein compensates for the toxic loss-of-function of Htt mutant protein (Leavitt, et al. 2001).

Aggregation of polyQ proteins *in vitro* is a complex process involving various oligomeric and protofibrillar aggregate species (Ross and Poirier 2005). Although nuclear and cytoplasmatic IBs are considered as a histological hallmark of polyQ disorders, their role in the disease pathogenesis is still unclear. IBs could impart the toxicity by physically interrupting the axonal transport (Morfini, et al. 2005). Conversely, a poor correlation between the presence of IBs in a disease-specific brain regions and pathological symptoms disfavors the role of the IBs in the toxicity *in vivo*. As an example, in the HD mice model harboring extensive striatal inclusions, almost no cell death has been observed (Mangiarini, et al. 1996). The disease symptoms have been shown to precede the IBs formation in a SCA1 mice model leading to a hypothesis that the aggregates might be a “by-product” of the disease pathology (Klement, et al. 1998). In HD cell-culture model, the cells containing inclusions survive significantly longer than the cells with diffused localization of the mutant protein suggesting even a protective role of inclusion bodies (Arrasate, et al. 2004). Furthermore, differentiated neuronal cells with soluble oligomers die faster than those with IBs or monomers of ATN1 fragment containing an expanded polyQ stretch (Takahashi, et al. 2008). Hence, current models favor a direct link between the abundance of small, intermediate species and cytotoxicity, which is also consistent with reported cytotoxicity of various aggregates in other neurodenerative diseases, including Aβ and α-synuclein oligomers (Caughey and Lansbury 2003; Klein, et al. 2001; Walsh, et al. 2002). These complex toxicity mechanisms result from a concerted action of the polyQ stretch, the sequences flanking it in the corresponding disease proteins and their interaction partners in the cell. Thus only a combined analysis of the effect of factors acting in *cis* and in *trans* on the dynamics of aggregation process will allow for the elucidation of the mechanisms underlying the pathogenesis of the polyQ diseases.

1.7 Aim of the thesis

The aggregation of a number of disease-relevant and model polyQ proteins *in vitro* has been suggested to be a multistep process that involves multiple aggregate intermediates with various morphologies which in turn reflect the cytotoxicity. Current models favor the prefibrillar aggregates as toxic species, whereas the end-stage fibrils are considered to be benign. Therefore understanding the structural changes in aggregation time course is essential to elucidate the relationship between polyQ aggregation and pathology. Details on the structure of the polyQ intermediates, however, particularly in the cellular context, are presently missing and have been limited by the technical difficulties due to their transient existence.

The main aim of this work was to systematically analyze and characterize the effect of the intrinsic and extrinsic factors on the ATN1 aggregation, a major culprit in DRPLA pathlogy. Murine neuroblastoma N2a cells were used as a cellular system. The properties and aggregation behavior of different aggregate species of ATN1 in both cytoplasm and nuclei were compared using dynamic imaging and biochemical and biophysical approaches. Furthermore, to specifically track the molecular architecture of the aggregates directly in the cell, a new approach, an orthogonal cross-seeding, has been developed.

The following specific questions were also addressed in this study:

1. Does the core of ATN1 aggregates structurally evolve with time?
2. What is the role of the flanking sequences and the polyQ stretch in the formation of aggregate core?

Subcellular localization, length of the polyQ stretch and differences in the composition and structure of the aggregate core may influence the recruitment-sequestration ability of aggregate species. Thus, the impact of the polyQ expansion in the disease state on the interactions of ATN1 in the nucleus and the cytoplasm of the N2a cells was studied using co-immunoprecipitation followed by mass spectrometry.

2. Materials and Methods

2.1. Materials

2.1.1 Escherichia coli strains

Strain	Genotype	Reference
DH5α	F^+/*endA1 hsdR17*(r_k^-, m_k^+) *glnV44 thi-1 recA1 gyrA1* (Nal^r) *relA1 ∆(lac/ZYA-argF) U169 deoR (φ80dlac∆(lacZ)M15)*	Novagene
BL21 (DE3)	B F^- *dcm*$^+$ The *omp T hsdS*(r_B^- m_B^-) *gal λ* (DE3)	Stratagene

2.1.2 Mammalian cell lines

Cell line	Description	Reference
N2a/Tet-Off	murine neuroblastoma N2a cell line stably transfected with the pTet-Off plasmid	A gift of Dr. P. Breuer
N2a/Tet-Off/LacI	N2a/Tet-Off cell line stably transfected with the pCMV-LacI vector	this work

2.1.3 Vectors used in this study

The following vectors were used for the genetic manipulations:

Vector	Description	Reference
pDsRed2	Prokaryotic, encoding red fluorescent protein DsRed2 from the *Discosoma sp.*	Clontech
pLAC	eucaryotic, lac-operator, *LacI*-regulated, MCS introduced in the pOPRSVCAT vector (Stratagene),	Matsumoto et al., 2006
pTRE2hyg	eucaryotic expression vector, doxycycline-responsive *pTRE* promoter (Tet-Off system)	Clontech
pEGFP-CMV-FL19Q/71Q	pEGFP-C2 vectors for constitutive expression (CMV promoter) of FL-ATN1 with 19Q or 71Q	Miyashita et al. 1998
pEGFP-CMV-ΔN19Q/71Q	pEGFP vectors for constitutive expression (CMV promoter) of ΔNLS-ATN1	Miyashita et al. 1998

The constructs used for the protein expression and analysis:

Vector	Description	Reference
pET16b-CRABP-Htt53Q	prokaryotic, expressing CRABP1-Htt53Q under the control of *T7* IPTG-inducible promoter	group stock
pBAD33-P39A CRABP	prokaryotic, expressing P39A CRABP1-myc under P_{BAD} promoter (arabinose-dependent)	group stock
pET16b-P39A CRABP	prokaryotic, expressing P39A CRABP1 under *T7* promoter	group stock
pBAD33-Htt20Q	prokaryotic, expressing Htt-exon1 with 20Q under the control of P_{BAD} promoter	group stock

The constructs used for the protein expression and analysis:

Vector	original backbone vector/Description	Reference
pGEX-GST 6P1-Htt53Q	prokaryotic, expressing Htt-exon1 with 53Q	group stock
pET-β_2m	prokaryotic, expressing $\beta_2$microglobulin under the control of *T7* promoter	Kad et al., 2001
pET16b-Luc	procaryotic, expressing firefly luciferase (*T7*)	group stock
pBAD33-Luc	procaryotic, expressing firefly luciferase (P_{BAD})	group stock
pEGFP-FL19Q/71Q	pEGFP-C2 vectors expressing FL-ATN1: FL19Q or FL71Q under doxycycline-responsive *pTRE* promoter	this work
pEGFP-ΔN19Q/71Q	pEGFP-C2 vectors expressing ATN1 lacking N-terminal NLS: ΔN19Q or ΔN 71Q (*pTRE*)	this work
pEGFP-C2	eucaryotic expression vector with EGFP tag upstream the MCS, constitutive CMV promoter	Clontech
pLAC-DsRed	pLAC vector expressing DsRed protein	this work
pLAC-DsRed-F_N	pLAC-DsRed vector with the N-terminus of human atrophin-1 downstream the DsRed	group stock
pLAC-DsRed-F_C	pLAC-DsRed with the C-terminus of human atrophin-1 downstream the DsRed	this work
pLAC-DsRed-Q19/Q71	pLAC-DsRed with the polyQ-containing fragment of atrophin-1 downstream the DsRed	group stock
pCMV-LacI-NLS	eukaryotic, constitutively expressing *LacI,* IPTG-dependent (LacSwitch I system)	Stratagene,

2.1.4 Antibodies

2.1.4.1 Primary antibodies

Antigen	Host	Monoclonal	Working dilution	Reference
GFP	Mouse	Yes	1:1000	Roche
GFP	Mouse	Yes	1:200	Miltenyi (GFP-tagged magnetic μMACS beads)
GAPDH	Mouse	Yes	1:2000	Ambion
lamin B1	Rabbit	No	1:250 (microscopy) 1:1000 (WB)	Abcam
nucleolin	Rabbit	No	1:1000	Abcam
LacI	Mouse	Yes	1:2000	Millipore
HA	Mouse	Yes	1:3000	Covance, Berkley CA
myc	Mouse	No	1:5000	Upstate biotechnology
CRABP	Mouse	Yes	1:1000	Abcam
MW1	Mouse	Yes	1:1000	Dev. Studies Hybridoma Bank, Iowa, USA
β_2m	Rabbit	No	1:5000	Strategic Diagnostic, USA

2.1.4.2 Secondary antibodies

Antigen	Host	Labeling	Working dilution	Reference
Mouse IgG	Mouse	HRP-conjugated	1:3000	ECL/Amersham
Rabbit IgG	Mouse	HRP-conjugated	1:3000	ECL/Amersham
Mouse IgG	Rabbit	Alexa 568-tagged	1:1000	Invitrogen

2.1.5 Enzymes and kits

2.1.5.1 Enzymes

Enzyme	Reference
Benzonase	Sigma-Aldrich
Herculase (DNA Polymerase)	Stratagene
Pfu DNA Polymerase	Stratagene
Pfu Turbo DNA Polymerase	Fermentas
Restriction enzymes	Fermentas, NEB
Calf intestine alkaline phosphatase	New England Biolabs
T4 DNA Ligase	New England Biolabs
Trypsin (for MALDI-TOF MS)	Roche
Lysosyme	Sigma-Aldrich

2.1.5.2 Kits

Kit	Reference
ECL detection kit	Rodeo^{TM} ECL western Blotting Detection
Nucleo Spin Extract II kit	Macherey-Nagel
Plasmid Miniprep kit	Macherey-Nagel
EndoFree Plasmid Maxi Kit	Qiagen
µMACS Epitope Tag Protein Isolation Kit	Miltenyi
jetPRIME DNA & siRNA transfection reagent	Polyplus Transfection
Lipofectamine Plus transfection kit	Invitrogen
Luciferase Assay system	Promega
Antifade mounting kit	Invitrogen

2.1.6 Frequently used buffers, reagents and media

2.1.6.1 Buffers

DNA analysis	
50x TAE (for agarose gel)	242g Tris base, 57.1ml Acetic acid, 100ml 0.5M EDTA, water up to 1l, pH=8.5
SDS-PAGE	
10x SDS-PAGE running buffer	30.3g Tris, 144g glycin, 10g SDS in 1l
5x SDS-PAGE loading buffer	3.79g Tris, 1g SDS, 0.5g bromophenol blue, 50ml glycerol, in 200ml water, pH=6.8, 5% ß-mercaptoethanol added before use
Coomassie staining solution	1.2 g/l Coomassie Brilliant Blue R-250, 50% ethanol, 10% acetic acid
Destaining solution	10% ethanol, 10% acetic acid
Western Blot	
Wet transfer western blot buffer	3.03g/l Tris, 14.4g/l glycine, 20% methanol
Blocking buffer	1x TBS, 5% skimmed milk
Antibody buffer	1x TBS, 1% skimmed milk
ECL-solution 1	100µl Luminol (250mM in DMSO), 44µl p-Cumaric acid (90mM in DMSO), 1 ml Tris/HCl 1M, pH 8.5, 8.85 ml H_2O
ECL-solution 2	6µl H_2O_2 (30%), 1ml Tris-HCl (1 M, pH 8.5), 9 ml H_2O
Stripping buffer 1	62.5 mM Tris-HCl, pH 6.7, 2% SDS, 100 mM β-mercaptoethanol
Stripping buffer 2	10 mM Tris, pH 8.0
IEF and MALDI-TOF MS	
DeStreak Rehydration Solution	GE Healthcare
IPG buffer pH 3-10 NL	GE Healthcare
Ultrodex suspension	20 mg Ultrodex + 666µl DeStreak Rehydration Solution (GE Healthcare)
SDS equilibration buffer (100 ml stock)	30% glycerol, 50 mM Tris-HCl pH 8.8, 6 M Urea, 2% SDS
Bacterial cell-lysis	
Lysis buffer	20mM Tris-HCl, pH 8.0, 1mM PMSF (Sigma-Aldrich), 5µg/ml lysosyme, 50ng/ml DNase, 0.1% Triton X-100

Mammalian cell lysis / fractionation	
1x TBS	10mM Tris, 154mM NaCl, pH=7.5
1X TBST	1x TBS, 0.2% Tween-20
Sucrose/TBS (ultracentrifugation)	2.5%, 15%, 25% or 30% sucrose, 1x TBS, Complete Protease Inhibitors cocktail, pH=7.5
Sucrose/PBS buffer	0.25M sucrose, 1XPBS, Complete Protease Inhibitors cocktail (Roche), pH=7.5
Buffer H	50mM HEPES in water, pH=7.5, Complete Protease Inhibitors cocktail (Roche)
Buffer H/$MgCl_2$	50mM HEPES, Complete Protease Inhibitors cocktail (Roche), pH=7.5, 20U/0.5 mio cells Benzonase
Lysis buffer T	1x TBS, Complete Protease Inhibitors cocktail (Roche), 100mM $MgCl_2$, pH=7.5, 20U/0.5 mio cells Benzonase
Fixing buffer (microscopy)	4% paraformaldehyde, 1x PBS
Permeabilization (microscopy)	0.1% Triton X-100, 1X PBS
PBS-B	1% BSA, 1x PBS

2.1.6.2 Media for bacterial culture

Luria-Bertani (LB) culturing medium	10g/l tryptone, 5g/l yeast extract, 10g/l NaCl (+ 15g/l agar for solid medium) Autoclave sterilization.
Ca/glycerol buffer (for competent cells)	60mM $CaCl_2$, 10mM PIPES, 150ml/l glycerol, pH=7.0

The stocks of antibiotics ampicilin or kanamycin prepared in water were added to LB medium at working concentrations 100µg/ml and 25µg/ml, respectively. Chloramphenicol stock in methanol was used at working concentration 25µg/ml.

2.1.6.3 Reagents for mammalian cell culture

Culturing full medium	*Dulbeco's Modified Eagle's Medium* (=DMEM) (PAN), 10% Fetal Calf Serum (=FCS) (PAN), 2mM Glutamine (Gibco) 1x non-essential aminoacids (Gibco) 100U/ml Peniciline (Gibco) 100 µg/ml Streptomycine (Gibco)
Tet-System Approved FCS	(Clontech) - for N2a-Tet-Off and N2a-Tet-Off-LacI cells
G418 (geneticin)	(Calbiochem) – 0.3mg/ml for maintenance of N2a-Tet-Off and N2a-Tet-Off-LacI cells
Hygromycin B	(Clontech) – 0.7 mg/ml for selection and 0.2mg/ml for maintenance of N2a-Tet-Off-LacI cells

1x PBS	(PAN)
Opti-MEM	Optimum Minimum Eagle's Medium (Invitrogen)
DMEM/F12	DMEM: Nutrient Mixture F-12 with L-Glutamine (Gibco), 10% Fetal Calf Serum (=FCS) (PAN), 1x non-essential aminoacids (Gibco) 100U/ml Peniciline (Gibco) 100 µg/ml Streptomycine (Gibco)
Trypsin-EDTA solution	(Gibco)
Freezing medium	10% DMSO (Sigma) in FCS

2.2 Methods

2.2.1 Molecular cloning methods

2.2.1.1 Plasmid preparation and DNA purification

Plasmids were isolated from *E. coli* DH5α cells. The transformed cells were grown at 37°C for at least 4 hours or overnight at constant shaking of 250rpm. Plasmid minipreps were performed with 5ml bacterial culture with Macherey-Nagel miniprep kits. Endonuclease-free maxipreps for transfections of mammalian cells were performed with 250ml overnight bacterial culture with Qiagen kit. Macherey-Nagel NucleoSpin ® Extract II kit was used to purify DNA from PCR, restriction digestion or dephosphorylation enzyme reaction mixtures or to extract it from agarose gels.

2.2.1.2 DNA analytical methods

DNA concentrations were measured by UV absorption spectrometry at 260nm.
1 OD_{260nm} = 50ng/µl double stranded DNA.
Agarose gel electrophoresis was used to analyze the DNA fragments. The 0.85-2.5% agarose gels (20~30ml) were prepared with low melting point agarose, TAE buffer and 2µl ethidium bromide stock solution. Electrophoresis was performed in TAE buffer, 70~90V. The DNA bands were visualized by fluorescent excitation on a

254nm UV table. For preparative purposes, inserts and vectors to be ligated double-digested with restriction enzymes were purified from 2.5% agarose gels (see 2.2.1.1). DNA sequencing service was provided by the core facility of MPI of Biochemistry (Martinsried, Germany) and GATC Biotech (Konstanz, Germany).

2.2.1.3 Restriction digestion

For the restriction enzymes purchased from Fermentas or New England Biolabs, the restriction digestion reactions were performed at the optimal buffer and optimal temperature for 1 hour. 1µl enzyme was used for up to 50µl reaction mixture. The products were then purified with PCR purification kit (Macherey-Nagel).

2.2.1.4 PCR reactions

In the experiments, the following PCR protocol was applied when a DNA fragment was being subcloned (for example, one of ATN1 fragments).
Reaction mixture composition (50µl scale):

Template	1µl
Primers (100~150µM)	1µl each
10x Herculase reaction buffer	5µl
Water	39.5µl
dNTPs(10mM each)	1.5µl
Herculase	0.5~1µl

PCR program:

95°C	2 min	
95°C	30 sec	10 cycles
55°C	45 sec	
72°C	1 min/kb	
95°C	30 sec	20 cycles
55°C	45 sec	
72°C	1 min/kb + 10 sec/cycle	
4°C	-	

For site-directed mutagenesis, the following PCR protocol was applied.
Reaction mixture composition (50µl scale):

Template (1:5 dilution)	1µl
Primers (10µM)	1µl each
10x *Pfu* buffer	5µl
Water	39.5µl
dNTPs (10mM each)	1.5µl
Pfu polymerase	1µl

PCR program:

95°C	2 min	
95°C	30 sec	18 cycles
55°C	45~60 sec	
68°C	2 min/kb + 1min	
4°C	-	

All the PCR reactions were performed on a VWR Thermocycler (VWR).

2.2.1.5 Site-directed mutagenesis

Site directed mutagenesis in this study was based on the strategy of QuikChange™ site-directed mutagenesis kit. *Pfu* or *Herculase* polymerases and DpnI enzyme were separately purchased. The primers were designed based on the Tm equation provided by Stratagen using a *ComplimentDNA* program developed by Dr. Zhang Gong based on the manual of QuikChange™ site-directed mutagenesis kit. The primers were 21~50 bases long and the calculated Tm were greater than 78°C. PCR reactions were performed according to the protocol in chapter 2.2.1.4. 1µl DpnI enzyme was added directly into the PCR reaction mixture and the digestion reaction was carried out at 37°C for 1 hour. 7µl of reaction mixture was directly transformed into 150µl of DH5α competent cells.

2.2.1.6 DNA dephosphorylation

Before DNA ligation, the vector and the fragment were double digested by restriction enzymes. The vector was then dephosphorylated by 1µl of Calf Intestine Alkaline

Phosphatase (CIP, from New England Biolabs) in a suitable buffer in 50 µl volume for 30 min. at 37°C.

2.2.1.7 DNA ligation

DNA ligation was performed in a total volume of 20µl with 1µl T4 DNA ligase from New England Biolabs at 12°C overnight. The concentration of vectors was kept approximately 1~2ng/µl. The molar ratio of vector: fragment was 1:6. Protocols were generated automatically by a *Ligation Calculator* program developed by Dr. Zhang Gong. After ligation, 10µl of ligation mixture was directly transformed into 150µl DH5α competent cells.

2.2.1.8 Competent cells and transformation

All the competent cells used in this study were made chemically.
DH5α *E. coli* cells were grown in optimal conditions (LB medium, 37°C, 250rpm shaking) until OD_{600nm} = 0.25~0.4. The culture was chilled on ice for 5 minutes. The cells were collected by centrifugation at 4°C and resuspended in cold Ca/glycerol buffer twice. The resuspended cells were incubated in the Ca/glycerol buffer for 30 minutes and then collected by centrifugation. For cells in 500ml culture, the pellet was resuspended in 6ml Ca/glycerol buffer, alliquoted into 150µl portions and snap-frozen in liquid nitrogen. They were kept in -80°C for up to half a year ensuring their competency. For transformation, the competent cells were thawed on ice. The DNA was added into the competent cells, mixed gently and kept on ice for 40 minutes. Then the cells were heat-shocked at 42°C for 1 minute and put back on ice for additional 2~3 minutes. 850µl pre-warmed LB medium was added into the competent cells and the cells were incubated at 37°C for 1 hour with 900rpm shaking. Then the cells were plated on proper antibiotic-containing LB-agar plates for colonies or inoculated to LB medium with the proper antibiotics.

2.2.2 General protein analytical methods

2.2.2.1 SDS-PAGE

SDS-PAGE was used to analyze proteins according to their molecular weights. The electrophoresis was performed using a discontinuous buffer system in MiniProtean 3 system (Bio-Rad). The gels were prepared as the following recipe:

	Stacking gel	Separating gel	
Concentration	5%	8%	12%
30% poly-acrylamide (ml)	0.85	3.2	4.8
1M Tris (pH=6.8) (ml)	0.63	-	-
1.5M Tris (pH=8.8) (ml)	-	3	3
10% APS (ml)	0.05	0.12	0.12
10% SDS (ml)	0.05	0.12	0.12
Water (ml)	3.4	5.56	3.96
TEMED (ul)	5	7	5
Total (ml)	5	12	12

The samples of mammalian total cell lysates or fractions were mixed with 5x loading buffer and heated up to 95°C for 5 minutes, then loaded on the gel. The gels were run in 1x SDS running buffer. The current applied was 12mA/gel for stacking gel and 24mA/gel for separating gel for optimal speed and resolution.
The SDS-PAGE were stained with Coomassie staining solution for 20-30 minutes and then destained in destaining solution until the bands were clearly visible.

2.2.2.2 Western blot

Proteins were transferred to nitrocellulose membranes after SDS-PAGE with wet-transfer method in western-blot transfer chamber supplied by Bio-Rad. Transfer was performed in 1x western blot transfer buffer with 100V voltage for 1-2h. The membranes were then blocked with 5% milk in TBS for 1 hour, washed with TBST twice, and then incubated in antibody buffer with the appropriate primary antibody at room temperature for 1~3 hours or at 4°C overnight. The membranes were then washed with TBST twice, incubated in antibody buffer with secondary antibody at room temperature for 1 hour, washed with TBST twice, and visualized with ECL

detection. The two ECL reagents were mixed directly before detection. The membranes were incubated in this mixture for 1~2 minutes and then exposed in Image Reader LAS-3000 (Fujifilm).

2.2.2.3 Filter-retardation-assay and native slot blot

SDS-insoluble aggregates were detected using slot blot filter retardation assay (Wanker, et al. 1999). Purified proteins, cell lysates or lysate fractions were adjusted to 2% SDS and 50 mM DTT. After heating at 95°C for 5 minutes, they were applied onto the slot blot manifold (Hoefer) and filtered through a cellulose acetate membrane (Waterman, 0.2 µm pore size) calibrated with 0.1% SDS, retaining only SDS-resistant aggregates. Following that membranes were washed twice with a solution containing 2% SDS and 50 mM DTT. For native slot blots purified proteins, lysates or lysate fractions were filtered through nitrocellulose membranes, calibrated with 1x TBS, retaining both SDS-resistant and SDS-labile species (Waterman 0.4µm pore size). Directly following the filtration through the slot blot manifold, the membranes were blocked with 5% milk in TBS for 1 h and the retained proteins were detected using the appropriate primary antibodies as described in chapter 2.2.2.2. To enable reprobing the membranes with another primary antibody the membranes were treated with stripping buffer 1 for 30 min. in 50°C to remove the antibodies and rinsed three times with a stripping buffer 2. The intensity of the slots was quantified using AIDA software version 4.15.025 or ONE-Dscan™ (Scananalytics, CSPI, USA). In the time-based assays the intensity of the spots at each time was converted into relative intensity and the intensity of slots among different experiments was compared as already decribed (Borwankar, et al. 2011).

2.2.3 Bacterial culture methods

2.2.3.1 Protein expression and growth curve

Plasmids containing *T7* (IPTG-inducible) or P_{BAD} (arabinose-inducible) promoters were used to express proteins in *E.coli* BL21 (DE3). The cells transformed with target plasmids were grown at 37°C, 250 rpm till OD_{600}=0.8. Following that, protein

expression was induced by adding to the medium isopropyl-β-thiogalactopyranoside (IPTG, Roth) to 0.4 mM or arabinose to 0.2%. Growth curves of different cells were monitored by optical density at 600nm.

2.2.3.2 *In vivo* orthogonal cross-seeding

The full-length CRABP-Htt53Q (*T7* promoter, ampicillin resistance) or either P39A CRABP (P_{BAD} promoter, chloramphenicol resistance) or Htt20Q (P_{BAD} promoter, chloramphenicol resistance) were cotransformed in *E. coli* BL21 (DE3) host. For expression, only freshly transformed cells bearing the double antibiotic resistance were used. A single colony was used to inoculate LB medium, containing 100 μg/ml ampicillin or 25 μg/ml chloramphenicol. Protein expression was induced either by adding IPTG (to 0.4 mM) for the *T7* promoter based constructs or arabinose (to 0.2%) for the P_{BAD} promoter-controlled constructs. In the co-expression experiments, expression of the full-length CRABP-Htt53Q chimera or β_2m (the plasmid was kindly provided by Prof. Sheena Radford, University of Leeds) was induced by adding IPTG for 60, 120, 180, and 240 min. after the culture reached OD_{600}=0.8. To turn off the protein expression IPTG was depleted by centrifuging the cells at 867x*g* for 5 minutes and washing the cells twice with fresh medium. The cells were resuspended in the same volume of fresh medium supplemented with the corresponding antibiotics, and the expression of the short fragments was induced by adding arabinose (to 0.2%) for 30 minutes. Following that, at different times after induction intact aggregates were isolated and analyzed by native slot-blots.

2.2.3.3 Isolation of intact aggregates from *E.coli* BL21 (DE3)

Intact aggregates of CRABP-Htt53Q were isolated at different times after induction from 250 ml of BL21 (DE3) culture. The cells was harvested at 2,060×*g* for 5 minutes at 4°C and pellets were re-suspended in 10 ml of lysis buffer and sonicated on ice for 5 minutes (50% duty cycle). Cell debris was removed by low speed centrifugation at 376×*g* for 3 minutes at 4 °C, and the supernatant comprising intact aggregates was aliquoted, frozen in liquid nitrogen, and stored at −80 °C. Small aliquots of the *in vivo* aggregates were dissolved either in 10 mM Tris·HCl, pH 8.0, containing 8 M urea or

in formic acid (for the later fibrillar species), and their concentration was determined spectrophotometrically using the [cepsilon]$_{280}$ of 21.750 M^{-1} cm^{-1} (a corrected value for wild-type CRABP1 with four additional cysteines). Buffer containing 8 M urea or formic acid served as a blank.

2.2.3.4 Protein purification

For protein purifications Htt53Q (in pGEX-GST 6P1 plasmid, *tac* promoter, IPTG-inducible) or P39A CRABP (pET16b vector, *T7* promoter) with N-terminal GST and His tag, respectively, were expressed in *E. coli* BL21 (DE3) cells in LB medium supplemented with 100 µg/ml ampicillin.

The cells transformed with the GST-Htt53Q plasmid were grown at 30°C till OD_{600}=0.4. The cells were then induced with 0.6 mM IPTG at 30°C for 6h. Next, the cells were centrifuged at 3400 rpm for 30 minutes and the pellets were stored at -80°C. The cell pellets were thawed and resuspended in 40 ml lysis buffer (50 mM Na_2HPO_4 pH 8.0, 100 mM NaCl, 10% glycerol, 0.1 mM DTT, 0.1 mM Complete protease inhibitor cocktail (Roche)). After adding 0.5 mg/ml lysozyme, 0.1 µl/ml benzonase and 0.1% Triton X-100 the lysates were incubated on ice for 30 minutes, the cells were further lysed using a French press and the lysate was centrifuged at 30,000xg for 30 minutes at 4°C. 2.5 ml GST 4 Fast Flow resin in a column was equilibrated with 25 ml lysis buffer and the supernatant was loaded on the column. The column was washed sequentially with 12.5 ml (each) of wash buffer 1 (lysis buffer + triton X-100), buffer 2 (50 mM Na_2HPO_4 pH 8.0, 500 mM NaCl, 10% glycerol, 0.1 mM DTT, 0.1 mM Complete protease inhibitor cocktail (Roche)) and buffer 3 (100 mM Tris-HCl pH 8.5, 100 mM NaCl, 10% glycerol, 0.1 mM DTT, 0.1 mM Complete protease inhibitor cocktail (Roche)). The protein was eluted with 7.5 ml of elution buffer (100 mM Tris pH 8.5, 100 mM NaCl 10% glycerol, 0.1 mM DTT, 0.1 mM Complete protease inhibitor cocktail (Roche), 20 mM reduced glutathione was added freshly to the buffer) and dialyzed with a dialysis buffer (50 mM Tris-HCl pH 8.0, 150 mM NaCl, 10% glycerol) for 16 hrs at 4°C. The protein concentration was measured using the Bradford assay and the protein aliquots were frozen in liquid nitrogen and stored at -80°C. Cells bearing the plasmid encoding P39A CRABP were cultivated at 37°C. After reaching OD_{600}=1 protein expression was induced with 0.4 mM IPTG for

4 h, the cells were harvested by centrifugation at 3700 rpm for 30 minutes, cell pellets were re-suspended in 20 ml of SL buffer (20 mM Tris-HCl pH 8.0, 500 mM NaCl) and treated for 15 minutes on ice with 5 mg/ml lysozyme and 5mg/ml DNase. After cell lysis with sonication for 5 minutes on ice (50% duty cycle) and centrifugation at 30,000xg for 30 minutes at 4°C the supernatants were applied on Ni-NTA columns (Qiagen, Valencia, CA) balanced with SL buffer. Following elution with a linear gradient of imidazole (20–500 mM) (Clark, et al. 1998), the protein fractions were dialyzed successively in 10 mM and 1 mM Tris-HCl buffer (pH 8.0; 10 mM β-mercaptoethanol) at 4°C overnight. 150-200 µM protein solutions were usually stored at 4 °C and were used within 2 weeks. Concentrations were determined spectrophotometrically using the $[cepsilon]_{280}$ value of 21750 $M^{-1}cm^{-1}$. The purity of the proteins was analyzed by SDS-PAGE and western blot analysis.

2.2.3.5 *In vitro* aggregation and seeding

In vitro aggregation of a 10 µM purified P39A CRABP protein was initiated by its destabilization with 1.7 M urea at 37°C. Prior to withdrawal of 50µl aliquots at different times the reaction mixture was gently mixed to ensure an equal distribution of the aggregates. GST-Htt53Q fusion contains a PreScission protease recognition site between the GST-tag and Htt53Q. To release the Htt53Q and initiate its aggregation the purified GST-Htt53Q protein was adjusted to a concentration of 3 µM in the cleavage buffer and PreScission protease was added at 0.8 U per 1 µM protein. To monitor the aggregation kinetics at 37°C with gentle agitation at 300 rpm 50µl aliquots were withdrawn at different times and analyzed.

To test the *in vitro* seeding activities of P39A CRABP and Htt53Q, aggregates of both proteins were grown overnight at 37 °C to allow complete aggregation. The aggregates were sonicated for 2 min in 30s bursts on ice to improve their seeding potency. 5% of such seeds were added to a reaction mixture at the beginning of the aggregation reaction. Aggregation reaction of 10 µM P39A CRABP was seeded with preformed Htt53Q aggregates and aggregation of 3µM Htt53Q with P39A CRABP seeds. Next the aggregation kinetics was monitored by withdrawing aliquots as described above. The aggregation reactions were stopped by heating the aliquots at

95°C with 2% SDS and 50mM DTT and the aggregation kinetics was further analyzed by filter-retardation assay (Wanker, et al. 1999).

2.2.3.6 FlAsH in-cell labeling and FlAsH fluorescence analysis

To estimate the tightness of the bacterial *T7* promoter the time-course of the CRABP-Htt53Q chimera expression was monitored using the FlAsH fluorescence as a read-out (Ignatova and Gierasch 2004). CRABP-Htt53Q protein contains a binding site (tetra-Cys motif) for the fluorescent dye, 4',5′-bis (1,3,2-dithioarsolan-2-yl) fluorescein (FlAsH, from the group stock) within an internal loop of the CRABP domain (Ignatova and Gierasch 2006). The *E. coli* BL21 (DE3) cells expressing CRABP-Htt53Q, cultivated in LB medium up to an OD_{600} of 0.5, pretreated with lysozyme (50 ng/ml, 10 minutes on ice) to make the outer membrane permeable to dye, were washed, resuspended in LB, and preloaded with FlAsH-EDT_2 (150 µM) and EDT (150 µM) to suppress the labeling of endogenous cysteine pairs (Adams, et al. 2002; Griffin, et al. 2000). The cells were preloaded with FlAsH-EDT_2 one generation prior to induction of CRABP-Htt53Q with 0.4 mM IPTG at OD_{600} = 0.8. At 60, 120, 180 or 240 minutes after induction 500 µl were withdrawn and the expression of the CRABP-Htt53Q was turned off by re-suspending the cells in IPTG-depleted LB-medium. The changes in the FlAsH fluorescence intensity were continuously monitored at 530 nm (bandwidth 2 nm) with excitation at 500 nm (Photon Technology International QM-1 fluorometer) over an interval of 30 minutes. The fluorescence of controls without protein was used as a blank and subtracted from each time point.

2.2.3.7 Firefly luciferase luminiscence analysis

The tightness of the *T7* and P_{BAD} promoters was tested by expressing the firefly luciferase cloned in the pBAD33 (chloramphenicol resistance, ATCC 87402) and pET16b (ampicillin resistance, Novagen) vectors, respectively, in *E.coli* BL21 (DE3). After the culture has reached OD_{600}=0.8 the expression of the firefly luciferase under the control of *T7* promoter was induced with 0.4 mM IPTG for 60 minutes.
The expression of the firefly luciferase under the control of P_{BAD} promoter was induced for 30 minutes by adding arabinose (to 0.2%) at various time points (60, 120, 180 and 240 minutes) after the culture has reached OD_{600}=0.8. Cells were collected,

lysed with the CCLR lysis reagent (Promega) following the manufacturers instructions and the luciferase activity was measured at 560 nm (using luciferase assay system (Promega)).

2.2.4 Mammalian cell culture methods

2.2.4.1 Culturing of adherent cell lines

Two adherent mammalian cell lines were used in this study. Murine neuroblastoma N2a cells stably transfected with pTet-Off plasmid (N2a/Tet-Off cells, a kind gift from Dr. P. Breuer), were used for doxycycline-controlled gene expression of FL-ATN1 and ΔN-ATN1 constructs under the minimal immediate early CMV promoter (*pTRE*). To enable that a constitutive *pCMV* promoter from the pEGFP-C2 constructs expressing FL- and ΔN-ATN1 variants (kindly provided by Dr. T. Miyashita) was exchanged with *pTRE* promoter from pTRE2hyg plasmid (Tet-Off system, Clontech). For the co-expression of FL/ΔN-ATN1 and ATN1 fragments in Tet-Off and LacSwitchI expression systems, respectively, N2a/Tet-Off cells were stably transfected with pCMV-LacI-NLS plasmid (Stratagene) bearing the Lac-repressor (*LacI*) gene and N2a/Tet-Off/LacI cell line was developed. The adherent mammalian cell lines were grown in a humid atmosphere containing 5% CO_2 at 37°C. Neuroblastoma N2a cells, were cultured in a full DMEM medium supplemented with 10% fetal bovine serum, 100 units/ml penicillin, 0.1 mg/ml streptomycin, 0.3 mg/ml L-Gln and 1 x non-essential amino acids. In order to avoid the interference with *pTRE* promoter-driven expression Tet-Off cell lines were cultured in the medium containing Tet-system approved FCS, without traces of tetracycline or its derivatives. For the maintenance of stably transfected N2a/Tet-Off cells 0.3 mg/ml of a selection antibiotic G418 (geneticin) was included in the full DMEM medium. N2a/Tet-Off-LacI cells containing stably integrated pCMV-LacI-NLS plasmid were selected in G418 containing full medium additionally supplemented with 0.7 mg/ml hygromycin B and further maintained using 0.3 mg/ml of the hygromycin B. Stably transfected N2a/Tet-Off/LacI cell line was developed from the positive clone chosen as described in Appendix 6.2. For the maintenance 250ml flasks (Falcon) and for the selection of the stably transfected cell line 15 cm culturing plates (VWR) were used. After reaching

confluency the cells were washed once in 1x PBS and harvested using Trypsin-EDTA solution. After adding fresh culturing medium to inhibit the action of Trypsin protease the cells were resuspended by repetitive pipeting and further cultured after diluting the cell suspension 1:5 to 1:10 times.

2.2.4.2 Cryopreservation

For the long-term preservation the cells cultured in 250 ml flasks until reaching the confluency were harvested, pelleted down for 5 minutes at room temperature, at 270xg and resuspended in 1ml of freezing medium. Followig that the cells were step-wise frozen: 1h at -20°C, overnight at -80°C and finally stored in a liquid nitrogen. After thawing the cryo-stocks freezing medium was removed by centrifugation at 270xg and the cells were resuspended and further cultured in a suitable medium.

2.2.4.3 Transfection and gene expression in mammalian cells

For the transient transfections cells were plated in the culturing medium with selection antibiotics in the numbers that allow obtaining 70% confluency at the day of transfection. Cells grown in 3 cm culturing plates (6-well-plates, Falcon) were transfected with 2µg of endonuclease-free plasmid DNA (from Maxi-*Preps*). For *in vivo* cross-seeding N2a/Tet-Off/LacI cells were co-transfected with the FL and ATN1 fragments at stoichiometric ratio 1:1 (0.5 µg:0.5 µg plasmid DNA per 1 well of 8-well µ-slide, ibidi). The transfections were performed using Lipofectamine Plus (Invitrogen) or JetPrime Reagent (PeqLab) following the manufacturers instructions. Briefly, DNA pre-complexed with Lipofectamine and Plus reagents diluted in Opti-MEM medium were incubated with the cells for 3h in 37°C, 5% CO_2 humid atmosphere. Otherwise, the cells were transfected with the DNA-JetPrime reagent complexes in full DMEM for 4h. Following that, transfection mixes were replaced with the fresh full DMEM and the cells were grown for further 12-72h. For long experiments the medium was changed every 24h. In order to exclude the interference with gene expression the selection antibiotics were ommited from the medium during and after transfection.

2.2.4.4 *In vivo* cross-seeding experiments in mammalian cells

The tight control of expression of FL/ΔN-ATN1 variants and ATN1 fragments in N2a/Tet-Off/LacI cells was provided by two modified mammalian expression systems: doxycycline-responsive Tet-Off (see 2.2.4.1) and IPTG-dependent LacSwitch I (Matsumoto et al., 2006), respectively. In the doxycycline-responsive Tet-Off expression system (Clontech) doxycycline inhibits the expression of the transcriptional activator protein (*tTA*) thus blocking the expression of the gene of interest under the control of the minimal immediate early CMV promoter (*pTRE* promoter). LacSwitch I inducible mammalian expression system (Stratagene) utilizes modified lac operon from E.coli. Binding of IPTG to the constitutively expressed Lac repressor protein (*LacI*) changes its conformation and results in the removal of the repressor from the operator thus enabling the expression of the gene of interest under the control of *RSV* promoter. Here, the fragments covering for different parts of the FL-ATN1 were cloned to the pLac-DsRed vector, downstream the DsRed gene. pLac-DsRed plasmid was obtained by cloning the DsRed sequence from the pDsRed2 plasmid (Clontech) to the pLac/MCS plasmid (kindly provided by Dr. R. Morimoto), an engineered pORSVI/MCS plasmid (Stratagene). The expression of constructs under the control of *pTRE* promoter was switched off by addition of 0.3 µg/ml doxycycline. The expression ATN1 fragments controlled under the LacSwitch I expression system was initiated by adding 15 mM IPTG to the medium. To monitor the recruitment of different parts of ATN1 to the early aggregates the expression of ATN1 fragments was turned on for 24h and after that it was stopped by depleting IPTG from the medium. The expression of FL or ΔN-ATN1 constructs was turned on for 12 h, 12 h after switching on the expression of the fragments. To test the recruitment ability of late ATN1 species FL or ΔN-ATN1 variants were expressed for 36 h. Following that, the expression was stopped by adding doxycycline to the medium. 12 h later the expression of the fragments was switched on for 24 h by adding IPTG to the medium. The recruitment of ATN1 fragments to early and late aggregates was analyzed by confocal imaging microscopy of transiently transfected live N2a/Tet-Off/LacI cells (see 2.2.4.8).

2.2.4.5 Preparation of mammalian cell lysates and fractionations

For preparation of the total lysates N2a/Tet-Off cells were washed twice in PBS and harvested in a lysis buffer T using a cell scraper, lysed on ice at the lowest blender-homogenizer power and subsequently treated with Benzonase™ (Sigma-Aldrich) for 20 min on ice. The total lysates were centrifuged for 10 minutes, at low speed (80xg) at 4°C and the pellet fraction was resuspended in the lysis buffer T. The supernatants were further fractionated into five fractions by ultracentrifugation (50000xg, Ti65-Beckman-Coulter rotor) for 45 minutes at 4°C in a discontinuous sucrose density gradient in 50mM Tris buffer pH 7.5, containing 150mM NaCl and protease inhibitors cocktail. For fractionation into nuclear and cytoplasmic fractions, cells were washed twice in PBS and harvested using a cell scraper in PBS buffer containing 0.25 M sucrose and protease inhibitors cocktail, centrifuged at 300xg for 3 minutes and resuspended in hypotonic buffer H. After swelling for 10 minutes on ice the cells were dounce-homogenized, centrifuged for 10 minutes at 80xg at 4°C to separate the non-disrupted cells and the largest cytoplasmatic inclusions (without precipitating the nuclei), and the nuclear fraction was further pelleted by 600xg for 10 minutes at 4°C. Both, the pellet after the first, slow-centrifugation step and the nuclei fraction were resuspended in the hypotonic buffer H containing 100 mM $MgCl_2$ to a volume equal of the supernatant and subjected to an additional mechanical disruption on ice at the lowest blender-homogenizer power and incubated for 15 minutes with Benzonase on ice. All the buffers used for preparation of the cell lysates and fractionations were filter-sterilized. Samples were further subjected to immunoprecipitation followed by 2-D and mass spectrometry analysis (see: 2.2.4.6 and 2.2.4.7) or were directly analyzed by immunoblot on nitrocellulose membrane or filter-retardation assay (Scherzinger, et al. 1999) on cellulose acetate membrane (0.2 µm pore size) and detected using anti-GFP (1:1000, Roche), anti-nucleolin (1:1000, Abcam), anti-lamin B1 (1:1000, Abcam) as primary antibodies.

2.2.4.6 Immunoprecipitation and two-dimensional gel analysis

2.2.4.6.1 Immunoprecipitation

25-30 millions of transiently transfected N2a-Tet-Off cells expressing FL-ATN1 proteins for 48h were fractionated into nuclear and cytoplasmic fractions, as described in 2.2.4.5 and immunoprecipitated using µMACS Epitope Tag Protein Isolation Kit (Miltenyi). The manufacturer's immunoprecipitation procedure was modified. Briefly, cytoplasmic and nuclear fractions were incubated with anti-GFP µMACS MicroBeads for 30 minutes. The magnetically labeled GFP-tagged species were separated in the magnetic field and retained on the µ Columns (Miltenyi). To avoid losing SDS-labile ATN1 species the unbound material was removed by washing the columns four times with buffer H/$MgCl_2$ instead of the SDS-containing Wash Buffer 1 (Miltenyi). The residual salts were removed with Wash Buffer 2 (Miltenyi). The immuno-complexes were eluted and solubilized by using 50 µl of DeStreak Rehydration Solution (GE Healthcare), containing urea, thiourea, CHAPS and DeStreak Reagent, supplemented with 2% IPG buffer pH 3-10 NL (GE Healthcare) and pre-heateing to 95^{o}C. The whole procedure was performed on ice or at 4^{o}C except for the last washing and elution steps, performed at room temperature. Following that the samples were immediately subjected to western blot or two-dimensional gel analysis.

2.2.4.6.2 Isoelectric focusing (IEF) and SDS-PAGE

In the first dimension the isolated FL-ATN1 species were separated according to their isoelectric point (pI) by using 7 cm immobilized pH gradient (IPG) Immobiline DryStrip Gels with non-linear pH range 3-10 (GE Healthcare). Prior to isoelectric focusing (IEF) the IPG strips were rehydrated in DeStreak Rehydration Solution (GE Healthcare) for 12h at room temperature. The sample diluted 1:1 with the Ultrodex suspension was applied using cups immediately prior to IEF. The IEF was performed on a Multiphor II Electrophoresis (Amersham Pharmacia Biotech) unit with Immobilline DryStrip Kit (GE Healthcare) at the temperature set at 20^{o}C using a programmed voltage gradient:

Phase	Voltage (V)	Duration (h:min)
1	150	0:15
2	300	0:15
3	500	0:10
4	1000	0:10
5	1500	0:10
6	2000	0:10
7	2500	0:10
8	3000	0:10
9	3500	1:30

In the second dimension the proteins were separated according to their molecular weights using SDS-PAGE in MiniProtean 3 system (Bio-Rad). Following the IEF the IPG gel strips were equilibrated in two-steps in SDS-containing buffers, involving the protein modification with iodoacetamid (buffer 1: SDS equilibration buffer with 10 mg/ml DTT; buffer 2: SDS equilibration buffer with 25 mg/ml iodoacetamid) in the second step and placed on 10% SDS-polyacralamide gels, prepared according to the following recipe:

Solution	Amount
Glycerol (g)	1.96
30% poly-acrylamide (ml)	4.42
1.5M Tris (pH=8.8) (ml)	2.23
10% APS (ml)	0.33
10% SDS (ml)	0.133
Water (ml)	4.92
TEMED (ul)	6
Total (ml)	13.65

The gels were run in 1x SDS running buffer using the following conditions:

Phase	Voltage (V)	Duration (h:min)
1	100	0:20
2	200	3:15

To visualize the proteins SDS-PAGE gels were stained overnight using sensitive Coomassie staining solution and then destained for 1h in destaining solution (Neuhoff, et al. 1988). Following that chosen protein spots were further analyzed by MALDI-TOF MS

2.2.4.7 Matrix-assisted laser desorption/ionization time-of-flight mass spectrometry (MALDI-TOF MS)

2.2.4.7.1 Sample preparation

The protein spots of choice were excised from keratin-free gels. The gel pieces were destained by shaking in 37°C in acetonitril - 50 mM ammoniumhydrogencarbonate washing solution freshly mixed in proportion 4:6 (v/v), shrank in acetonitrile, vacuum dried and subjected to in-gel trypsin digestion. The gel pieces were incubated in trypsin digestion solution overnight, at 37°C. The resulting peptides were extracted from gel pieces by incubation with shaking at 1000 rpm, at 37°C sequentially in 10 µl of water for 15 minutes, 20 µl of acetonitril for 5 minutes, 30 µl of 5% formic acid for 20 minutes and 20 µl of acetonitril for 5 minutes. The supernatants from all steps were pooled together, vacuum dried and peptides were dissolved in 5µl of 0.1% TFA (trifluoroacetic acid) and 50% acetonitrile. The resuspended peptides were spotted onto the MALDI target with α-cyano-4-hydroxycinnamic acid (CHCA) as matrix and further analyzed.

2.2.4.7.2 MALDI TOF MS analysis and protein identification

The tryptic peptides were analyzed using MALDI TOF mass spectrometer (microflex LRF, Bruker Daltonics), equipped with a nitrogen laser with variable repetition rate. Spectra were acquired by summing the signals recorded after 150-200 laser shots. Singly charged monoisotopic peptide masses were generated and used as inputs for database searching after external and internal calibration of spectra. Database searching was performed against SwissProt database, employing Mascot online engine (http://www.matrixscience.com/cgi/search_form.pl?FORMVER=2&SEARCH=PMF) and using a Peptide Mass Fingerprint as protein identification method. The following search parameters were employed: *all entries* and *Mus musculus* for the taxonomic cathegory, peptide mass range of 0-200 kDa, iodoacetamide modified cysteines, maximum of 2 missed cleavage sites and mass tolerance of 0.1 Da.

2.2.4.8 Fluorescent microscopy and cell imaging

The mammalian cells expressing ATN1 variants were imaged on LSM710 Axiovert confocal microscope (Zeiss), equipped with the x63 objective lens, and images were taken at 488-nm, 405-nm, 561-nm laser wavelengths for GFP, DAPI and DsRed/Alexa568, respectively.

2.2.4.8.1 Fixed microscopy preparations

Transfected N2a/Tet-Off cells were grown on poly-L-lysine pre-coated cover slides. 12h -72h post-transfection the cells expressing ATN1 constructs tagged with GFP or DsRed were washed three times for 5 minutes with 1x phosphate-buffered saline (PBS) fixed for 1h in 4% paraformaldehyde, again washed three times for 5 minutes in 1xPBS and permeabilized for 2 minutes with 1% Triton X-100 (Sigma). After washing three times in 1xPBS the preparations were blocked for 1 h in PBS-B and the nuclei were counterstained for 10 minutes with DAPI (4',6-diamidino-2-2-phenylinodol, 0.25 µg/ml) (Sigma) in PBS-B. Following the three 5 minutes washings in 1xPBS and removing the salts with water, the cover slides were mounted using anti-fade mounting kit (Invitrogen) and sealed with the nail polish. For immunofluorescent analysis of endogenous lamin B1 localization, following the blocking step, the cover slides were additionally incubated for 1 h with the primary anti-lamin B1 antibody (1:250, Abcam) in PBS-B. Subsequently, after washing three times for 5 minutes in PBS-B the cells were incubated for 1 h with Alexa568-labelled anti-mouse IgG antibody (1:1000, Invitrogen) and DAPI in PBS-B. Following that the procedure was carried on as described above. The whole procedure was performed at room temperature. The ready fixed preparations were stored in dark in 4^0C.

2.2.4.8.2 Live-cell imaging, FRAP, iFRAP

For imaging of live cells, FRAP (Fluorescence Recovery After Photobleaching) and iFRAP (inverted FRAP) transfected N2a/Tet-Off or N2a/Tet-Off/LacI cells were grown in poly-L-lysine pre-coated 8-well µ-slides (ibidi). FRAP experiments were conducted at room temperature, using CO_2-insensitive medium DMEM/F12, buffered with

HEPES, without phenol red. Individual slides were imaged up to 1.5 h. For FRAP experiments an area of 2.98 μm^2 was photobleached for 1s (120 iterations) with 488-nm laser wavelength at 100 % power and single images were collected before and every 1.5 s after photobleaching within an interval of 8.5 minutes. For the iFRAP experiments the area of interest was defined using Zen software (Zeiss) and the whole cell outside the defined area was photobleached for 4.5 s (90 iterations) with 488-nm laser wavelength at 100 % power. 300 or 500 z-stacks, each consisting of 5 slices in 0.7 µm intervals or 7 slices in 0.9 µm intervals, were collected for each single image in the FRAP and iFRAP experiments, respectively. The intensity of the images recorded in FRAP was normalized to relative intensity (*RI*) as established for in-cell FRAP analysis (Kim, et al. 2002; Lippincott-Schwartz, et al. 2001; Stenoien, et al. 2002): $RI_{t=i} = (I_i/I_{nbi})/(I_0/I_{pb})$, where I_i and I_{nbi} are the integrated intensities of the bleached and non-bleached area at any given time point, and I_0 and I_{pb} are the integrated intensities before photobleaching of the bleached and non-bleached area, respectively. The fluorescence intensity was recorded from the image with the highest contrast within each z-stack accounting for the alterations in the position of the photobleached species due to slight diffusive movements using software written in Visual BASIC.NET (by Prof. Zhang Gong). The total mobile fraction and the fast and slow phases of recovery were determined as described by Laporte and co-workers (Laporte, et al. 2011). The images recorded in iFRAP were normalized to the relative intensity values $RI_{t=i} = (I_i/I_{nbi})$. The constitutive photobleaching in the iFRAP experiments during the long-time illumination with low intensity laser was measured by collecting control images of at least 10 non-bleached cells. The relative intensity values were corrected for the constitutive bleaching, plotted against the time and fit in MatLab R2009b using standard three- or five-parameter exponential functions. The half-life time was determined as described elsewhere (Stenoien, et al. 2002) and the standard deviation was calculated from three independent cells.

3. Results

3.1 Expansion of the polyQ stretch changes the inclusion dynamics

Cellular aggregates of polyQ proteins may differ in size and structure, including the core and flexible regions (Ignatova, et al. 2007; Thakur, et al. 2009), compositions in terms of other cellular proteins (Chai, et al. 2001; Matsumoto, et al. 2006) and subcellular localization (Ko, et al. 2001). These differences may be reflected by the changes in the biophysical and dynamic properties of the various aggregate species. To address this we first systematically analyzed the dynamic properties of the ATN1 aggregates. The *in vivo* dynamics of full-length (FL) and ΔN-ATN1 with a polyQ tract in the non-pathological (Q19) or pathological (Q71) length was monitored in neuroblastoma N2a/Tet-Off cells, by tagging them N-terminally with GFP protein and controlling their expression in Tet-Off doxycycline-responsive mammalian system (Clontech). We modified the Tet-Off system by exchanging the *pCMV* constitutive promoter of the ATN1 constructs to the *pTRE* promoter (Tet-Off).

Murine neuroblastoma N2a cells represent a cellular medium highly relevant to the pathophysiological medium of polyQ diseases and have been shown by a few groups as a suitable model for studying the aggregation of polyQ proteins (Haacke, et al. 2006; Jana, et al. 2000; Nucifora, et al. 2001; Yamamoto, et al. 2006).

The pathological FL71Q variant readily localized mainly into hyperfluorescent loci in both, cytoplasm and nucleus, even at 24 h post-transfection (Fig. 3-1 and Table 3-1). A fraction of it, however, remained diffusely distributed throughout the cell even at later times of expression thus recapitulating the expression pattern of ATN1 with expanded polyQ tract previously observed in degenerated neurons (Nucifora, et al. 2003). At early time point (24 h), FL19Q exhibited a predominantly diffuse pattern of localization throughout the cell with some rarely detectable, small hyperfluorescent puncta mostly in the nuclei of some cells (Fig. 3-1 and Table 3-1). The fraction of the FL19Q hyperfluorescent loci increased with the expression time (48 h) with much higher proportion of the inclusions in the nucleus compared to the cytosol (Fig. 3-1 and Table 3-1). Interestingly, FL19Q and FL71Q proteins typically formed in the nuclei 1-3 inclusions of 1-3 µm in diameter, regardless of the polyQ length and the

time of expression. The cytoplasmatic assemblies were heterogeneous in number, with their sizes ranging from 0.5µm-5µm.

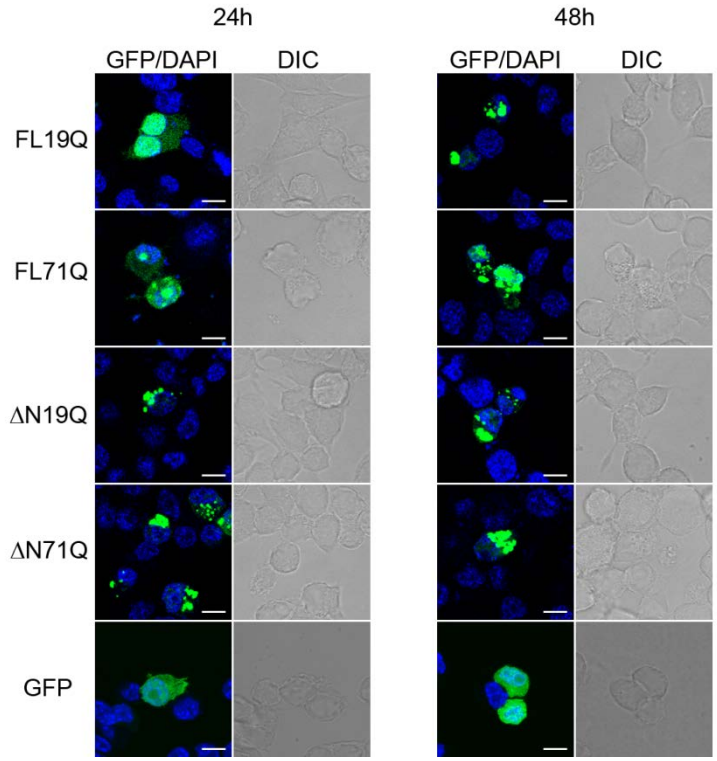

Figure 3-1: Cellular localization of the ATN1 variants. *GFP-tagged FL-ATN1 variants partitioned between the cytoplasm and the nucleus and ΔN-ATN1 variants were localized in the cytoplasm. The nuclear localization was confirmed with DAPI counterstaining. N2a/Tet-Off cells were transiently transfected with GFP-tagged ATN1 variants and visualized by the fluorescence (GFP) and differential interference-contrast (DIC) microscopy after 24 and 48 h. GFP control was soluble over the whole expression cycle. Scale bar, 10 µm.*

Notably, only the FL71Q variant formed SDS-insoluble species, with the detergent-resistance occurring for the first time only 36h post-transfection (Fig. 3-2). The resistance to even high concentrations of detergents represents an important pathological hallmark of polyQ-aggregates with fibrillar structures (pre-aggregates or mature fibrils) (Kazantsev, et al. 1999). This property of the fibrillar aggregates was studied here using a filter-retardation assay, an approach designed to monitor the

formation of high molecular weight fibrillar protein aggregates (Scherzinger, et al. 1997).

The nucleo-cytoplasmic shuttling of ATN1 is mediated by the two functional NLS and NES sequences and can be abrogated by a putative caspase cleavage at Asp109 which removes the NLS and alters the localization of the protein solely to the cytoplasm (Nucifora, et al. 2003). Such N-terminally truncated ATN1 fragments (ΔN-ATN1) have been identified in DRPLA disease model mice and DRPLA patients (Nucifora, et al. 2001; Schilling, et al. 1999). To compare the cytoplasmic inclusions of FL-ATN1, we expressed the corresponding N-terminally truncated ATN1 variants with short (ΔN19Q) or expanded (ΔN71Q) polyQ stretch, lacking the initial 78 amino acids sequence, that comprises the NLS. Both, ΔN19Q and ΔN71Q formed hyperfluorescent loci which were undistinguishable in shape and size (Fig. 3-1); however, similar to the FL-ATN1 proteins, only the variant with the expanded polyQ stretch (ΔN71Q) assembled into detergent-resistant aggregates 36h post-transfection (Fig. 3-2). Taken together, the data suggest that FL-ATN1 and ΔN-ATN1 variants independent of the polyQ length formed discernible inclusions however the polyQ expansion shortened the time of appearance and introduced differences in their detergent resistance.

Table 3-1: Quantification of the localization pattern of GFP-ATN1 variants. *Cells expressing FL-ATN1 and ΔN-ATN1 proteins were counted in three independent blind experiments for the presence of inclusions and diffusive staining in nucleus and cytoplasm.*

Protein	Time of expression h	Nuclear localization		Cytoplasmic localization	
		Diffuse distribution, %	Hyperfluore-scent loci, %	Diffuse distribution, %	Hyperfluore-scent loci, %
FL19Q	24	74 ± 4	26 ± 4	93 ± 3	5 ± 1
	48	36 ± 3	63 ± 4	73 ± 2	29 ± 4
FL71Q	24	34 ± 5	65 ± 4	48 ± 4	51 ± 3
	48	23 ± 4	77 ± 5	38 ± 5	61 ± 5
ΔN19Q	24	n.d.	n.o.	22 ± 4	78 ± 4
	48	n.d.	n.o.	20 ± 6	80 ± 6
ΔN71Q	24	n.d.	n.o.	21 ± 3	79 ± 3
	48	n.d.	n.o.	21 ± 4	79 ± 4

n.o., not observed; n.d., not determined

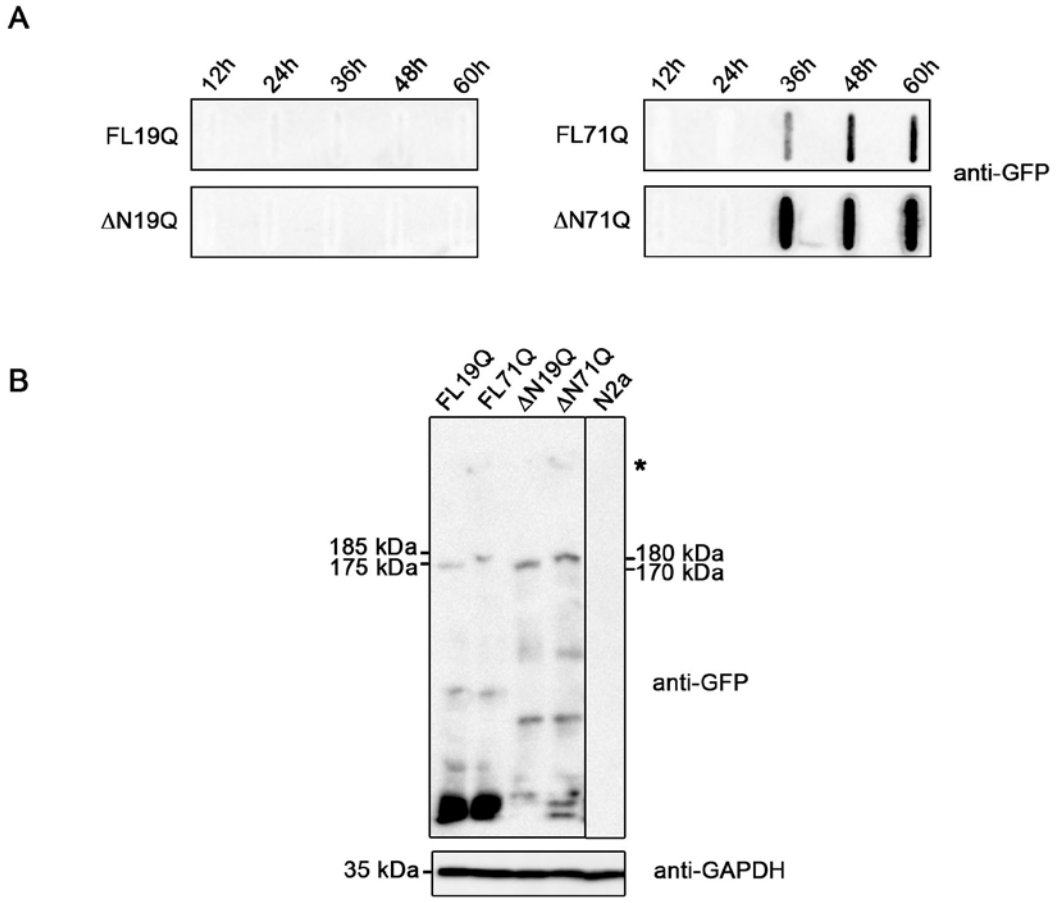

Figure 3-2: FL-ATN1 and ∆N-ATN1 with expanded polyQ tracts form detergent-resistant aggregates. *(A) Filter-retardation assay. Three million N2a/Tet-Off cells expressing each protein at different times were lysed, applied to the cellulose acetate membrane and washed with SDS-containing buffer. (B) The lysates prepared from 0.3 million N2a/Tet-Off cells expressing ATN1 variants for 48h were separated by SDS-PAGE and blotted on the nitrocellulose membrane. The low amount of the SDS-insoluble FL71Q and ΔN71Q aggregates in the stacking gel is a result of low number of the lysed cells loaded on the gel. The GFP-positive bands of approximately 175 kDa, 185 kDa, 170 kDa and 180 kDa correspond to the monomeric form of FL19Q, FL71Q, ΔN19Q and ΔN71Q, respectively. The lower molecular weight GFP-positive bands are probably degradation products of the ATN1 proteins during the processing of the sample. Mock-transfected N2a/Tet-Off cells provide a negative control (N2a). The ATN1 proteins were probed with anti-GFP antibodies (A, B). Note that here total lysates, comprising the cytoplasmic and nuclear fraction, were loaded onto the membranes (A, B). Asterisk (*) denotes the beginning of the stacking gel.*

This raised the question as to whether the hyperfluorescent loci of ATN1 with non-pathological and pathological polyQ-length, even though with the undistinguishable morphology on the static microscopy images, have different mobility and dynamic properties. The dynamic properties of the nuclear and/or cytoplasmatic inclusions were assessed using FRAP which is usually employed to assess the diffusion and mobility of fluorescently-tagged species (Lippincott-Schwartz, et al. 2001). In the case of inclusions, a small sector of a hyperfluorescent spot is directly bleached and the degree of fluorescence recovery within this area is informative of the mobility of the fluorescent species within the inclusion. The nuclear inclusions of FL19Q were all highly mobile, displaying nearly complete recovery within 100 sec (Fig. 3-3 A, B, Table 3-2). In contrast, FL71Q formed two types of nuclear inclusions with high and low recovery (two representative examples are included in Fig. 3-3 A, B).

Intriguingly, the profile of the high-recovering FL71Q nuclear inclusions showed an initial fast recovery phase followed by a slower, incomplete recovery (Fig. 3-3 B). Mathematical analysis of the FRAP data supported these assertions, as the curve fit to a recovery is consistent with two populations: a mobile fraction which accounted for 69% ± 7% and a less mobile fraction 31 ± 4% within aggregates (Fig. 3-3 B, Table 3-2). This recovery pattern strongly differs from the observation of a single protein population detected in the aggregates of Htt-exon 1 with expanded polyQ stretch (Holmberg, et al. 2004; Kim, et al. 2002). The nuclear, diffusely distributed fractions of both, FL71Q and FL19Q, were highly mobile and displayed immediate recovery comparable to the GFP recovery; the complete recovery was reached within the first postbleach measurement (at 1.5 s) (data not shown).

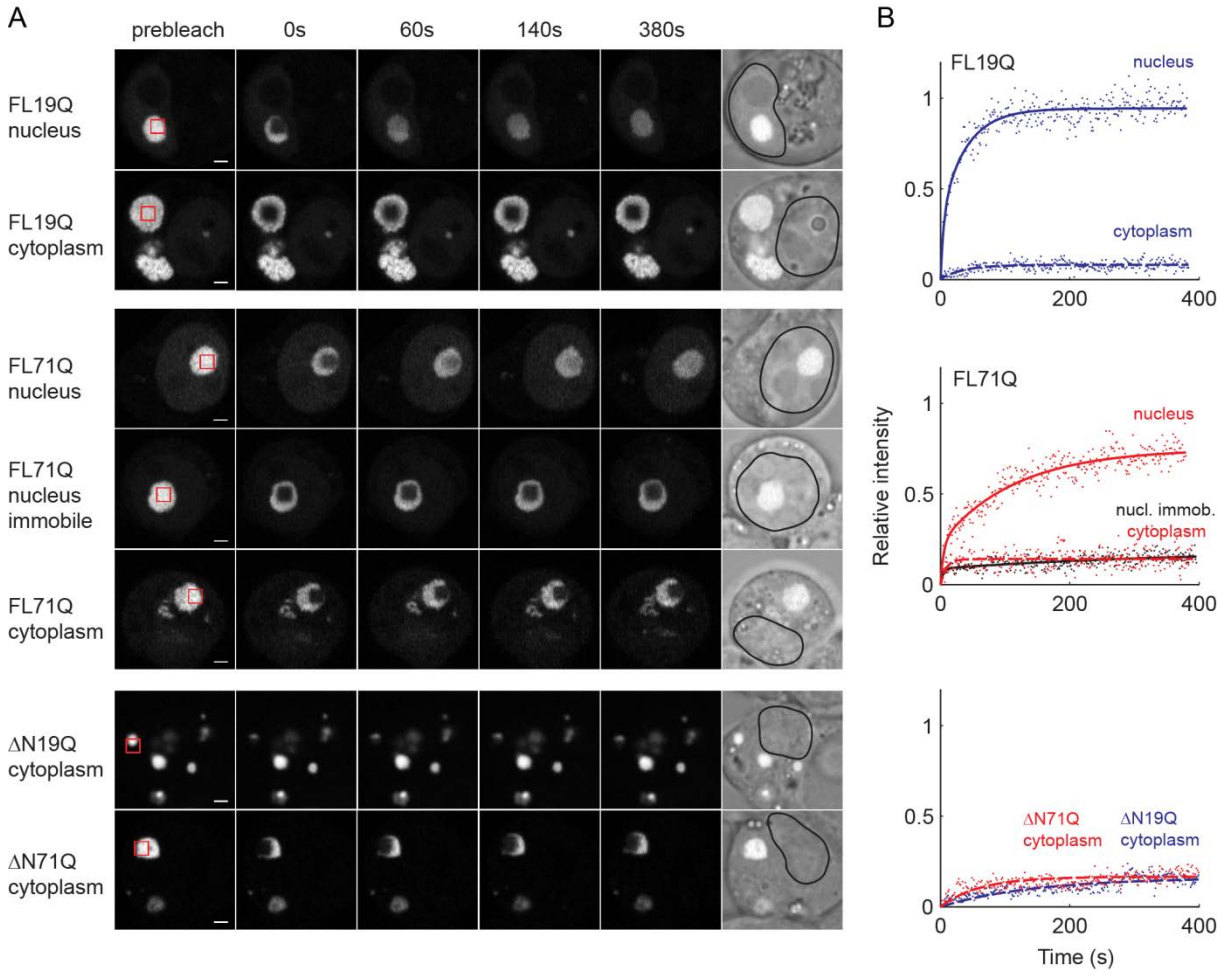

Figure 3-3: Mobility analysis of ATN-1 aggregates. *(A) FRAP analysis of FL-ATN1 and ΔN-ATN1 aggregates. Different ATN1 variants were transiently expressed in N2a/Tet-Off cells for 48 h. The red box on the prebleach image marks the area of bleaching. Scale bar, 2 µm. (B) Quantitative analysis of the FRAP images. Fluorescence intensity in the bleached area of each FRAP image (A) is converted into relative fluorescence intensity. Solid or dashed lines represent a curve-fit to three-parameter single or a five-parameter double exponential function.*

Cytoplasmic aggregates, whether built of the FL-ATN1 or ΔN-ATN1 variants with pathological and non-pathological Q-length, exhibited poor recovery profiles (Fig. 3-3 A, B and Table 3-2) which correspondes to stable aggregate structures with immobile proteins in them.

Table 3-2: Quantitative analysis of the mobility of the ATN-1 variants. *The mobile fraction was calculated from the FRAP measurements and the half-life time from the iFRAP experiments. The standard deviation is a mean value of the analysis in at least 10 cells for FRAP and three to five cells for iFRAP experiments. FL71Q protein forms two distinct aggregate types in the nucleus: high-recovering ([a]) and low-recovering ([b]) species in the FRAP experiments; '−' non-decaying species; n.d., not determined.*

Protein	Localization	Expression time, h	FRAP	iFRAP
			Mobile Fraction, %	Half-life time, min
FL19Q	nucleus	24	87.6 ± 12.2	48 ± 7
		48	78.4 ± 16.3	182 ± 74
	cytoplasm	24	13.5 ± 7.4	−
		48	14.7 ± 9.6	−
FL71Q	nucleus[a]	24	79.6 ± 19.0	110 ± 13
		48	64.9 ± 14.5	206 ± 73
	nucleus[b]	24	30.6 ± 7.7	1440 ± 212
		48	28.1 ± 9.1	2937 ± 860
	cytoplasm	24	13.6 ± 6.8	−
		48	13.8 ± 4.4	−
ΔN19Q	cytoplasm	24	17.6 ± 5.2	−
		48	16.8 ± 4.3	n.d.
ΔN71Q	cytoplasm	24	15.7 ± 5.5	−
		48	11.1 ± 4.4	n.d.

FRAP analyses suggested that two populations with different mobility are present within the nuclear FL71Q inclusions, however this dynamics may represent variations in the ability of the aggregates to exchange with the external mobile protein pool (outside of the inclusion). Thus, a complementary assay was employed, inverted-FRAP (iFRAP), which reports on the exchange of fluorescently-labeled species from aggregates or with the neighboring environment or compartment (Krol, et al. 2008). In brief, in iFRAP the whole cell, leaving the inclusion of interest intact, is completely photobleached. If a mobile species can dissociate from the inclusions, it would be expected that the fluorescence of the inclusions will decrease based on their migration to the near environment. The fluorescence of the nucleoplasmic FL19Q inclusions decreased rapidly, with a half-life time of 48 min at 24 h of expression (Table 3-2), suggesting that the FL19Q monomer is loosely incorporated. Similar to the FRAP results, the nuclear FL71Q inclusions exhibited two different half-life times of decay (Table 3-2): the low-recovering FL71Q assemblies in the FRAP experiments

decayed with an order of magnitude longer half-life time than compared to the high-recovering FL71Q species. Moreover, the fluorescence decay of the high-recovering inclusions can be better fitted to a two-phase exponential decay curve supporting the presence of at least two distinct protein populations within these inclusions. The fluorescence intensity of the cytoplasmic assemblies of all constructs remained constant, implying that the corresponding monomers are stably associated in them (Table 3-2).

3.2 ATN1 with expanded polyQ stretch forms detergent-resistant inclusions which associate with nuclear membranes

Next, to determine if the observed differences in the inclusions dynamics correlate with the composition and structural features of the aggregates, the inclusions were separated into nuclear and cytoplasmic and their detergent-resistance was analyzed. SDS-insoluble FL71Q aggregates, which account for fibrillar species (Kazantsev, et al. 1999), were bulky structures that sedimented at very low velocity (Fig. 3-4). A small SDS-resistant fraction was also found in the nucleus which most likely represents the low-recovering species in the FRAP experiments (Fig. 3-3 A, B).
The lysates of cells expressing FL-ATN1 or ΔN-ATN1 variants were also fractionated by size and density by means of non-continuous sucrose gradient centrifugation (Fig. 3-5 A). ΔN71Q, similarly to FL71Q, built bulky SDS-resistant aggregates which sediment at very low velocity in the pellet fraction (Fig. 3-5 B). No SDS-resistant species were detected in the supernatant obtained in the slow centrifugation step (Fig. 3-5 B), identical to that of nucleo-cytoplasmatic fractionation, where this fraction was shown to comprise detergent-soluble cytoplasmic fraction and a nuclear fraction, containing detergent-resistant species (Fig. 3-4 B). This might be explained by much lower cell numbers used to prepare total lysates for the sucrose density centrifugation (note the description of Fig. 3-4 and Fig. 3-5). The amount of the FL71Q nuclear SDS-insoluble fraction already low in the lysates prepared from the higher cell numbers (Fig. 3-4 B) was non-detectable in the supernatants prepared for the fractionations in sucrose density gradient. Thus the supernatants which generally

comprised the SDS-labile, small-size nuclear and cytoplasmic aggregates (Fig. 3-5 A) were further subjected to sucrose density centrifugation.

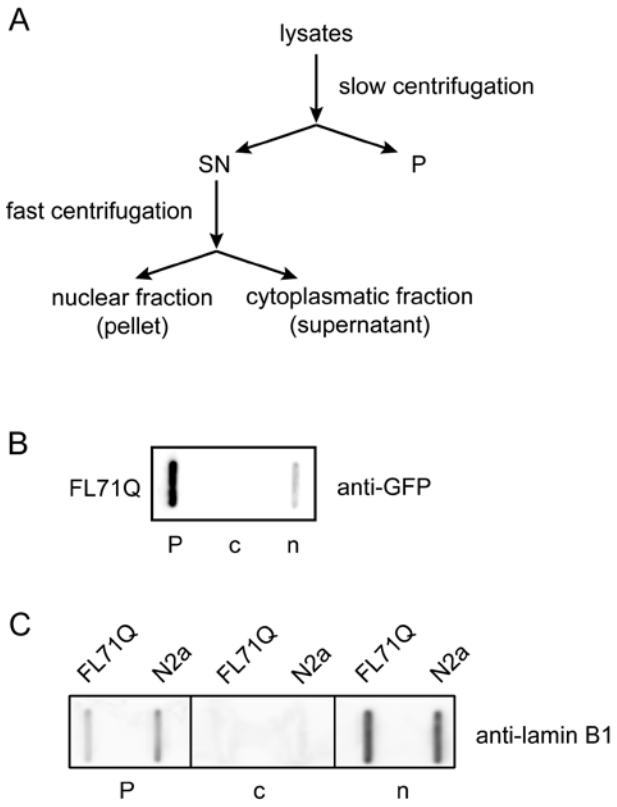

Figure 3-4: Nuclear and cytoplasmic FL71Q aggregates contain detergent-resistant species. *(A) Five million N2a/Tet-Off cells expressing FL71Q for 48 h were fractionated into nucleoplasmic (n) and cytoplasmic (c) fractions. SN, denotes supernatant, P, low-speed sedimenting pellet fraction. (B) Analysis of the FL71Q fractions for detergent resistance using filter-retardation assay. The fractions in panel A were applied to the cellulose acetate membrane, washed with SDS-containing buffer and probed with anti-GFP antibodies. (C) Counterstaining of the fractions with anti-lamin B1 antibodies (note, here the nitrocellulose membrane that retains all proteins was used). Large aggregates co-sediment at low velocity into the P fraction which contains cell debris and a small fraction of intact cells (the latter is responsible for the low positive lamin B1 signal). Mock-transfected N2a/Tet-Off cells (N2a) were used as a control.*

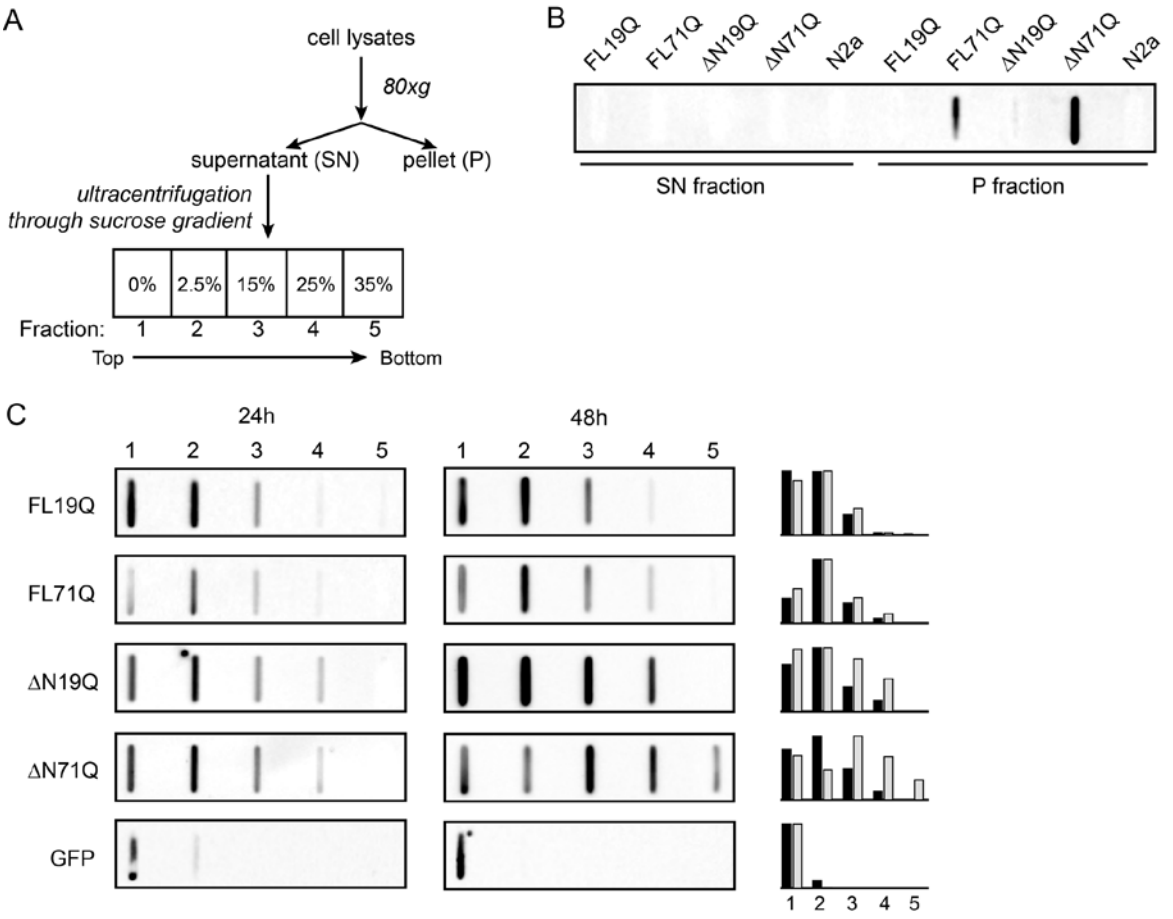

Figure 3-5: The detergent-labile inclusions of the FL-ATN1 and ΔN-ATN1 with expanded polyQ differ in their density. *(A) Schematic of the fractionation procedure of the inclusions. (B) Very large inclusions pellet at low centrifugation speed in the pellet fraction (P). Only FL71Q and ΔN71Q form detergent-resistant species. The supernatant (SN) and P-fractions were obtained after lysis of two million N2a/Tet-Off cells expressing FL-ATN1 and ΔN-ATN1 variants for 48 h. The SDS-insolubility was monitored by filter-retardation assay and probed with anti-GFP antibodies. Mock-transfected N2a/Tet-Off cells (N2a) served as a control. (C) Fractionation of the inclusions in the SN fraction on a non-continuous sucrose gradient. Two million N2a/Tet-Off cells transfected with all FL-ATN1 and ΔN-ATN1 variants were lysed after 24 or 48 h. The fractions were loaded onto nitrocellulose membrane, retaining all proteins, and visualized by immunostaining with anti-GFP antibodies. The intensity of the GFP-ATN1 positive fractions was related to the spot with the highest intensity within each blot and the relative intensity is graphically summarized for 24 h (black) and 48 h (gray) for each construct (at the right side of the immunoblots). The numbers over the blots correspond to the fractions from the sucrose gradient in (A). Cells expressing GFP protein serve as a control of completely soluble protein which is found in the lightest fraction.*

At early time point of expression (24 h), those SDS-labile aggregates showed similar pattern for each pair, FL19Q/FL71Q and ΔN19Q/ΔN71Q (Fig. 3-5 C).

While the density of the non-pathological FL19Q and ΔN19Q did not change at later expression time (48 h), the FL71Q and ΔN71Q aggregates migrated at higher density (fraction 3 and 4 was enriched of FL71Q and fractions 3-5 of ΔN71Q; Fig. 3-5 C). The separation of the aggregates by density centrifugation is determined by their mass, density and shape, i.e. the enrichment of FL71Q and ΔN71Q aggregates in the higher-density fractions would account for species with higher mass, larger density and/or increased compactness. These changes in the global structure of the FL71Q and ΔN71Q aggregates mirrored the decrease in mobility observed in the FRAP analyses (Table 3-2).

Interestingly, the fraction of the bulky, detergent-resistant FL71Q aggregates that sedimented at very slow centrifugation speed was strongly lamin B1-positive (Fig. 3-4 C), even though the majority of those aggregates are localized in the cytoplasm as suggested by the FRAP experiments (Fig. 3-3). As already observed, other proteins with expanded polyQ stretch assemble into perinuclear aggregates which typically associate with the nuclear membrane forming a characteristic distortion of the nuclear surface (Chapple, et al. 2008; Waelter, et al. 2001). Next, the state of the nuclear envelope was analyzed using lamin B1 as a marker for nuclear integrity (Lammerding, et al. 2006) (Fig. 3-6).

Immunostaining analysis revealed that small nuclear FL71Q inclusions were clearly associated with the nuclear envelope and caused discernible discontinuity in the lamin B1 rim. In addition, the cytoplasmic aggregates also associated with the nuclear membrane forming a local depression in the nuclear envelope (Fig. 3-6).

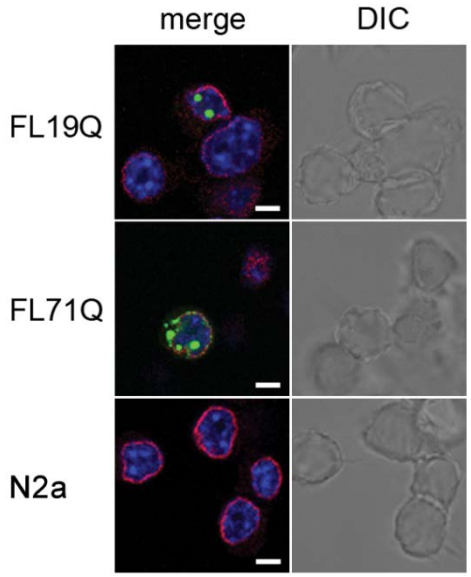

Figure 3-6: Nuclear and cytoplasmic FL71Q inclusions associate with the nuclear envelope but they do not alter lamin B1 distribution. *N2a/Tet-Off cells were transiently transfected with FL19Q or FL71Q and visualized by the GFP fluorescence after 24 h. Nuclei were counterstained with DAPI and the nuclear envelope comprising lamin B1 with anti-lamin B1 antibody and Alexa-568 labeled secondary antibody (red channel). Mock transfected N2a/Tet-Off cells (N2a) served as a control. Scale bar, 5µm.*

3.3 An approach to explore the evolution of the aggregate core in living cells

CRABP-Htt53Q chimera is a protein which represents a summarized model of polyQ proteins. It comprises cellular retinoic acid binding protein 1 (CRABP), a well-folded and stable β-sheet protein fused N-terminally to exon1 of huntingtin (Htt) containing a consecutive polyQ repeat in the pathological range (53Q) (Ignatova and Gierasch 2006). CRABP-Htt53Q has been shown to form *in vitro* and in *E. coli* cells aggregates that, similarly to those of SCA3 and Htt-exon1 (Ellisdon, et al. 2006; Gales, et al. 2005; Poirier, et al. 2002), evolve in time from SDS-labile to SDS-resistant species (Ignatova and Gierasch 2006). The change in the CRABP-Htt53Q solubility coincides with the morphological evolution from small spherical to bulky fibrillar aggregates (Ignatova, et al. 2007) and the fact that only the early spherical aggregates cross-react with the A11 antibody confirms their oligomeric character. A11 is a

conformation-sensitive antibody, raised against the Aβ (1-40) peptide that has been reported to recognize a generic most likely structural epitope present in early aggregate species of many amyloidogenic peptides (Kayed, et al. 2003).

This time-dependent evolution of physico-chemical properties of the CRABP-Htt53Q aggregates have been suggested to result from changes in the composition of the aggregate core (Ignatova, et al. 2007).

A limited trypsinolysis is an approach allowing identification of the protein/peptide segments that are not protected in the amyloidogenic core (Kheterpal, et al. 2001; Myers, et al. 2006; von Bergen, et al. 2006). However this approach is based on aggregate isolation from the cells and the *in vitro* trypsinization. The isolation procedure may alter the structure of the transient intermediates. Although the end-stage fibrillar aggregates are stable easily detectable structures, (Groenning, et al. 2007; Nilsson 2004; Scherzinger, et al. 1997) the structural characterization of the early prefibrillar aggregate species is technically difficult due to their transient character. Therefore we sought to develop an approach to map directly in the cell structural changes in the aggregates. We designed an orthogonal cross-seeding assay that can be applied to identify sequences or domains involved in the core of aggregates directly in living cells. A characteristic feature of the nucleated polymerization growth mechanism of amyloid formation is that preformed aggregates or seeds of the same protein can bypass the initiating energetically unfavorable nucleation event (Chen, et al. 2001; Harper and Lansbury 1997). This feature is the conceptual core of the orthogonal cross-seeding assay, which is based on the highly discriminating ability of these seeds to recruit new monomers with equivalent sequences (Chien and Weissman 2001; Krebs, et al. 2004; O'Nuallain, et al. 2004) and the degree of sequence identity determines the efficiency of the seeding process (Krebs, et al. 2004). To experimentally probe the nature of the aggregates of an amyloidogenic protein, the model expression host is co-transformed with multiple plasmids, one encoding the full-length amyloidogenic protein and others encoding fragments comprising different parts of the full-length protein (Fig. 3-7). Provided there is tight control of the promoters, the synthesis of the fragments can be turned on and off in a tightly controlled, time-dependent manner. Recruitment of any of the fragments into the aggregates of the full-length parental protein will suggest that a

portion of the full-length protein sequentially equivalent to the fragments comprises the aggregate core.

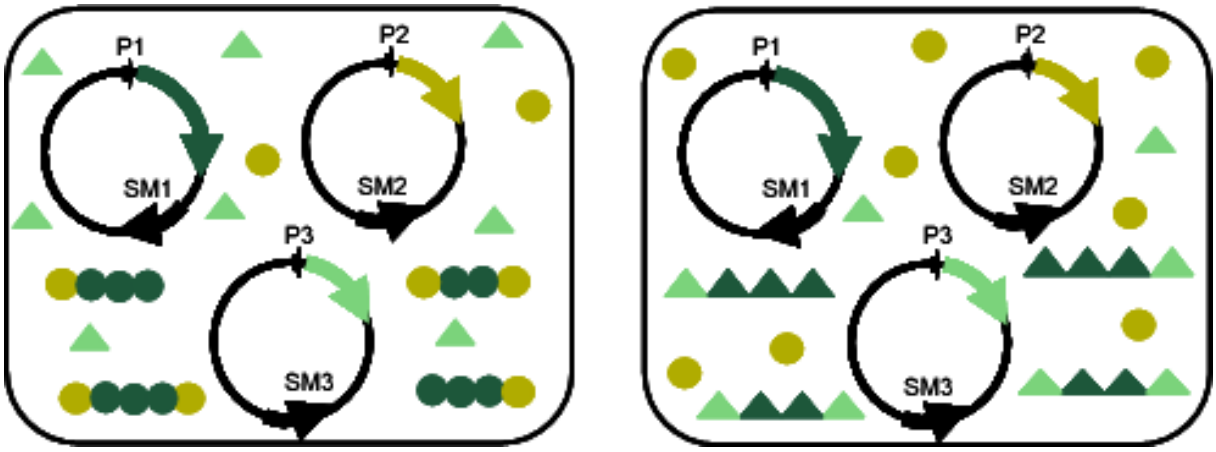

Figure 3-7: Principle of the in vivo cross-seeding approach. *The full-length aggregating protein (dark green) and segments of it (light green or dark yellow) are co-expressed on different plasmids under different promoters (marked P1, P2, and P3). The plasmids also bear various selection markers (marked SM1, SM2, and SM3). Only soluble fragments which sufficiently resemble the core structure of the aggregates can be recruited to the various aggregates.*

3.3.1 The aggregate core of CRABP-Htt53Q evolves structurally in the time course of aggregation

To test the applicability of the cross-seeding assay for probing the sequences and/or domains forming the aggregation core directly in the cellular environment, we first monitored the evolution of the aggregates of the CRABP-Htt53Q. Although *E.coli* is not a natural cellular environment for the polyQ pathologies it has been shown to support the formation of the cellular aggregates structurally homologous to those formed in eukaryotic cells (Carrio, et al. 2005; Gonzalez-Montalban, et al. 2007). Hence, given also its easy manipulability, *E.coli* was chosen as a first system to test the applicability of the cross-seeding approach.

The full-length CRABP-Htt53Q protein was co-transformed and co-expressed in *E. coli* with either an N-terminally *HA*-tagged Htt-exon 1 with 20Q (Htt20Q) or with a C-terminally *myc*-tagged point mutant of CRABP, consisting each of the domains of the chimera (Fig. 3-8).

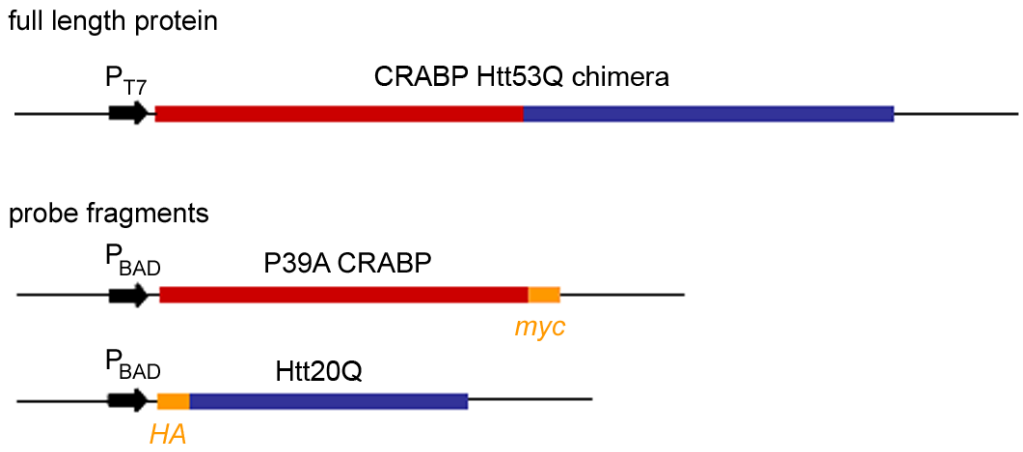

Figure 3-8: Schematic representation of the CRABP-Htt53Q constructs used for the cross-seeding experiments. *The expression of the amyloidogenic CRABP-Htt53Q chimera was controlled under* the *T7 IPTG-inducible promoter. The two orthogonally expressed probe fragments P39A CRABP (red) and Htt-exon 1 with 20Q (blue) with a detection tag at either their N- or C-terminus represent the two domains of the full-length chimera; their expression is under the control of the arabinose-inducible P_{BAD} promoter. Both constructs with the CRABP domain contained a tetra-Cys motif for FlAsH binding, which was used as a read-out to follow the time-course of expression and aggregation (Ignatova and Gierasch 2004; Ignatova and Gierasch 2006); insertion of this motif does not alter properties of the CRABP (Ignatova and Gierasch 2005).*

The expression of CRABP-Htt53Q chimera under the control of the *T7* promoter was induced by adding isopropyl-β-thiogalactopyranoside (IPTG) for various periods of time and was terminated by depletion of the IPTG-inducer by changing to fresh medium. Subsequent to turning-off the expression of the full-length chimera, the expression of probe fragments controlled by the P_{BAD} promoter were pulse-induced with arabinose and their incorporation in the intact CRABP-Htt53Q aggregates was

detected using the immunoreactivity of the corresponding tag after isolation of the intact aggregates from *E.coli* cells (Fig. 3-8, Fig. 3-11).

A prerequisite for the orthogonal cross-seeding approach is that the co-expressed fragments remain soluble over the entire cycle of expression, hence ensuring that the monomeric peptides are recruited to the aggregates of full-length protein based on the primary sequence equivalence. In contrast to the pathological variant with 53Q, the Htt-exon 1 with non-expanded polyQ stretch is not aggregation-prone (Ignatova and Gierasch 2006) and Htt-exon1 with 20Q (Htt20Q) remained soluble during the entire cycle of expression (data not shown). Therefore, its detection in the CRABP-Htt53Q aggregates would reflect the intrinsic ability of CRABP-Htt53Q aggregates to recruit polyQ species. P39A tetra-Cys CRABP1 protein is aggregation-prone and partitions between the soluble and insoluble fraction at later time points of expression, however it remains soluble in the first 60 minutes (Ignatova and Gierasch 2004) thus covering the time-frame of its expression during the cross-seeding experiments.

Another requirement that must be fulfilled to make the orthogonal cross-seeding method valid is the tight control and sufficiently high level of expression of the full-length protein and its fragments. Tightness of the regulation of *T7 and* P_{BAD} promoters was tested prior to the cross-seeding experiments using the activity of firefly luciferase as a read-out. Adding to the medium IPTG allowed an efficient induction of the luciferase expression under the control of the *T7* promoter (Fig. 3-9 A). Subsequent withdrawal of the IPTG by re-suspending the cells in the fresh medium without the IPTG led to almost complete repression of the *T7* promoter. In the non-induced sample, almost no luciferase was detectable confirming the tightness of the expression control by the *T7* promoter (Fig. 3-9 A).

The expression of CRABP-Htt53Q after labeling the cells with FlAsH-reagent was measured with the FlAsH-fluorescence as a read-out. The intensity of FlAsH fluorescence reports on both expression and aggregation and misfolded and aggregate species are hyperfluorescent compared to the native state (Ignatova and Gierasch 2006). Depleting the IPTG from the medium at different times of induction efficiently arrested the expression of full-length CRABP-Htt53Q protein under the control of *T7* promoter (Fig. 3-9 B).

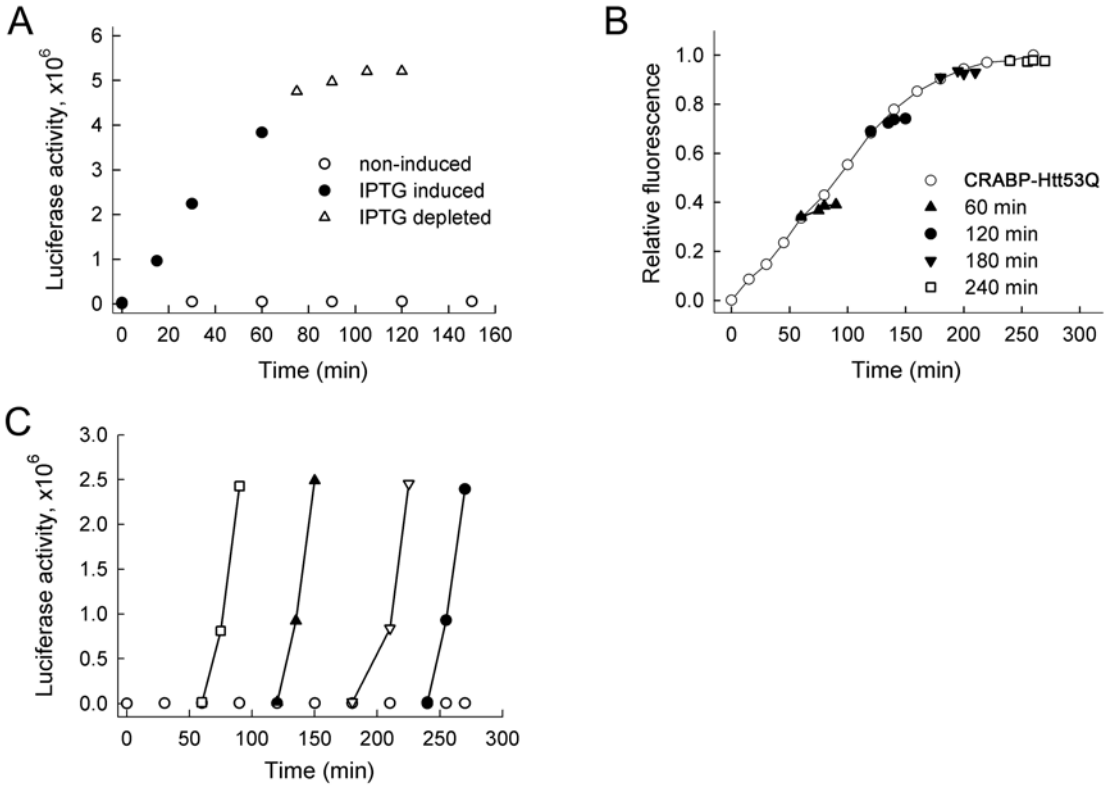

Figure 3-9: Tightness of the regulation of the T7 and arabinose-inducible P_{BAD} promoters. *(A) Luciferase expressed under the control of the T7 promoter was induced by adding IPTG to the medium to 0.4 mM and incubating for 60 minutes (IPTG-induced). Then, its expression was turned off by re-suspending cells in fresh, IPTG-depleted LB-medium (IPTG-depleted). In the non-induced sample, almost no luciferase was detectable (open circles). (B) The expression of CRABP-Htt53Q (induced by adding 0.4 mM IPTG at OD_{600} =0.8) under the T7 IPTG-inducible promoter was almost completely stopped after depletion of the IPTG from the medium. The time-course of expression was monitored using the FlAsH-fluorescence as a read-out (depicted as CRABP-Htt53Q). At different times after induction, the expression of the CRABP-Htt53Q was turned off by re-suspending the cells in an IPTG-depleted LB-medium (filled symbols and opened squares). (C) The P_{BAD} promoter ensures an equal amount of active luciferase independent of the time point of induction. Firefly luciferase was induced for 30 minutes at various time points by adding arabinose (to 0.2%): 60 min (open squares), 120 min (closed triangles), 180 min (open inverted triangles) and 240 min (closed circles). The times of induction represent various times after the culture has reached OD_{600} =0.8, and correspond to the times at which the fragment expression was induced in the co-expression experiments (see Fig. 3-11). In the non-induced sample no luciferase activity was measured (open circles).*

P_{BAD} promoter ensured an equally strong level of pulse-expression regardless of the time-point of induction as measured by the activity of the firefly luciferase (Fig. 3-9 C). The lack of the luciferase activity in the control cells that were not induced with arabinose confirmed that also the P_{BAD} promoter allows a tight control of expression (Fig. 3-9 C).

To test the strength of the pulse-expression under the control of *T7 and* P_{BAD} promoters the expression of the CRABP-Htt53Q was induced for different times by IPTG and the expressions of *myc*-tagged P39A CRABP and *HA*-tagged Htt20Q were induced for 30 minutes by adding 0.2% arabinose (Fig. 3-10). Following that, the equal amounts of *E. coli* cells were lysed and analyzed using SDS-PAGE. Since the longer times of CRABP-Htt53Q expression (180 and 240 minutes) result in the formation of SDS-insoluble aggregates (Ignatova, et al. 2007) the samples were treated with formic acid to ensure the solubilization and allow the quantitative estimation of expression of the chimera (Fig. 3-10). It is important to note that *HA*-tagged Htt20Q expressed alone (i.e., not as a part of a larger fusion protein) has a reduced electrophoretic mobility and consequently low molecular weight correlation, as noted for Htt-exon1 and other polyQ proteins (Kegel, et al. 2010; Miyashita, et al. 1998; Miyashita, et al. 1997; Preisinger, et al. 1999).

Both *T7 and* P_{BAD} promoters were shown to ensure a high level of the pulse-expression and the P_{BAD} promoter allowed a rapid increase of the concentration of either of the probe fragments within the test time of 30 minutes (Fig. 3-9 and 3-10).

The cross-seeding experiments showed that from the earliest time points tested, CRABP-Htt53Q aggregates efficiently recruited the P39A CRABP species (anti-*myc* positive), with the highest activity at the earliest time-point (60 min.) (Fig. 3-11 A). In contrast, the early aggregates showed almost no ability to stimulate polyQ-mediated elongation as evidenced by the lack of recruitment of the Htt20Q (anti-*HA* positive species) (Fig. 3-11 B).

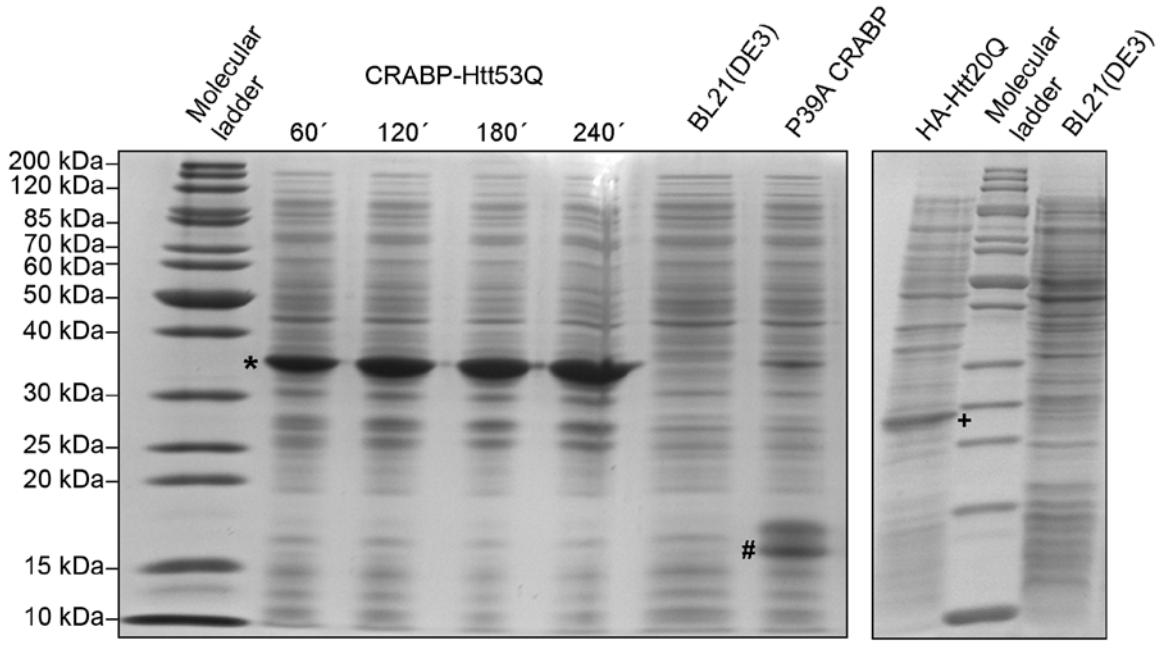

Figure 3-10: Expression profile of CRABP-Htt53Q protein constructs. *Expression of CRABP-Htt53Q chimera in E.coli BL21 (DE3) was induced by adding IPTG to 0.4 mM at OD_{600}=0.8 and incubating for different times at 37°C. P39A CRABP-myc and HA-tagged Htt-exon 1 with 20Q were induced for 30 minutes by adding 0.2% arabinose. The CRABP-Htt53Q band is marked with *, P39A CRABP with #, and Htt20Q with +. Equal amounts of cells were loaded in each lane on the 15% SDS-PAGE. Non-transformed E. coli BL21 (DE3) cells served as a negative control.*

At the later time point (240 min) CRABP-Htt53Q aggregates, for which a fibrillar phenotype have been detected (Ignatova, et al. 2007), showed the opposite trend. They significantly enhanced the deposition of the polyQ-containing fragments (*HA*-positive) and were not able to recruit the *myc*-tagged CRABP mutant (Fig. 3-11 A, B). This result strongly suggests that different regions of the full-length CRABP-Htt53Q chimera are transiently forming the aggregate core at different stages in the aggregation process: CRABP domain was participating in the aggregate core at the early time points whereas the polyQ segments formed the core at later time points. The evolution to polyQ-based aggregate core correlated with the changes in the detergent-solubility of the aggregates.

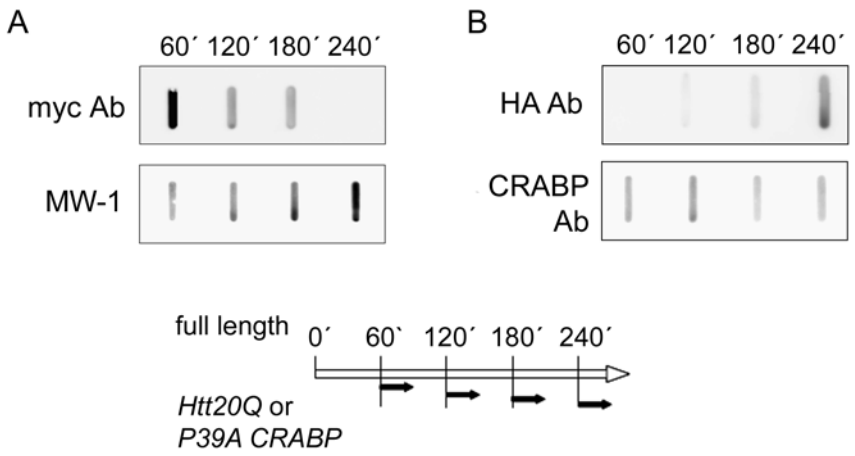

Figure 3-11: The seeding ability of aggregates of the CRABP-Htt53 chimera evolves over time in the cellular environment. *E. coli BL21 (DE3) cells were co-transformed with CRABP-Htt53 and either P39A CRABP (A) or Htt20Q (B). At different times after induction (as indicated in the expression schemes), the expression of the CRABP-Htt53 chimera was turned off, and probe fragments were pulse-expressed for 30 min. The recruitment of either P39A CRABP or Htt20Q into the aggregates of CRABP-Htt53 chimera was detected by immunoreactivity using* myc *or HA-antibodies, respectively. The nitrocellulose membrane retained both soluble (oligomeric) species and insoluble aggregates. The same blots were also stripped and re-probed with CRABP antibody or the polyQ specific antibody MW-1 to validate that the aggregates arose from the CRABP-Htt53 chimera. Although equal amounts of the aggregates of CRABP-Htt53 (3 µM) isolated at different times were loaded onto the membrane, their immunoreactivity towards the CRABP and MW-1 antibodies varies. A lower MW-1 reactivity of the early species and lower anti-CRABP reactivity for aggregates isolated at later time was consistently observed, probably because of variations in the exposure of both epitopes (Ignatova, et al. 2007) and unpublished results). It should be noted that MW-1 binds preferably to elongated polyQ stretches and does not recognize short polyQ segments.*

Control experiments indicated that there were no non-specific cross-seeding activities of both fragments (i.e., P39A CRABP monomers recruited into aggregates with polyQ-dominated aggregate cores, or vice versa) (Fig. 3-12). Seeds from P39A CRABP or Htt 53Q were prepared *in vitro* and used in cross-seeding reactions *in vitro*. P39A CRABP aggregates failed to shorten the lag time of aggregating Htt53Q protein, and vice versa the preformed Htt53Q aggregates did not seed P39A CRABP

aggregation (Fig. 3-12). This strongly supports the notion that sequence equivalence to the aggregate core is required for the probe fragment to elongate any of the aggregate species.

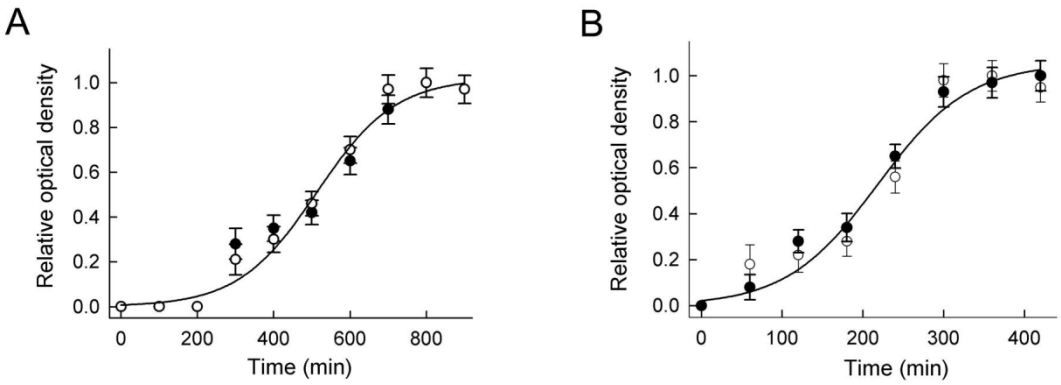

Figure 3-12: In vitro cross-seeding activities of P39A CRABP and Htt53Q. *P39A CRABP and Htt53Q do not seed each other's aggregation in vitro. To prepare the aggregation seeds P39A CRABP and Htt53Q were expressed in E. coli BL21 (DE3) cells and purified. (A) In vitro aggregation of 10 µM purified P39A CRABP alone (open symbols) at 37°C or seeded with 5% (w/w) of in vitro grown pre-formed aggregates of Htt53Q (filled symbols). (B) Aggregation kinetics of 3 µM Htt53Q at 37 °C alone (open symbols) or seeded with 5% (w/w) of pre-formed aggregates of P39A CRABP (filled symbols)* in vitro*. The aggregation was analyzed by filter-retardation assay using an acetate cellulose membrane, retaining only SDS-resistant fibrillar aggregates. P39A CRABP species were probed with CRABP antibody (1:1000) and Htt53Q with polyQ specific antibody MW-1 (1:1000). The intensity of the slots was quantified using AIDA software.*

3.3.2 Specificity of the cross-seeding approach

Next, we explored the specificity of the orthogonal cross-seeding approach using a sequence-unrelated amyloidogenic protein, β_2-microglobulin (β_2m), which is amyloidogenic and forms fibrils in patients suffering from hemodialysis-related amyloidosis (Gejyo, et al. 1986). Similarly to CRABP-Htt53Q chimera, β_2m construct (Kad, et al. 2001) was expressed under the control of the *T7* promoter. At different

times the β_2m expression was turned off and the probe fragments (Htt20Q or P39A CRABP) were pulse-expressed for 30 min. Neither fragment was recruited into the β_2m aggregates, further arguing that sequence similarity is a prerequisite for recruitment into aggregates (Fig. 3-13).

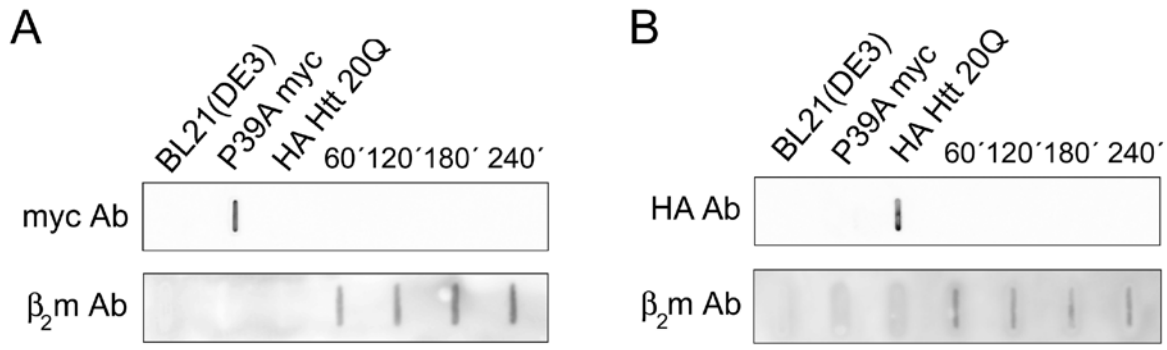

Figure 3-13: Specificity of the cross-seeding approach. *Aggregates of β_2m protein do not recruit soluble P39A CRABP or* Htt20Q. *E. coli BL21 (DE3) cells were co-transformed with β_2m and either P39A CRABP (A) or Htt20Q (B), and the same expression pattern of the constructs as in Fig. 3-11 was used. The slot blots with the intact aggregates were probed with myc and HA-antibodies and reprobed after stripping with β_2m antibody. Cells expressing only P39A CRABP (depicted as P39A myc) or HA-Htt20Q were induced for 30 min by the addition of 0.2% arabinose, and total lysates were loaded as positive controls. Lysates of nontransformed E. coli BL21 (DE3) cells (marked BL21 (DE3)) served as a negative control.*

Promiscuous cross-seeding would suggest substantial heterogeneity of the aggregate core within a single fibril. More broadly, such a result could account for how one amyloidogenic disease might influence or even promote another. The protein deposits, however, are typically dominated by a single primary amyloidogenic protein, which is consistent with the idea that the forces driving amyloid formation are highly discriminating (Chien and Weissman 2001; Krebs, et al. 2004; O'Nuallain, et al. 2004).

3.4 Expansion of the polyQ stretch changes the aggregate core of ATN1

The orthogonal cross-seeding assay proved to be a highly suitable approach to specifically map the sequences from the aggregating protein that form the aggregate core. Thus, in order to address the question whether the observed evolution in the detergent-resistance of FL71Q and ∆N71Q inclusions (Fig. 3-2) is determined by changes in the structure of the aggregate core we applied the orthogonal cross-seeding assay directly in live N2a cells. For this reason we co-expressed FL19Q and FL71Q proteins or their N-terminal truncations (∆N19Q and ∆N71Q) with various fragments of them which were N-terminally tagged with the fluorescent protein DsRed (Fig. 3-14). The full-length and ΔN-ATN1 variants were expressed for different times to allow formation of SDS-soluble or SDS-resistant aggregate species. Together with or subsequently to their pulse-expression the fragments were pulse-expressed in a tightly controlled manner and their incorporation in the inclusions was monitored by confocal imaging microscopy (Fig. 3-17 to Fig. 3-22). Similarly to the observation in bacterial system, we expected that FL19Q or FL71Q aggregates would recruit only the fragment bearing the sequence that resembles the sequence of the parental protein that participates in the aggregate core. The co-expression of the full-length proteins and their fragments was tightly controlled by two mammalian expression systems. The expression of the full-length ATN1 variants was controlled by *pTRE* promoter in a doxycycline-responsive Tet-Off system (Clontech), modified in frame of this project, whereas ATN1 fragments were expressed in a modified (Matsumoto, et al. 2006) IPTG-dependent LacSwitch I system (Stratagene) (details in the description of Fig. 3-14).

To enable the co-expression of full-length proteins and fragments of the ATN1 a stably-tranfected N2a/Tet-Off/LacI cell line containing stably integrated genes expressing *tTA* expression transactivator (Tet-Off system) and *LacI* (Lac repressor from LacSwitch I system) was created. To achieve this N2a/Tet-Off cell line was stably transfected with a pCMV-LacI-NLS plasmid encoding the Lac repressor (detailed description in 2.2.4.1 and in the Appendix).

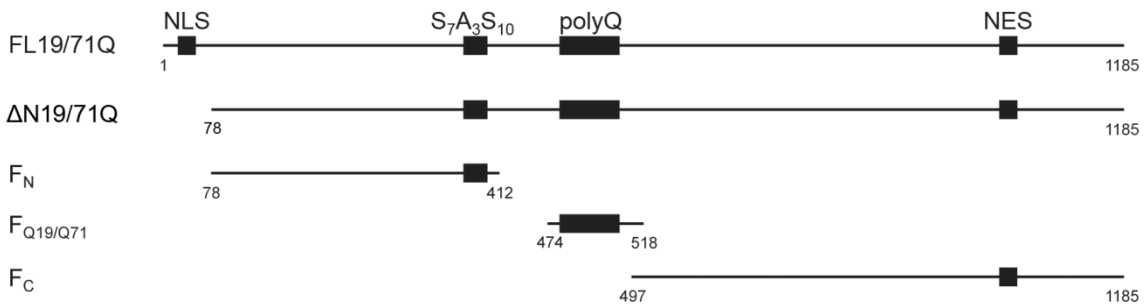

Figure 3-14: Schematic representation of the constructs used in ATN1 cross-seeding experiments. *The expression of FL19Q, FL71Q, ΔN19Q and ΔN71Q constructs N-terminally tagged with GFP was controlled by doxycycline responsive Tet-Off expression system (Clontech). Doxycycline inhibits here the expression of a transcriptional activator protein (tTA) thus blocking the expression of the gene of interest under the control of the pTRE promoter. F_N, F_C, F_{Q19} and F_{Q71} fragments, N-terminally tagged with DsRed protein were expressed using modified LacSwitch I IPTG-inducible mammalian expression system that utilizes modified lac operon from E.coli (Stratagene). The numbering is according to the amino acid sequence of FL19Q. NLS, nuclear localization signal, NES, nuclear export signal.*

A prerequisite for this approach is that co-expressed fragments remain soluble over the cross-seeding cycle while having a sufficiently strong, tightly controlled pulse-expression. Therefore to test this full-length ATN1 variants or fragments were expressed in N2a/Tet-Off/LacI cells alone and the protein synthesis and aggregation were analyzed by confocal imaging microscopy and filter-retardation assay (Fig. 3-15, Fig. 3-16). To determine the concentration of doxycycline that can efficiently turn off the expression under control of the p*TRE* promoter, doxycycline at different concentrations was added to the growth medium simultaneously with transfecting FL19Q and FL71Q into N2a/Tet-Off/LacI cells (Fig. 3-15 A). All tested concentrations of doxycycline tightly inhibited *pTRE*-promoter-dependent protein synthesis (Fig. 3-15 A) and the concentration 300 ng/ml was chosen to be used in the following cross-seeding experiments. To analyze the composition of aggregate core of the SDS-resistant aggregates, the FL-ATN1 protein should be expressed for at least 36h. The pulse-expression of the fragments itself is also a time-consuming procedure and we tested whether the amount of aggregates would change during this time. The filter-

retardation assay demonstrated that the FL71Q aggregates persisted over the time of expression of the fragments (Fig. 3-15 B).

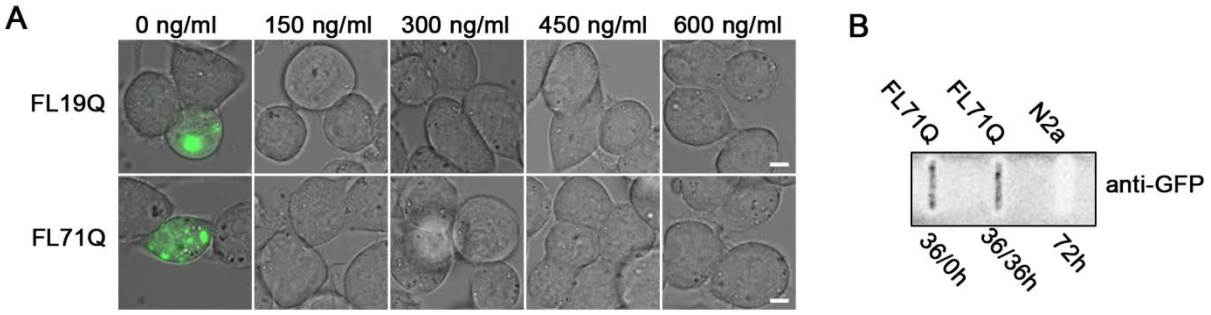

Figure 3-15: Controls of the in vivo cross-seeding experiments. *(A) Addition of doxycycline tightly inhibited the pTRE-promoter-controlled protein synthesis. FL19Q and FL71Q were transfected into N2a/Tet-Off/LacI cells and the de novo protein synthesis was inhibited by addition of different concentrations of doxycycline (denoted over the images). Cells were analyzed after 36 h using a confocal microscope. Merged images of the cells imaged with 488-nm laser wavelength for GFP and differential interference-contrast microscopy. Scale bar 5 µm. (B) Filter-retardation assay of N2a/Tet-Off/LacI cells expressing FL71Q for 36 h compared to the mock-transfected N2a/Tet-Off/LacI cells (N2a). The times 36/0h and 36/36h denote the expression time of FL71Q (36 h) followed by the time of analysis (0 and 36h) after the inhibition of the FL71Q expression with 300 ng/ml doxycycline. The unchanged intensity of the signal indicates that the amount of the SDS-resistant FL71Q aggregates did not change with the time of expression of the fragments in Fig. 3-17 to 3-22.*

During the cross-seeding experiments the F_N, F_C, F_{Q19} and F_{Q71} fragments were supposed to be expressed for 24h. Their solubility over the duration of the cross-seeding cycle was tested by monitoring their expression in live N2a/Tet-Off/LacI cells over 48 h using confocal imaging microscopy. F_N, F_C and F_{Q19} fragments retained the solubility after 48h. At this time F_{Q71} fragment formed well discernible aggregates, however it remained soluble up to 36h post-transfection. Thus even the F_{Q71} fragment is soluble within the time-frame of the cross-seeding experiments (Fig. 3-16). It should be noted that the fragments, albeit lacking any NLS, were equally

distributed between the nucleoplasm and cytoplasm (Fig. 3-16), probably due to a free diffusion as observed for small peptides and proteins (Allen, et al. 2000; Weis 2003). This uniform distribution of the fragments over the cell volume allowed for examination of the recruiting properties of both nuclear and cytoplasmic inclusions.

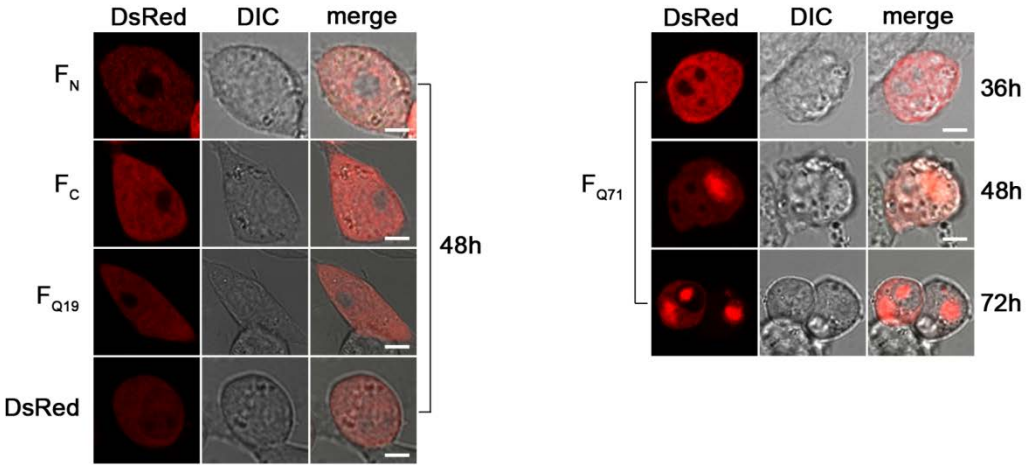

Figure 3-16: Control of the in vivo cross-seeding experiments. *ATN1 fragments remained soluble during the cross-seeding cycle. F_N, F_C, F_{Q19} and F_{Q71} fragments (Fig. 3-14) were transfected in N2a/Tet-Off/LacI cells and their expression was induced by adding 15 mM IPTG. The expression time is indicated at the right of each image series. Cells were visualized using a confocal microscope with 561-nm laser wavelength for DsRed and differential interference-contrast microscopy (DIC). The fragment F_{Q71} formed aggregates in a time-dependent manner (right panel), whereas all other fragments showed a diffuse staining accounting for a soluble expression (left panel). Therefore the expression of the ATN1 fragments in the cross-seeding experiment was limited to 24 h, at which all fragments were present in a soluble state. It should be noted that all fragments co-localized in the nucleus and cytosol albeit the lack of a NLS sequence. Scale bar, 5.5 µm.*

Orthogonal cross-seeding *in vivo* revealed polymorphic interactions of nuclear FL19Q and FL71Q inclusions with the ATN1 fragments (Fig. 3-17 - Fig.3-18). The N- and C-terminal sequences flanking the polyQ region (F_N and F_C), but not the polyQ-containing fragments, co-localized with the nuclear FL71Q aggregates formed at early expression time (Fig. 3-17 A).

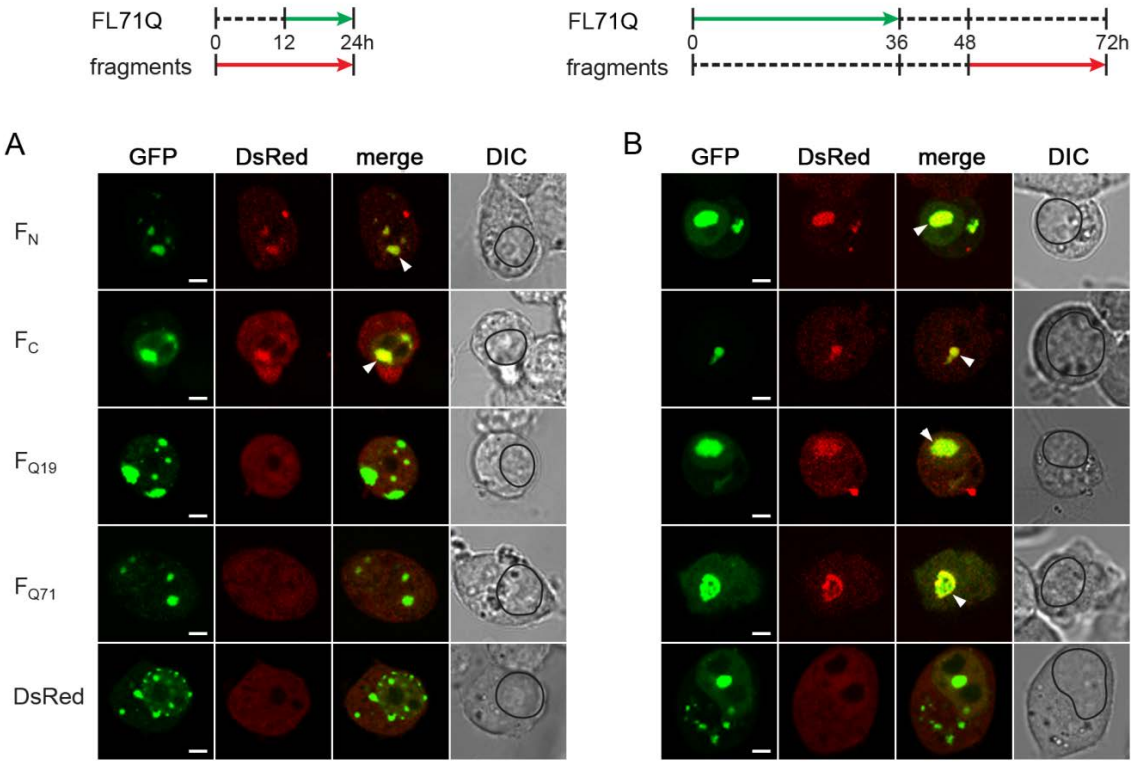

Figure 3-17: Orthogonal cross-seeding in vivo of nuclear FL71Q inclusions with the ATN1 fragments. *The upper panel depicts the co-expression schemes of the fragments and FL-ATN1, representative for the image series below. Nuclear FL71Q aggregates recruited F_N and F_C fragments at early expression times (A) and additionally F_{Q19} and F_{Q71} at later expression times (B). N2a/Tet-Off/LacI cells were co-transfected with GFP-tagged FL71Q and a DsRed-tagged fragment thereof (marked on the left of each image row). The degree of co-localization is illustrated by merging the GFP and DsRed images. The persistence of fluorescence in a red emission channel after extinguishing 488nm laser for GFP excitation excluded the possibility that observed co-localization was a result of an overlap between GFP and DsRed emission spectra. The recruited fragments in the FL-ATN1 inclusions are marked with an arrow on the merged images. The boundaries of the nuclei are designated with a black line on the DIC images. DIC denotes differential interference-contrast microscopy. A hyperfluorescent spot on the F_{Q19} (Fig 3-17 B) image (on the DsRed image) of unclear origin most likely is a debrie from neighboring cell as it is localized at the edge of the cells. Scale bar, 4 µm. The images originate from the diploma thesis of S. Zakrzewski, supervised by the author of this dissertation.*

This implies that at early time point FL71Q associates into inclusions through interactions of the N- and C-terminal regions. At later time-point, nuclear FL71Q

aggregates also recruited both Q-rich fragments (F_{Q19} and F_{Q71}) suggesting a change in the aggregate core to polyQ-containing one (Fig. 3-17 B). The late time-point nuclear and cytoplasmic FL71Q aggregates partitioned between the detergent-resistant and detergent-labile fractions (Fig. 3-5 and Fig. 3-4), suggesting that the ability to recruit polyQ-fragments followed the appearance of the SDS-insolubility.

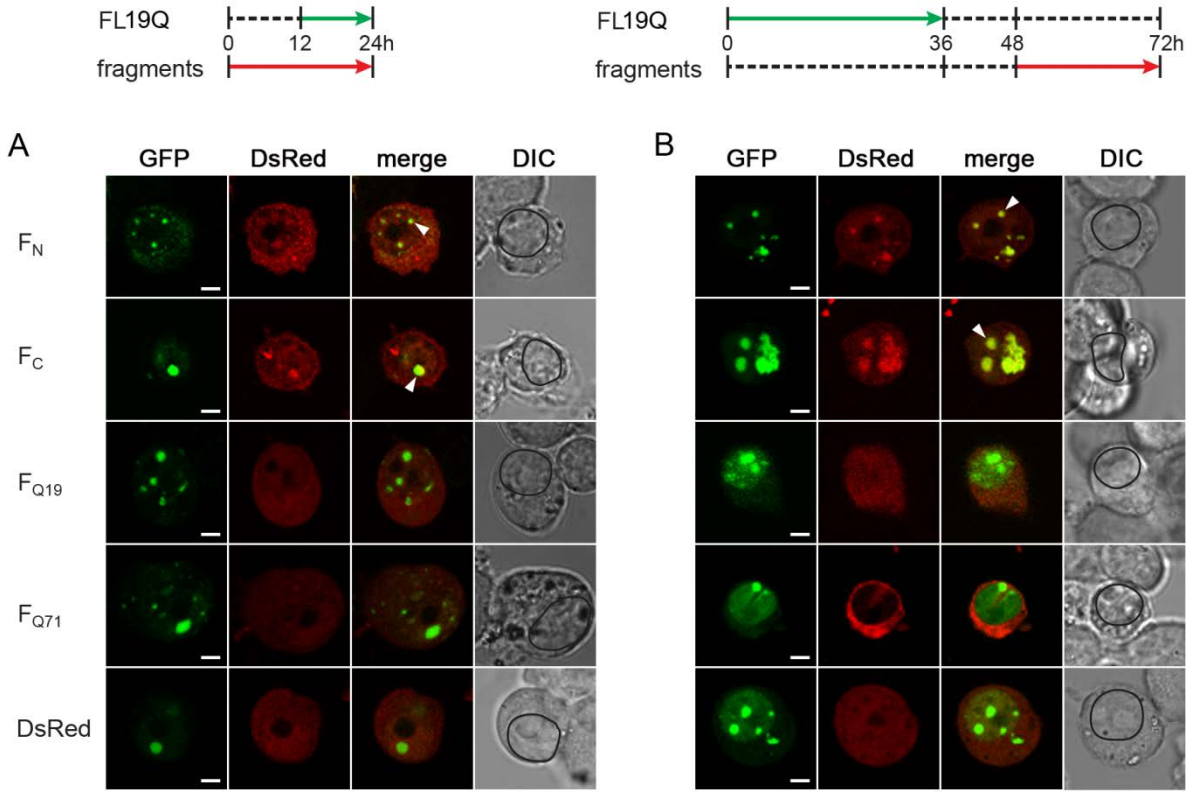

Figure 3-18: Orthogonal cross-seeding in vivo of nuclear FL19Q inclusions with the ATN1 fragments. *Expression schemes for the co-expression of the fragments and FL19Q in the upper panel are representative for the image series below them (A,B). Nuclear FL19Q aggregates recruited F_N and F_C fragments at early (A) and later expression times, but not F_{Q19} and F_{Q71} fragments (B). The recruited fragments in the FL-ATN1 inclusions are marked with an arrow on the merged images. DIC denotes differential interference contrast. The hyperfluorescent spots on the F_C (Fig 3-18 B) images (on the DsRed images) of unclear origin are; most likely, the debris from neighboring cells. Scale bar, 4 µm. For the details see the description of Fig. 3-17. These images originate from the diploma thesis of S. Zakrzewski, supervised by the author of this dissertation.*

The cytoplasmic FL71Q aggregates mirrored the recruiting ability of the nuclear inclusions. F_N and F_C fragments co-localized with the cytoplasmic FL71Q aggregates at early time points (Fig. 3-19 A). At late time of expression, the cytoplasmic FL71Q inclusions represent a mixed population of aggregates with different core structures as they recruited all type of fragments (Fig. 3-19 B).

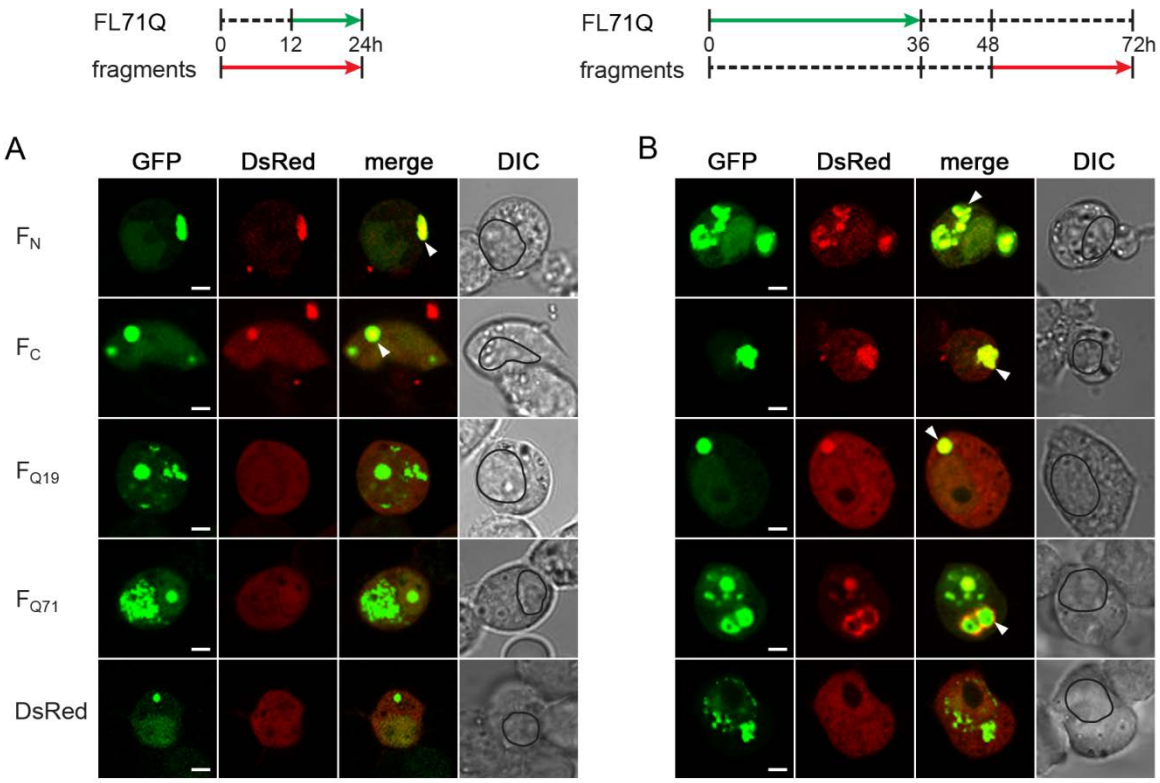

Figure 3-19: Orthogonal cross-seeding in vivo of the cytoplasmic FL71Q inclusions with the ATN1 fragments. *(A, B) Cytoplasmic FL71Q aggregates recruited F_N and F_C fragments at early expression times (A) and additionally F_{Q19} and F_{Q71} at later expression times (B). The schemes for the co-expression of the fragments and FL-ATN1 included in the upper panel are representative for the image series below them. The recruited fragments in the FL71Q inclusions are marked with an arrow on the merged images. DIC denotes differential interference contrast microscopy. Scale bar represents 4 µm. Details are included in the legend of Fig. 3-17. The images originate from the diploma thesis of S. Zakrzewski, supervised by the author of this dissertation.*

The nuclear and cytoplasmic inclusions of the non-pathological variant FL19Q did not evolve over the expression time and were able to recruit only the F_N and F_C fragments (Fig. 3-18 A, B and Fig. 3-20 A, B).

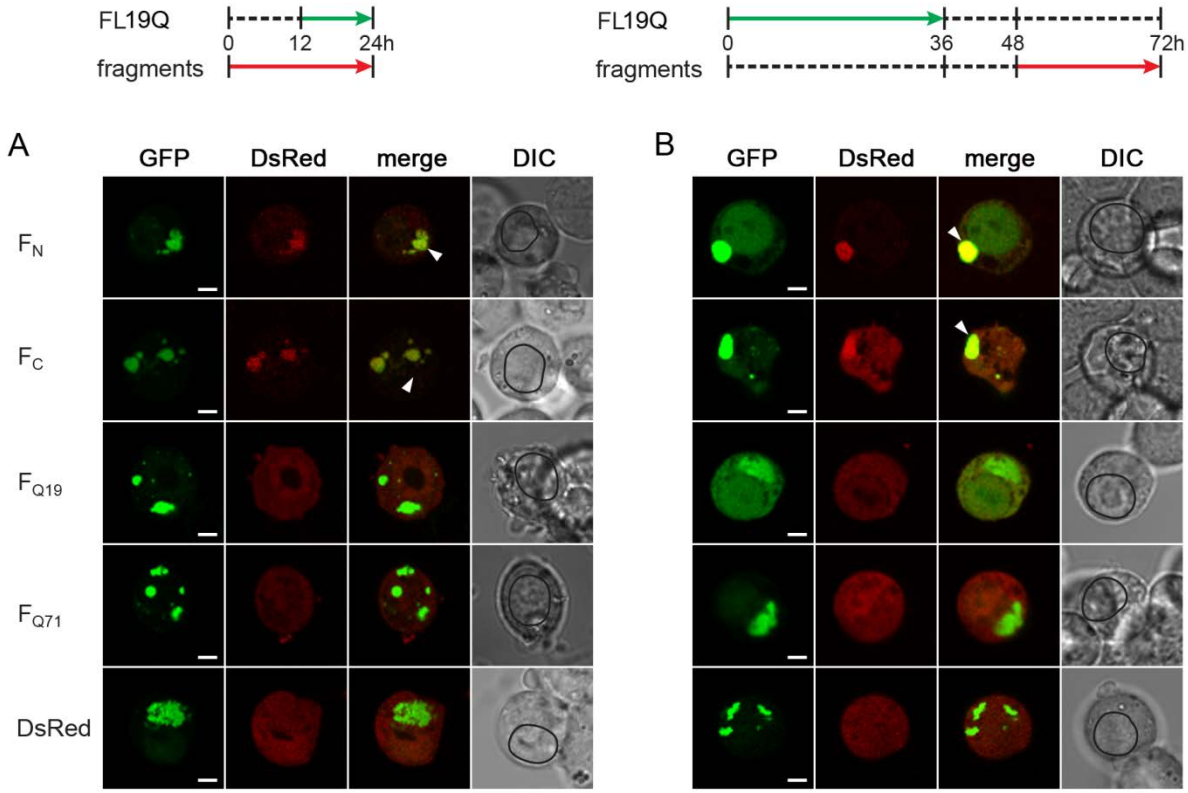

Figure 3-20: Orthogonal cross-seeding in vivo of the cytoplasmic FL19Q inclusions with the ATN1 fragments. *The scheme for the co-expression of the fragments and FL-ATN1 is included in the upper panel and each scheme is representative for the image series below it. (A, B) Cytoplasmic FL19Q aggregates recruited only F_N and F_C fragments at early (A) and later expression times, however, (B) the FL19Q species were not capable of recruiting F_{Q19} and F_{Q71} fragments. The recruited fragments in the FL19Q inclusions are marked with an arrow on the merged images. DIC denotes differential interference contrast microscopy. For details see the description of Fig. 3-17. Scale bar represents 4 µm. These images originate from the diploma thesis of S. Zakrzewski, supervised by the author of this dissertation.*

Interestingly, the cytoplasmic inclusions of ΔN-ATN1 resembled the phenotype of the cytoplasmic FL-ATN1 inclusions. An evolution of the recruiting ability was observed only for the cytoplasmic ΔN71Q aggregates (Fig. 3-21 A, B).

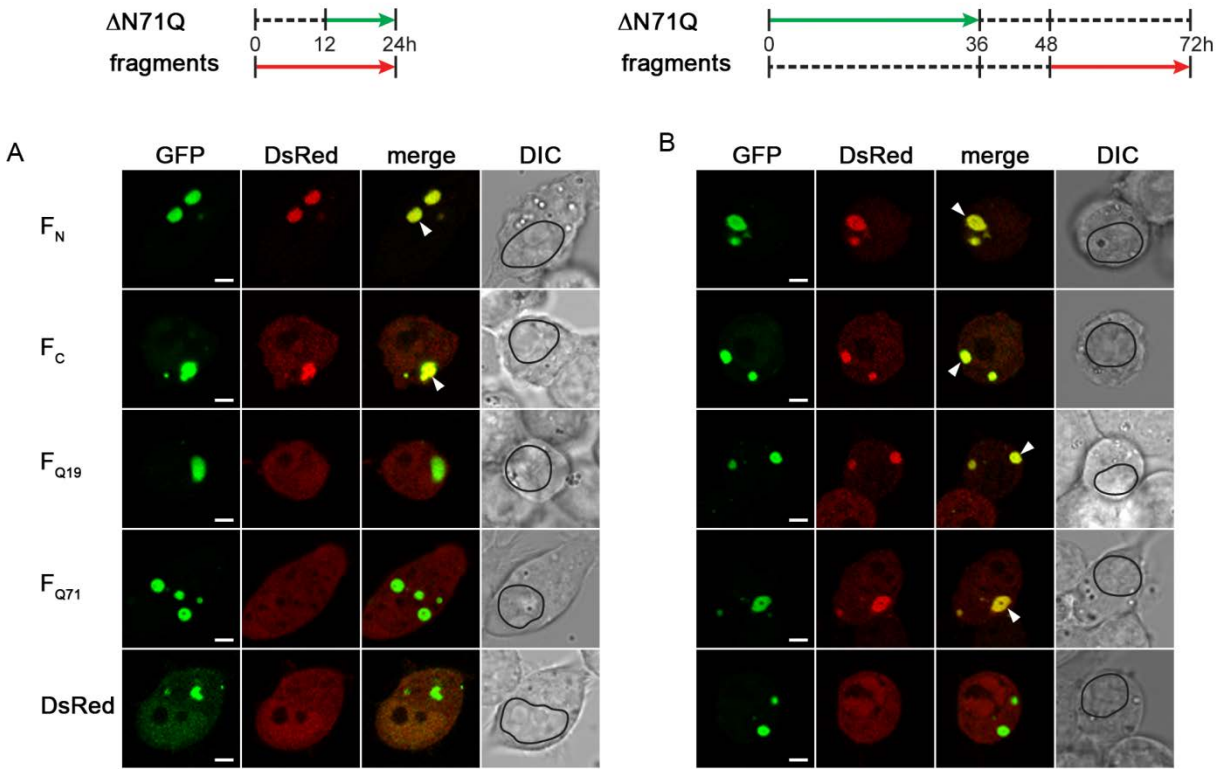

Figure 3-21: Orthogonal cross-seeding in vivo of ΔN71Q inclusions with the ATN1 fragments. *(A, B) ΔN71Q aggregates recruited F_N and F_C fragments at early (A) and also F_{Q19} and F_{Q71} at later times of expression (B). The schemes of the co-expression of the fragments and ΔN-ATN1 in the upper panel are representative for the image series below. The recruited fragments in the ΔN-ATN1 inclusions are marked with an arrow on the merged images. DIC denotes differential interference contrast microscopy. Details in the description are included in the legend of Fig. 3-17. Scale bar represents 4 µm.*

In contrast, the inclusions composed of the non-pathological ΔN19Q variant did not evolve over time and were able to recruit only the fragments covering the flanking sequences (Fig. 3-22 A, B), regardless of the aggregation time of ΔN19Q. These data

allow us to conclude that the expansion of the polyQ stretch beyond the pathological threshold induces a change in the aggregate core to polyQ-based.

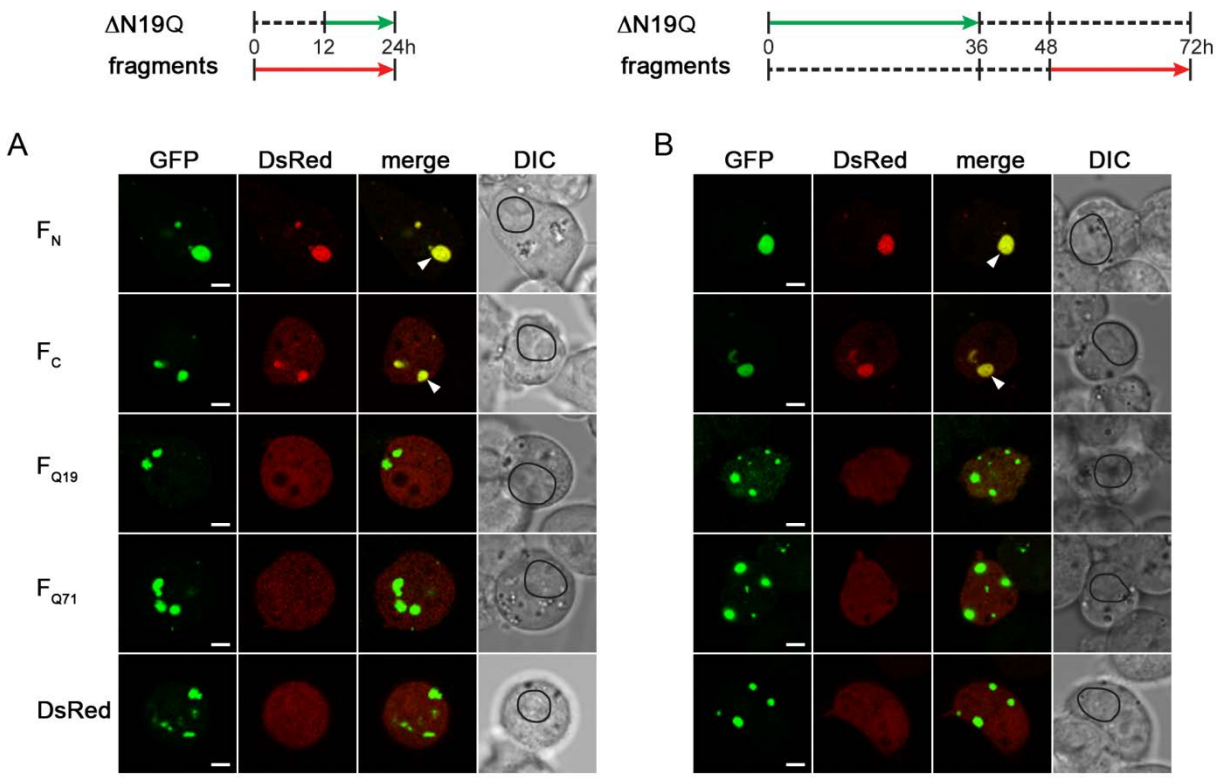

Figure 3-22: Orthogonal cross-seeding in vivo of ΔN19Q inclusions with the ATN1 fragments. *(A, B) ΔN19Q inclusions recruited only F_N and F_C fragments at early (A) and late expression times (B). The upper panel shows the schemes of the co-expression of the fragments and ΔN-ATN1 that are representative for the image series below them. The recruited fragments in the ΔN-ATN1 inclusions are marked with an arrow on the merged images. DIC denotes differential interference contrast microscopy. Details are in the description of Fig. 3-17. Scale bar represents 4 µm.*

3.5 Expansion of the polyQ stretch alters the dynamics of interactions with cellular proteins

Immunohistochemical and biochemical analyses established that aggregates of polyQ-containing proteins are associated with a variety of cellular proteins (Chai, et al. 2002; Cummings, et al. 1998; Kazantsev, et al. 1999; Kim, et al. 2002; Nucifora, et al. 2001; Rajan, et al. 2001; Steffan, et al. 2000; Stenoien, et al. 2002). The observed different composition and core structure of the FL19Q and FL71Q inclusions raised the question as to whether these structural variations will reflect the interactions with the cellular proteins. To test this FL19Q and FL71Q were expressed for 48h in N2a/Tet-Off cells and analyzed using 2D-gel and MALDI-TOF MS analyses. The cells were fractionated into nucleoplasmic and cytoplasmic fractions (Fig. 3-4 A) and FL19Q and FL71Q inclusions were immunoprecipitated using anti-GFP antibodies (Fig. 3-24, Fig. 3-25). Although most of large, bulky, SDS-resistant cytoplasmic FL71Q species co-precipitated with a slow centrifugation pellet fraction (P) (Fig. 3-4), this fraction was not amenable for further analysis, since it contained some intact cells (see the description of the Fig. 3-4 C). Next, the aggregates from nuclear and cytoplasmic fractions were dissolved and their protein composition was analyzed using two-dimensional (2D) gel electrophoresis. This technique separates proteins according to two independent properties in two consecutive steps: the first dimension step, isoelectric focusing (IEF), separates proteins according to their isoelectric points (pI) whereas the second step, SDS-PAGE, separates proteins according to their molecular weights (Gorg, et al. 1988). Because it is unlikely that two molecules will be similar in two distinct properties, the molecules are more effectively separated in 2-D electrophoresis than in 1-D electrophoresis.

Prior to the 2D-gel electrophoresis experiments the specificity of the immunoprecipitation of FL-ATN1 assemblies was confirmed. The inclusions were immunoprecipitated from the lysates of N2a/Tet-Off cells expressing FL19Q or FL71Q for 48 h and analyzed by immunoblot. The dominating GFP-tagged FL19Q and FL71Q bands suggest the specificity of the immunoprecipitation (Fig. 3-23).

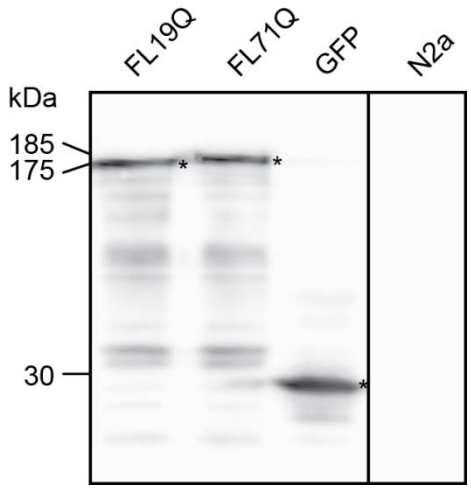

Figure 3-23: Specificity of the immunoprecipitation of the FL-ATN1 inclusions with the anti-GPF magnetic beads tested with the anti-GPF antibodies. *Five million N2a/Tet-Off cells expressing FL19Q or FL71Q for 48 h were lysed and subjected to immunoprecipitation with anti-GFP antibody-coupled magnetic beads then lysates were resuspended in Laemmli buffer, analyzed by immunoblot and stained with anti-GFP antibodies. The lower, GFP-positive bands are probably degradation products of FL-ATN1 during the processing of the samples. GFP expressing cells and mock-transfected N2a/Tet-Off (N2a) were used as a control. Bands corresponding to the monomeric FL19Q, FL71Q and GFP are highlighted with an asterisk on each lane.*

The interactome of the FL19Q with FL71Q inclusions was compared (Fig. 3-24 A, 3-25) and only spots that differ between the two proteins were identified (Table 3-3) using MALDI-TOF MS analysis, a sensitive method to identify proteins and peptides in the wide mass range (1-300 kDa) (Bonk and Humeny 2001).

For the nuclear inclusions mainly proteins that are involved in the RNA processing and DNA repair were identified (Fig. 3-24 A, B, Table 3-3).

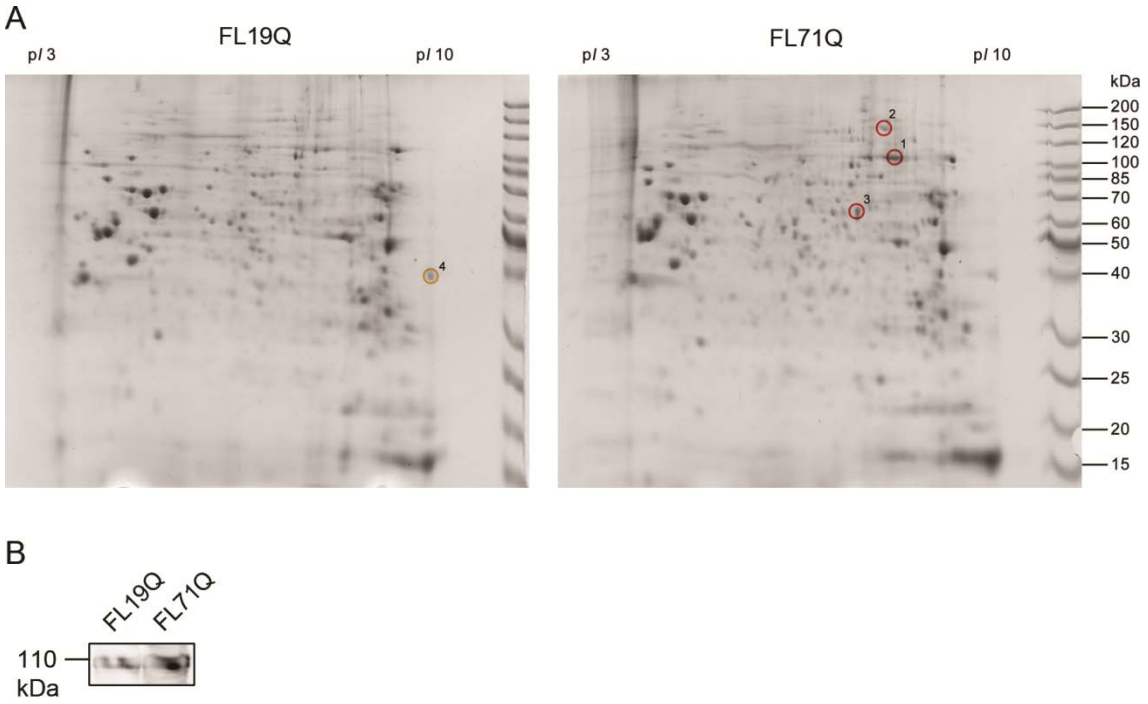

Figure 3-24: Identification of the proteins associated with the nuclear ATN1 aggregates. *(A) The nuclear fraction was isolated as described in Fig. 3-4 A, from the N2a/Tet-Off cells transiently expressing FL19Q or FL71Q for 48 h and inclusions-interacting proteins were immunoprecipitated with anti-GFP antibody and analyzed on 2D-gels. Proteins enriched in nuclear FL71Q aggregates are circled in (A) on the right panel; a protein depleted in nuclear FL71Q inclusions is marked on the left panel. The numbers of the spots correspond to the numbers in the Table 3-3. (B) The nucleoplasmic fraction of FL71Q (A) was immunoprecipitated and analyzed by immunoblot with anti-nucleolin antibody. It should be noted that there are two nucleolin-positive bands likely representing the two alternatively phosphorylated forms of the full-length protein.*

The transcriptional profiles of some of these proteins have been also found to be specifically altered in the DRPLA mouse model (Luthi-Carter, et al. 2002).

Some of the proteins interacting with the nuclear inclusions, including heterogeneous nuclear protein L and endoplasmin, show overlapping changes in the microarray transcriptional profiling common to different polyQ-disease proteins (Luthi-Carter, et al. 2002) and are most likely caused by the expanded polyQ stretch regardless of the protein context. In the nuclear FL71Q species intensive spot of nucleolin was

observed (Fig. 3-24 A and Table 3-3), which is a crucial protein involved in the first steps of the ribosome biogenesis (Ginisty, et al. 1998; Ginisty, et al. 1999; Srivastava and Pollard 1999). Its presence in the FL71Q nuclear aggregates was confirmed by immunoblotting of the fractionated nucleoplasmic FL71Q aggregates with anti-nucleolin antibody (Fig. 3-24 B).

The difference between the detergent-labile cytoplasmic FL19Q and FL71Q inclusions was a depletion of two proteins from the FL71Q interactome that belong to the group of molecular chaperones (Fig. 3-25, Table 3-3).

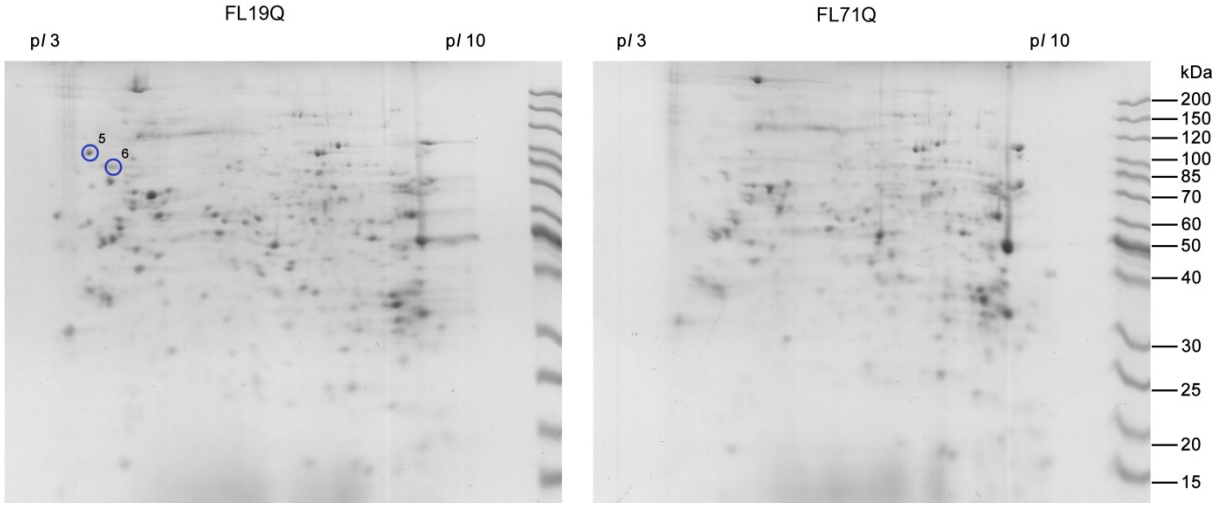

Figure 3-25: Identification of the proteins associated with the cytoplasmatic ATN1 aggregates. *FL19Q or FL71Q were transiently expressed in N2a/Tet-Off cells for 48 h, the cytoplasmic fraction was isolated as described in Fig. 3-4 A and inclusions-interacting proteins were immunoprecipitated with anti-GFP antibody and analyzed on 2D-gels. Proteins depleted in cytoplasmic FL71Q aggregates are circled on the left panel. The numbers of the spots correspond to the numbers in the Table 3-3.*

Murine Hsp cognate 90β protein and Hsp90B1 chaperone murine homolog, endoplasmin (Coe and Michalak 2009), were depleted in the cytoplasmic FL71Q aggregates as opposed to the inclusions of the non-pathological FL19Q counterpart (Fig. 3-25). Consistently, a decrease of the level of the Hsp90 transcript has been detected in the DRPLA mouse model (Luthi-Carter, et al. 2002).

Table 3-3: Proteins with aberrant association patterns in the FL71Q aggregates as compared to the corresponding FL19Q inclusions. *Proteins that were specifically influenced by the nuclear and cytoplasmic FL71Q aggregates were classified into two groups: depleted and enriched in the FL71Q aggregates as compared to the FL19Q inclusions.*

Aggregate type	**Compared to FL19Q**	**Protein**		**Cellular function**
nuclear FL71Q	enriched	1	Nucleolin	Pre-rRNA transcription and ribosome biogenesis
	enriched	2	Chromosomal protein 1A	Chromosome cohesion and DNA repair
	enriched	3	Heterogeneous nuclear protein L	Component of the heterogeneous nuclear ribonucleoprotein (hnRNP)
	depleted	4	Nuclear ribonucleoprotein G	Pre-mRNA splicing
cytoplasmic FL71Q	depleted	5	Endoplasmin (murine Hsp90B1)	Molecular chaperone
	depleted	6	Heat shock cognate Hsp protein 90β	Molecular chaperone

4. Discussion

4.1 General aspects of ATN1 aggregation

A multistep aggregation process of polyQ proteins may proceed through heterogeneous populations of different aggregate intermediates with various structural, dynamic and physicochemical properties which might be on- or off-pathway to the amyloid structures (Chai, et al. 2002; Kim, et al. 2002; Matsumoto, et al. 2006; Ross and Poirier 2005; Stenoien, et al. 2002; Wacker, et al. 2004). ATN1 variants with a polyQ length in the non-pathological (FL19Q) or pathological (FL71Q) range localize into nuclear and cytoplasmic hyperfluorescent loci, which on static images obtained in fixed cell studies may support the notion of immobile aggregates (Fig. 3-1). However, the systematic biophysical analysis of these inclusions in this study revealed various aggregates with different dynamic properties and molecular architecture. The pathological FL71Q protein forms at least two types of inclusions with distinct dynamic properties that coexist in the nucleus: (*i*) inclusions composed of high-mobility species that exchange quickly with the soluble nucleoplasmic pool, and (*ii*) aggregates consisting most likely of detergent-resistant, low-mobility species that exchanged with lower frequency with the surrounding environment (Fig. 3-2, Fig. 3-3). By contrast, SDS-labile FL19Q molecular species in the nuclei were also spatially sequestered in inclusions however they retained a high mobility within the inclusions and fast exchange with the surrounding environment (Fig. 3-2, Fig. 3-3). ATN1 and ATN2 are physically associated *in vivo*, though the functional significance of these interactions is still unknown. ATN2 associates mainly in promyelocytic leukemia protein nuclear bodies (Shen and Peterson 2009) and may sequester ATN1. This sequestration may be of functional relevance to ATN1 and the primary reason for the observed spatial confinement of FL19Q.

Unlike the nuclear aggregates, the cytoplasmic full-length and ΔN-ATN1 variants with pathological and non-pathological Q-lengths assemble into bulky, but compact and immobile structures (Fig. 3-1 to Fig. 3-3). Similarly, Htt-exon 1 with 103Q and the prion proteins, Rnq1 and Ure2, are also sequestered in bulky cytoplasmic structures in yeast and mammalian cell models which may facilitate their clearance

(Kaganovich, et al. 2008). Characteristic feature of those bulky structures is a decreased mobility of the sequestered misfolded proteins, similarly as we observed for the cytoplasmatic inclusions of the FL- and ΔN-ATN1 proteins Fig. 3-3, Table 3-2). Strikingly, only the cytoplasmic inclusions of ATN1 with expanded polyQ tract are detergent-resistant. Thus, the detergent insolubility, which is indicative of fibrillar aggregates (Kazantsev, et al. 1999) may account for the immobilization of the FL71Q and ΔN71Q proteins within the cytoplasmatic aggregates. Spatial sequestration and decreased protein mobility, however, may also be a result of its binding to macromolecular complexes (Lippincott-Schwartz, et al. 2001). Given that the nucleus and the cytoplasm may provide different sets of interaction partners (Hands and Wyttenbach 2010), differences in the mobility of the detergent-labile FL19Q and ΔN19Q assemblies formed in the cytoplasm and nucleus may be a result of compartment-specific protein-protein interactions or protein post-translational modifications. The intrinsic propensity of the 19Q ATN1 variants to associate may suggest another explanation of their spatial sequestration and this association can be driven by sequence elements outside the polyQ tract as suggested by the cross-seeding experiments (Fig. 3-18, Fig.3-20 and Fig. 3-22).

In analogy to our observations of ATN1, another polyQ disease-related protein, ataxin-3 with the polyQ stretch in the non-pathogenic range, has been shown to form *in vitro* SDS-soluble oligomeric aggregate species in nearly physiological conditions (Ellisdon, et al. 2006; Gales, et al. 2005). This property has been imparted on the non-expanded SCA3 protein by the Josephin domain, a flanking sequence involved in the initial, polyQ-independent step of aggregation of ataxin-3, that has an inherent tendency to aggregate *in vitro* (Ellisdon, et al. 2006; Masino, et al. 2004).

Taken together our results suggest that the aggregation of ATN1 *in vivo* comprises formation of species with heterogeneous biophysical properties that might be modulated by intrinsic and/or extrinsic, cell compartment-specific factors. The change in the detergent-solubility of the FL- and ΔN-ATN1 species with expanded polyQ implies that they evolve over time.

4.2 Flanking sequences modulate the aggregation of ATN1

Our in-cell, orthogonal cross-seeding analyses suggest that the architecture of the aggregate core of FL71Q inclusions in nucleus and cytoplasm evolves into polyQ-based and we propose that the polyQ-stretch expansion over the pathogenic threshold triggers a conformational switch to facilitate formation of amyloid structures. Our model is consistent with the 'conformational conversion' model of amyloid formation of yeast prion (Serio, et al. 2000) and the proposed multistep aggregation model for other disease-related polyQ proteins (Aiken, et al. 2009; Ellisdon, et al. 2006; Thakur, et al. 2009) and model proteins (Bulone, et al. 2006; Ignatova, et al. 2007). In these models the initial aggregation step is triggered by the association of folded domains (Aiken, et al. 2009; Ignatova, et al. 2007; Masino, et al. 2004; Thakur, et al. 2009) or secondary structure elements located N-terminally upstream of the polyQ sequence (Aiken, et al. 2009; Ignatova, et al. 2007; Masino, et al. 2004; Thakur, et al. 2009) and results in the formation of prefibrillar, detergent-labile aggregate species (Ignatova, et al. 2007; Masino, et al. 2004; Thakur, et al. 2009).
Unexpectedly, for ATN1 our cross-seeding analyses suggest that the N- and C-terminal domains initially associate in highly flexible inclusions with the polyQ sequence excluded from the aggregate core (Fig. 3-17 - Fig.3-22). Since changes in the conformational dynamics or stability of the structured flanking domains upon the pathological expansion of the polyQ stretch has been suggested to initiate the aggregation of some polyQ proteins (Chow, et al. 2004b; Ignatova and Gierasch 2006; Masino, et al. 2004), we compared the structural properties of ATN1, Htt-exon 1 and SCA3 with the same length of the polyQ expansion (71Q) using the disorder predictor PONDR (www.pondr.com) (Romero, et al. 2004).
PONDR analysis revealed that ATN1 sequence bears some unique features: both N- and C-terminal domains show a tendency toward order and the PONDR score well below 0.5 median in the C-terminus is associated with a higher tendency of being structured (Mohan, et al. 2006) (Fig. 4-1). In contrast, PONDR analysis of the Htt-exon 1 sequence predicts some order only in the N-terminal region (Fig. 4-1) which as experimentally suggested probably takes up an α-helical conformation and promotes the aggregation by interacting with itself and with the polyQ segment (Aiken, et al. 2009). The N-terminal segment of ataxin-3 with PONDR scores far

below 0.5 median comprises the globular, autonomously folded Josephine domain which alters the aggregation behavior on the polyQ stretch (Masino, et al. 2004). PONDR analysis suggests also tendency toward order in the C-terminal region of ataxin-3 (Fig. 4-1), however its impact on aggregation kinetics has not been experimentally addressed yet. PONDR analysis of initial 600 amino acids of ataxin-7 revealed a score above the 0.5 median for the N-terminal 29 amino acids ($AT7^{NT}$) and does not suggest any tendency towards order (Kar, et al. 2011). Consistently, a model polyQ peptide $AT7^{NT}Q_{30}K_2$ bearing this N-terminal sequence of AT7 undergoes the classic nucleated polymerization growth, with a direct formation of fibrils via monomeric nucleus and without any intermediate species; such aggregation behavior is typical for simple polyQ peptides (Kar, et al. 2011). The absence of an effect of the $AT7^{NT}$ cannot be due to its short length as the initial, 17 amino acid-long N-terminal domain of Htt-exon1 (HTT^{NT}), which is even shorter, significantly modulates the aggregation mechanism of $HTT^{NT}Q_{30}P_6$ peptide (Thakur, et al. 2009).

Although structural details on the mechanisms by which flanking regions initiate the aggregation of the polyQ disease proteins remain to be clarified, our data on ATN1 and the examples in the literature on other polyQ proteins clearly suggest that structurally stable elements can initially associate into flexible aggregates. Depending on the sequence features which are unique for each polyQ protein however, the structured regions can be N- or C-terminally localized (Fig. 4-1).

Similarly as observed for Htt-exon 1, CRABP-Htt-exon 1 chimera and SCA3 with expanded polyQ tract (Aiken, et al. 2009; Ignatova, et al. 2007; Masino, et al. 2004; Thakur, et al. 2009), the initial step in the aggregation of FL-ATN1 proteins is non-nucleated and independent of the polyQ length, as FL19Q and FL71Q in nucleus recruit both N- and C-terminal fragments and form inclusions with a mixed N- or C-cores (Fig. 3-17 - Fig. 3-18).

In the initial, soluble aggregate species of ATN1, polyQ-sequence is excluded from the aggregate core and it is possible that early association of the flanking domains might accelerate the nucleation of a polyQ-based amyloid structure by orienting and/or increasing the local concentration of the polyQ elements, as previously suggested for the flanking sequences of other polyQ proteins (Ellisdon, et al. 2007; Ignatova, et al. 2007; Thakur, et al. 2009). On a second stage, the initial, relatively loosely-packed FL71Q nuclear inclusions which intensively exchange with the

surrounding monomer pool convert to more stable, SDS-resistant amyloid structures with the polyQ-dominated aggregate core (Fig. 3-2 to Fig. 3-4, Fig. 3-17).

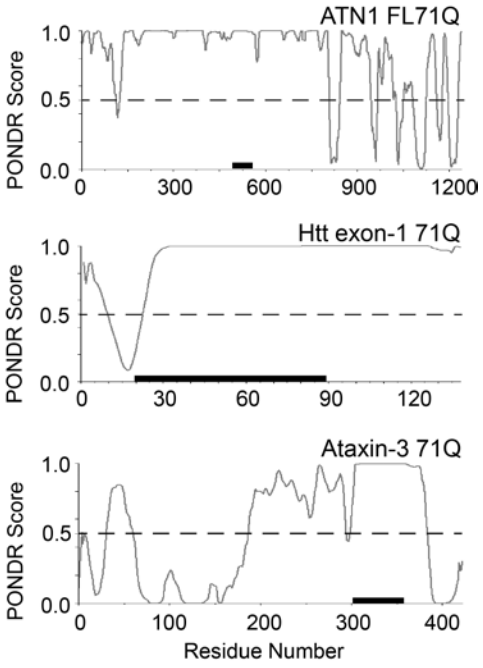

Figure 4-1: PONDR analysis of the FL-ATN1protein, Htt-exon 1 and ataxin-3. *Segments with PONDR score between 0 and 0.5 are predicted to be stably folded and scores near 1.0 are associated with disorder. In ATN1 polyQ sequence is located between residue 483 and 554 and is directly flanked by largely disordered regions, however both N-terminal and C-terminal sequences flanking the polyQ tract show a tendency towards order. The black bars represent the polyQ sequence; for comparison the polyQ stretches of all three proteins are set to 71Q. Access to PONDR (www.pondr.com) was provided by Molecular Kinetics.*

Strikingly, cytoplasmatic FL-ATN1 inclusions mirror the sequestration pattern of the corresponding nuclear FL-ATN1 assemblies as well as the aggregate core and solubility evolution observed for the FL71Q nuclear inclusions (Fig. 3-2, Fig. 3-19, Fig. 3-20). However, in contrast to the inclusions localized in the nucleus, the ability of the FL-ATN1 proteins in the cytoplasm to exchange with the protein pool within and outside the inclusion is equally restricted in the early and end-stage phase of aggregation. This suggests that although the compartment-dependent protein context may modulate the biophysical and perhaps also toxic properties of ATN1 aggregate

species, it does not appreciably change the aggregation mechanism which is mostly determined by the sequences of the host protein.
ΔN19Q and ΔN71Q proteins exhibit recruiting ability, dynamic properties and solubility similar to those of cytoplasmic FL-ATN1, suggesting that the proximal N-terminal segment deleted in the ΔN-ATN1 variants is not essential for the association of the FL-ATN1 flanking domains during the initial step of aggregation.

4.3 Changes in the interactome of mutant ATN1 occur in parallel to the evolution of the aggregate core

Pathological polyQ expansion may introduce differences in the interactomes of the disease-related polyQ proteins (Bauer and Nukina 2009). Certain non-native changes in the protein-protein interaction networks are common for different mutant polyQ proteins (McCampbell, et al. 2000; Shimohata, et al. 2000a; Strom and Sjogren 2005; Yamada, et al. 2000). Provided that the polyQ segment is the only primary amino acid sequence motif shared by the distinct polyQ proteins (Gatchel and Zoghbi 2005), it can be assumed that such common non-native protein-protein interactions occur via expanded polyQ stretch. Conversely, some interactome changes that are specific to pathogenic variants of distinct polyQ proteins are also likely to be mediated by the sequences flanking the polyQ tract, as expansion of the polyQ stretch may introduce some alterations in their conformation (Lam, et al. 2006; Yanagisawa, et al. 2000). By comparing the composition of the non-pathological FL19Q and FL71Q inclusions isolated 48h post-transfection we were able to detect some differences in the interaction partners of the FL71Q imparted by pathological expansion of the polyQ tract. Additionally, comparison of nuclear and cytoplasmic inclusions provided some hints on compartment-specific changes in the interactome of FL71Q upon the pathogenic polyQ expansion.
Intriguingly, some of the differences between FL-ATN1 with polyQ in the pathological and non-pathological length we found correlated with changes detected in the microarray transcriptional profiles analysis of different brain regions of DRPLA and HD mice (Luthi-Carter, et al. 2002). We identified four proteins that clearly differ in the nuclear inclusions of FL19Q versus FL71Q. Interestingly, one of the proteins

enriched in the FL71Q nuclear inclusions, heterogeneous ribonucleoprotein L that is involved in pre-mRNA splicing (Fig. 3-23, tabele 3-3) had a decreased transcript levels in the cerebella of DRPLA and HD mice (Luthi-Carter, et al. 2002). Given that similar transcriptional alteration might occur in N2a cells expressing FL71Q, enrichment of this protein in the nuclear FL71Q inclusions suggests that its sequestration in the ATN1 aggregates could further deplete it from the cellular pool and thus compromise its function.

Analysis of the cytoplasmatic fraction (Fig. 3-4 B) allowed us to compare soluble FL19Q and FL71Q inclusions (Fig. 3-4 B). We found that endoplasmin, a murine homolog of the human molecular chaperone Hsp90B1 and the Hsc90β proteins, in contrast with FL19Q species, were depleted from the cytoplasmic FL71Q aggregates and the former alteration coincided with a decrease of endoplasmin transcript in DRPLA mouse model in comparison to wild-type mice (Luthi-Carter, et al. 2002).

Hsp90, a highly conserved molecular chaperone family, assists folding, intracellular transport, maintenance, and cell signaling (Bukau, et al. 2006; Hohfeld, et al. 2001; Pratt, et al. 2006; Wandinger, et al. 2008). Recent studies using a yeast model suggest that transient binding of Hsp90 to the expanded polyQ stretches in cooperation with other heat shock proteins plays an important role in the maturation of polyQ aggregates (Walter, et al. 2011). The cytoplasmatic Hsp82 protein, a yeast homolog of Hsp90 together with Hsp26 and Hsp70 and a few other chaperones associates with the soluble species of Q103 peptides already at the early times of expression (Walter, et al. 2011). Hsp90, Hsp26 and Hsp70, however, appear to be partially released from 103Q before the maturation of the aggregates and prior to association of Hsp104 (Walter, et al. 2011). When binding of Hsp70 to Q103 was enhanced, Hsp70 and Hsp90 were retained within the polyQ species, which blocked the interaction with Hsp104 and formation of the SDS-resistant Q103 aggregates, suggesting that a release of Hsp90 might be essential for accomplishing the maturation process (Walter, et al. 2011). These findings may have implications for the polyQ pathology in general. Similar non-native interactions of Hsp90 proteins with the expanded polyQ stretch in the disease proteins might perturb formation of the insoluble end-stage aggregates, generally assumed to be benign, while increasing the pool of toxic soluble oligomeric species (Arrasate, et al. 2004). In this light depletion of the endoplasmin from the detergent-labile FL71Q species might be a

part of the cellular response to ATN1 aggregation preceding the transition to the detergent resistant species with polyQ-dominated aggregate core. Alternatively, given the decrease in level of endoplasmin transcript observed in DRPLA mice (Luthi-Carter, et al. 2002) it could mean that the expression of this chaperone is perturbed by the pathogenic polyQ expansion of ATN1 already at the level of transcription. If this is the case, it is likely that the level of the endoplasmin protein in the N2a cells is too low to allow performing its normal function from the beginning on, which in turn leads to the enhanced aggregation of FL71Q.

4.4 Relevance of the ATN-1 aggregation mechanism to pathology

The onset of the polyQ-associated pathology has been linked to a change in the subcellular localization of the aggregation-prone disease proteins. An accumulating body of evidence suggests the nucleus as the primary site of toxicity in the polyQ diseases (Klement, et al. 1998; Nucifora, et al. 2003; Saudou, et al. 1998).

Douglas and colleagues have shown in the yeast toxicity model, [RNQ+] cells, that re-directing of the mutant Htt-exon 1 with 103Q to the nucleus, either through nuclear localization of its interaction partner Rnq1 or by fusing the Htt-103Q with an NLS, inhibited the conversion of Htt-103Q into benign amyloid-like fibrillar aggregates, simultaneously increasing the pool of the soluble oligomeric cytotoxic species (Douglas, et al. 2009). Similarly, the nuclear inclusions of ataxin-1 with a pathologic polyQ length in mammalian cell models have been shown to retain increased solubility and contain both fast- and slow-exchanging components (Chai, et al. 2002; Krol, et al. 2008; Stenoien, et al. 2002). This model resonates with our finding that nuclear inclusions of FL-ATN1 are more dynamic and provides a mechanistic explanation of the enhanced cellular toxicity of the nuclear ATN1 aggregates (Nucifora, et al. 2003).

In contrast, Htt-exon 1 with an expanded polyQ tract forms immobile intranuclear inclusions (Chai, et al. 2002) underscoring the importance of the protein context in the polyQ diseases. Furthermore, we observed that intranuclear and cytoplasmic juxtanuclear FL71Q inclusions co-localize with the nuclear envelope component lamin B1 (Fig. 3-6). Similar alterations in the lamin B1 rim and mechanical depression

in the nuclear membrane are observed for mutant Htt-exon 1 (Chapple, et al. 2008). Aberrant interactions with the nuclear membrane are relevant to the pathophysiology of some neurological diseases (Iwahashi, et al. 2006). Together with the observation of highly dynamic and structurally heterogeneous nuclear inclusions our results provide a mechanistic explanation of why preferential accumulation of mutant ATN1 in the nucleus may confer cellular toxicity.

Furthermore, our results contribute to the emerging concept that the cellular aggregation is a dynamic, multistep process with different sequences of the aggregating protein transiently or stably involved in the aggregate core. The idea that in the aggregation time course various surfaces will be accessible for biophysical interactions with the cellular proteins goes beyond the role of the protein misfolding and may have important implications for a large number of other neurodegenerative pathologies.

4.5 Outlook and perspectives

Each of the disease-related polyQ proteins exhibits a cell-specific pattern of toxicity and triggers the degeneration of defined neuronal populations despite its widespread expression in different tissues. Although pathological polyQ expansion is necessary to trigger aggregation, the sequences flanking the polyQ stretch also modulate the initial aggregation steps (de Chiara, et al. 2005b; Ellisdon, et al. 2006; Ignatova, et al. 2007; Thakur, et al. 2009) and influence the morphology and stability of the various aggregates and their ability to recruit other cellular proteins (Ignatova, et al. 2007; Lam, et al. 2006; Legleiter, et al. 2010; Tam, et al. 2009; Yanagisawa, et al. 2000). Variations in the amino-acid compositions and native folds of the flanking sequences may account for different physico-chemical properties and toxicity of aggregates formed by distinct polyQ disease proteins (Gatchel and Zoghbi 2005).

The molecular and structural aspects of various intermediates formed in the aggregation of the polyQ proteins remain still poorly defined. The initial stages of polyQ aggregation are particularly difficult to track due to the transient appearance of the early aggregates. *Ex vivo* analyses, although contributing valuable insights into the aggregation mechanisms, involve isolation of the aggregates from the natural,

cellular environment which may alter the stability of the early aggregate species or may cause missing of some transient intermediates. Thus a combination between the *ex vivo* approaches with direct *in vivo* analyses of the aggregate architecture and dynamics is crucial for understanding the underlying molecular mechanisms of polyQ aggregation and increased toxicity of the early aggregates in the polyQ pathologies.

The factors modifying aggregation and toxicity of the polyQ disease proteins in *cis* and in *trans* may reciprocally or synergistically influence each other. The interplay between various domains of the host protein may influence the molecular architecture and toxicity of the aggregates by exposing regions that are usually buried in the native state, which in turn may alter post-translational modification patterns and/or interactions with cellular proteins. In turn, altered protein-protein interactions and post-translational modifications may change the structure, subcellular localization, turnover and consequently the toxicity of the aggregate species (Lim, et al. 2008; McCampbell, et al. 2000; Steffan, et al. 2000; Yamada, et al. 2000). Depending on the nature of these alterations (e.g., loss of functional interaction, new aberrant, non-native interaction, change in the strength of interactions) toxicity is likely to be conferred via distinct mechanisms. Intrinsic and extrinsic factors modulating the polyQ aggregation process may exert a toxic effect either by directly changing the native functions of the mutant polyQ proteins or by sequestration of other cellular proteins in the IBs and thus depleting their physiological function(s) from the cell. Coupling of the cytotoxicity directly to a toxic gain-of-function or loss-of-funtion of the mutant polyQ protein species provides a rationale for the therapeutic strategies, including enhancement of its degradation (Bauer, et al. 2009; Lai and Frishman 2005; Sarkar, et al. 2007b), stabilizing the monomeric native state (Nagai, et al. 2003; Sarkar, et al. 2007a), triggering the formation of benign oligomeric species which are off-pathway to the fibril formation (Behrends, et al. 2006; Borwankar, et al. 2011; Ehrnhoefer, et al. 2006) or acceleration of the aggregation to fibrillar aggregates which are suggested to be benign (Bodner, et al. 2006). In contrast, when the cytotoxic effect is a result of compromising the function(s) of a protein that is vital for the cellular functionality, other than that of the disease polyQ protein, therapeutic strategies aiming to compensate for the loss-of-function of this particular protein might prove effective (DeMarch, et al. 2008; Ferrante, et al. 2003; Giampa, et al. 2009; Ying, et al. 2006).

The alterations in the interaction networks, common for different polyQ proteins most likely result from the common pathological expansion of the polyQ stretch. Others, disease-specific, are likely to be influenced by the flanking sequences. Furthermore, an altered subcellular localization, with a preferential accumulation of misfolded species in the nucleus, has been suggested to add to the polyQ-associated toxicity due to compartment-specific protein context (Hands and Wyttenbach 2010). Thus comparative studies of the aggregate structure and interactomes of polyQ proteins with the polyQ expansion in the pathological and non-pathological range from different cellular compartments need to be performed to clearly define the origin of toxicity in nucleus vs. cytoplasm.

Here we systematically analyzed the intrinsic and extrinsic factors influencing the aggregation of ATN1 in different cellular compartments. We developed a novel orthogonal cross-seeding assay which allows for analysis of aggregate structure directly in the cell and enables tracking of the intrinsic determinants of the amyloidogenicity in different systems (here *E. coli* and mammalian N2a cells). Results presented in this work suggest that systematic, comparative studies based on the orthogonal cross-seeding approach and mobility measurements, combined with ex vivo analyses of physicochemical properties and interaction partners might contribute to elucidation of the disease-specific mechanisms of aggregation and neurodegeneration and thus help to develop medical applications efficient for the individual polyQ pathologies.

5. References

Adams, S. R., et al.
2002 New biarsenical ligands and tetracysteine motifs for protein labeling in vitro and in vivo: synthesis and biological applications. J Am Chem Soc 124(21):6063-76.
Aiken, C. T., et al.
2009 Phosphorylation of threonine 3: implications for Huntingtin aggregation and neurotoxicity. J Biol Chem 284(43):29427-36.
Allen, T. D., et al.
2000 The nuclear pore complex: mediator of translocation between nucleus and cytoplasm. J Cell Sci 113 (Pt 10):1651-9.
Ambrose, H. J., et al.
1994 A physical map across chromosome 11q22-q23 containing the major locus for ataxia telangiectasia. Genomics 21(3):612-9.
Andrew, S. E., Y. P. Goldberg, and M. R. Hayden
1997 Rethinking genotype and phenotype correlations in polyglutamine expansion disorders. Hum Mol Genet 6(12):2005-10.
Arrasate, M., et al.
2004 Inclusion body formation reduces levels of mutant huntingtin and the risk of neuronal death. Nature 431(7010):805-10.
Atwal, R. S., et al.
2011 Kinase inhibitors modulate huntingtin cell localization and toxicity. Nat Chem Biol 7(7):453-60.
—
2007 Huntingtin has a membrane association signal that can modulate huntingtin aggregation, nuclear entry and toxicity. Hum Mol Genet 16(21):2600-15.
Bailey, C. K., et al.
2002 Molecular chaperones enhance the degradation of expanded polyglutamine repeat androgen receptor in a cellular model of spinal and bulbar muscular atrophy. Hum Mol Genet 11(5):515-23.
Bauer, H. H., et al.
1995 Architecture and polymorphism of fibrillar supramolecular assemblies produced by in vitro aggregation of human calcitonin. J Struct Biol 115(1):1-15.
Bauer, P. O., and N. Nukina
2009 The pathogenic mechanisms of polyglutamine diseases and current therapeutic strategies. J Neurochem 110(6):1737-65.
Bauer, P. O., et al.
2009 Inhibition of Rho kinases enhances the degradation of mutant huntingtin. J Biol Chem 284(19):13153-64.
Becher, M. W., et al.
1998 Intranuclear neuronal inclusions in Huntington's disease and dentatorubral and pallidoluysian atrophy: correlation between the density of inclusions and IT15 CAG triplet repeat length. Neurobiol Dis 4(6):387-97.
Behrends, C., et al.
2006 Chaperonin TRiC promotes the assembly of polyQ expansion proteins into nontoxic oligomers. Mol Cell 23(6):887-97.
Bence, N. F., R. M. Sampat, and R. R. Kopito

2001 Impairment of the ubiquitin-proteasome system by protein aggregation. Science 292(5521):1552-5.

Berke, S. J., et al.
2004 Caspase-mediated proteolysis of the polyglutamine disease protein ataxin-3. J Neurochem 89(4):908-18.

Berson, J. F., et al.
2003 Proprotein convertase cleavage liberates a fibrillogenic fragment of a resident glycoprotein to initiate melanosome biogenesis. J Cell Biol 161(3):521-33.

Bhattacharyya, A. M., A. K. Thakur, and R. Wetzel
2005 polyglutamine aggregation nucleation: thermodynamics of a highly unfavorable protein folding reaction. Proc Natl Acad Sci U S A 102(43):15400-5.

Bhattacharyya, A., et al.
2006 Oligoproline effects on polyglutamine conformation and aggregation. J Mol Biol 355(3):524-35.

Bodner, R. A., et al.
2006 Pharmacological promotion of inclusion formation: a therapeutic approach for Huntington's and Parkinson's diseases. Proc Natl Acad Sci U S A 103(11):4246-51.

Bonk, T., and A. Humeny
2001 MALDI-TOF-MS analysis of protein and DNA. Neuroscientist 7(1):6-12.

Borwankar, T., et al.
2011 Natural osmolytes remodel the aggregation pathway of mutant huntingtin exon 1. Biochemistry 50(12):2048-60.

Breuer, P., et al.
2010 Nuclear aggregation of polyglutamine-expanded ataxin-3: fragments escape the cytoplasmic quality control. J Biol Chem 285(9):6532-7.

Brignull, H. R., J. F. Morley, and R. I. Morimoto
2007 The stress of misfolded proteins: C. elegans models for neurodegenerative disease and aging. Adv Exp Med Biol 594:167-89.

Bukau, B., J. Weissman, and A. Horwich
2006 Molecular chaperones and protein quality control. Cell 125(3):443-51.

Bulone, D., et al.
2006 The interplay between PolyQ and protein context delays aggregation by forming a reservoir of protofibrils. PLoS One 1:e111.

Busch, A., et al.
2003 Mutant huntingtin promotes the fibrillogenesis of wild-type huntingtin: a potential mechanism for loss of huntingtin function in Huntington's disease. J Biol Chem 278(42):41452-61.

Carrio, M., et al.
2005 Amyloid-like properties of bacterial inclusion bodies. J Mol Biol 347(5):1025-37.

Caughey, B., and P. T. Lansbury
2003 Protofibrils, pores, fibrils, and neurodegeneration: separating the responsible protein aggregates from the innocent bystanders. Annu Rev Neurosci 26:267-98.

Chai, Y., et al.
2002 Live-cell imaging reveals divergent intracellular dynamics of polyglutamine disease proteins and supports a sequestration model of pathogenesis. Proc Natl Acad Sci U S A 99(14):9310-5.

—

2001 The role of protein composition in specifying nuclear inclusion formation in polyglutamine disease. J Biol Chem 276(48):44889-97.

Chapman, M. R., et al.
2002 Role of Escherichia coli curli operons in directing amyloid fiber formation. Science 295(5556):851-5.

Chapple, J. P., et al.
2008 Focal distortion of the nuclear envelope by huntingtin aggregates revealed by lamin immunostaining. Neurosci Lett 447(2-3):172-4.

Chen, H. K., et al.
2003 Interaction of Akt-phosphorylated ataxin-1 with 14-3-3 mediates neurodegeneration in spinocerebellar ataxia type 1. Cell 113(4):457-68.

Chen, S., et al.
2002a Amyloid-like features of polyglutamine aggregates and their assembly kinetics. Biochemistry 41(23):7391-9.

—
2001 Polyglutamine aggregation behavior in vitro supports a recruitment mechanism of cytotoxicity. J Mol Biol 311(1):173-82.

Chen, S., F. A. Ferrone, and R. Wetzel
2002b Huntington's disease age-of-onset linked to polyglutamine aggregation nucleation. Proc Natl Acad Sci U S A 99(18):11884-9.

Chien, P., and J. S. Weissman
2001 Conformational diversity in a yeast prion dictates its seeding specificity. Nature 410(6825):223-7.

Chiti, F., and C. M. Dobson
2006 Protein misfolding, functional amyloid, and human disease. Annu Rev Biochem 75:333-66.

Chiti, F., et al.
2003 Rationalization of the effects of mutations on peptide and protein aggregation rates. Nature 424(6950):805-8.

—
2001 Reduction of the amyloidogenicity of a protein by specific binding of ligands to the native conformation. Protein Sci 10(4):879-86.

Cholfin, J. A., et al.
2001 The SCA12 mutation as a rare cause of spinocerebellar ataxia. Arch Neurol 58(11):1833-5.

Chow, M. K., et al.
2004a Polyglutamine expansion in ataxin-3 does not affect protein stability: implications for misfolding and disease. J Biol Chem 279(46):47643-51.

Chow, M. K., H. L. Paulson, and S. P. Bottomley
2004b Destabilization of a non-pathological variant of ataxin-3 results in fibrillogenesis via a partially folded intermediate: a model for misfolding in polyglutamine disease. J Mol Biol 335(1):333-41.

Claessen, D., et al.
2003 A novel class of secreted hydrophobic proteins is involved in aerial hyphae formation in Streptomyces coelicolor by forming amyloid-like fibrils. Genes Dev 17(14):1714-26.

Clark, H. B., et al.
1997 Purkinje cell expression of a mutant allele of SCA1 in transgenic mice leads to disparate effects on motor behaviors, followed by a progressive cerebellar dysfunction and histological alterations. J Neurosci 17(19):7385-95.

Clark, P. L., B. F. Weston, and L. M. Gierasch

1998 Probing the folding pathway of a beta-clam protein with single-tryptophan constructs. Fold Des 3(5):401-12.

Coe, H., and M. Michalak

2009 Calcium binding chaperones of the endoplasmic reticulum. Gen Physiol Biophys 28 Spec No Focus:F96-F103.

Collins, S. R., et al.

2004 Mechanism of prion propagation: amyloid growth occurs by monomer addition. PLoS Biol 2(10):e321.

Colomer Gould, V. F., et al.

2007 A mutant ataxin-3 fragment results from processing at a site N-terminal to amino acid 190 in brain of Machado-Joseph disease-like transgenic mice. Neurobiol Dis 27(3):362-9.

Cooper, J. K., et al.

1998 Truncated N-terminal fragments of huntingtin with expanded glutamine repeats form nuclear and cytoplasmic aggregates in cell culture. Hum Mol Genet 7(5):783-90.

Cornett, J., et al.

2005 Polyglutamine expansion of huntingtin impairs its nuclear export. Nat Genet 37(2):198-204.

Crick, S. L., et al.

2006 Fluorescence correlation spectroscopy shows that monomeric polyglutamine molecules form collapsed structures in aqueous solutions. Proc Natl Acad Sci U S A 103(45):16764-9.

Cummings, C. J., et al.

1998 Chaperone suppression of aggregation and altered subcellular proteasome localization imply protein misfolding in SCA1. Nat Genet 19(2):148-54.

Cummings, C. J., and H. Y. Zoghbi

2000 Fourteen and counting: unraveling trinucleotide repeat diseases. Hum Mol Genet 9(6):909-16.

Darnell, G., et al.

2007 Flanking polyproline sequences inhibit beta-sheet structure in polyglutamine segments by inducing PPII-like helix structure. J Mol Biol 374(3):688-704.

Davies, A. F., et al.

1999 Delineation of two distinct 6p deletion syndromes. Hum Genet 104(1):64-72.

de Chiara, C., et al.

2005a The AXH domain adopts alternative folds the solution structure of HBP1 AXH. Structure 13(5):743-53.

—

2005b Polyglutamine is not all: the functional role of the AXH domain in the ataxin-1 protein. J Mol Biol 354(4):883-93.

DeMarch, Z., et al.

2008 Beneficial effects of rolipram in the R6/2 mouse model of Huntington's disease. Neurobiol Dis 30(3):375-87.

DiFiglia, M., et al.

1997 Aggregation of huntingtin in neuronal intranuclear inclusions and dystrophic neurites in brain. Science 277(5334):1990-3.

Ding, T. T., et al.

2002 Annular alpha-synuclein protofibrils are produced when spherical protofibrils are incubated in solution or bound to brain-derived membranes. Biochemistry 41(32):10209-17.

Douglas, P. M., et al.
2009 Reciprocal efficiency of RNQ1 and polyglutamine detoxification in the cytosol and nucleus. Mol Biol Cell 20(19):4162-73.

Duennwald, M. L., et al.
2006 Flanking sequences profoundly alter polyglutamine toxicity in yeast. Proc Natl Acad Sci U S A 103(29):11045-50.

Durr, A., et al.
1999 Homozygosity in Huntington's disease. J Med Genet 36(2):172-3.

Ehrnhoefer, D. E., et al.
2006 Green tea (-)-epigallocatechin-gallate modulates early events in huntingtin misfolding and reduces toxicity in Huntington's disease models. Hum Mol Genet 15(18):2743-51.

Ellisdon, A. M., M. C. Pearce, and S. P. Bottomley
2007 Mechanisms of ataxin-3 misfolding and fibril formation: kinetic analysis of a disease-associated polyglutamine protein. J Mol Biol 368(2):595-605.

Ellisdon, A. M., B. Thomas, and S. P. Bottomley
2006 The two-stage pathway of ataxin-3 fibrillogenesis involves a polyglutamine-independent step. J Biol Chem 281(25):16888-96.

Fandrich, M., M. A. Fletcher, and C. M. Dobson
2001 Amyloid fibrils from muscle myoglobin. Nature 410(6825):165-6.

Faux, N. G., et al.
2005 Functional insights from the distribution and role of homopeptide repeat-containing proteins. Genome Res 15(4):537-51.

Ferrante, R. J., et al.
2003 Histone deacetylase inhibition by sodium butyrate chemotherapy ameliorates the neurodegenerative phenotype in Huntington's disease mice. J Neurosci 23(28):9418-27.

Ferreira, S. T., F. G. De Felice, and A. Chapeaurouge
2006 Metastable, partially folded states in the productive folding and in the misfolding and amyloid aggregation of proteins. Cell Biochem Biophys 44(3):539-48.

Fischbeck, K. H., et al.
1999 Androgen receptor mutation in Kennedy's disease. Philos Trans R Soc Lond B Biol Sci 354(1386):1075-8.

Gales, L., et al.
2005 Towards a structural understanding of the fibrillization pathway in Machado-Joseph's disease: trapping early oligomers of non-expanded ataxin-3. J Mol Biol 353(3):642-54.

Gatchel, J. R., and H. Y. Zoghbi
2005 Diseases of unstable repeat expansion: mechanisms and common principles. Nat Rev Genet 6(10):743-55.

Gauthier, L. R., et al.
2004 Huntingtin controls neurotrophic support and survival of neurons by enhancing BDNF vesicular transport along microtubules. Cell 118(1):127-38.

Gejyo, F., et al.
1986 Beta 2-microglobulin: a new form of amyloid protein associated with chronic hemodialysis. Kidney Int 30(3):385-90.

Giampa, C., et al.

2009 Phosphodiesterase type IV inhibition prevents sequestration of CREB binding protein, protects striatal parvalbumin interneurons and rescues motor deficits in the R6/2 mouse model of Huntington's disease. Eur J Neurosci 29(5):902-10.

Ginisty, H., F. Amalric, and P. Bouvet
1998 Nucleolin functions in the first step of ribosomal RNA processing. EMBO J 17(5):1476-86.

Ginisty, H., et al.
1999 Structure and functions of nucleolin. J Cell Sci 112 (Pt 6):761-72.

Goldberg, Y. P., et al.
1993 Molecular analysis of new mutations for Huntington's disease: intermediate alleles and sex of origin effects. Nat Genet 5(2):174-9.

Goldfarb, L. G., et al.
1996 Unstable triplet repeat and phenotypic variability of spinocerebellar ataxia type 1. Ann Neurol 39(4):500-6.

Gonzalez-Montalban, N., A. Villaverde, and A. Aris
2007 Amyloid-linked cellular toxicity triggered by bacterial inclusion bodies. Biochem Biophys Res Commun 355(3):637-42.

Gorg, A., W. Postel, and S. Gunther
1988 The current state of two-dimensional electrophoresis with immobilized pH gradients. Electrophoresis 9(9):531-46.

Goti, D., et al.
2004 A mutant ataxin-3 putative-cleavage fragment in brains of Machado-Joseph disease patients and transgenic mice is cytotoxic above a critical concentration. J Neurosci 24(45):10266-79.

Graham, R. K., et al.
2006 Cleavage at the caspase-6 site is required for neuronal dysfunction and degeneration due to mutant huntingtin. Cell 125(6):1179-91.

Griffin, B. A., et al.
2000 Fluorescent labeling of recombinant proteins in living cells with FlAsH. Methods Enzymol 327:565-78.

Groenning, M., et al.
2007 Study on the binding of Thioflavin T to beta-sheet-rich and non-beta-sheet cavities. J Struct Biol 158(3):358-69.

Gu, X., et al.
2009 Serines 13 and 16 are critical determinants of full-length human mutant huntingtin induced disease pathogenesis in HD mice. Neuron 64(6):828-40.

Guijarro, J. I., et al.
1998 Amyloid fibril formation by an SH3 domain. Proc Natl Acad Sci U S A 95(8):4224-8.

Gusella, J. F., and M. E. MacDonald
2000 Molecular genetics: unmasking polyglutamine triggers in neurodegenerative disease. Nat Rev Neurosci 1(2):109-15.

Haacke, A., et al.
2006 Proteolytic cleavage of polyglutamine-expanded ataxin-3 is critical for aggregation and sequestration of non-expanded ataxin-3. Hum Mol Genet 15(4):555-68.

Hackam, A. S., et al.
2000 Huntingtin interacting protein 1 induces apoptosis via a novel caspase-dependent death effector domain. J Biol Chem 275(52):41299-308.

Hands, S. L., and A. Wyttenbach

2010 Neurotoxic protein oligomerisation associated with polyglutamine diseases. Acta Neuropathol 120(4):419-37.

Harper, J. D., and P. T. Lansbury, Jr.
1997 Models of amyloid seeding in Alzheimer's disease and scrapie: mechanistic truths and physiological consequences of the time-dependent solubility of amyloid proteins. Annu Rev Biochem 66:385-407.

Harper, J. D., C. M. Lieber, and P. T. Lansbury, Jr.
1997 Atomic force microscopic imaging of seeded fibril formation and fibril branching by the Alzheimer's disease amyloid-beta protein. Chem Biol 4(12):951-9.

Hershko, A., and A. Ciechanover
1998 The ubiquitin system. Annu Rev Biochem 67:425-79.

Hodges, M., et al.
1998 Structure, organization, and dynamics of promyelocytic leukemia protein nuclear bodies. Am J Hum Genet 63(2):297-304.

Hohfeld, J., D. M. Cyr, and C. Patterson
2001 From the cradle to the grave: molecular chaperones that may choose between folding and degradation. EMBO Rep 2(10):885-90.

Holmberg, C. I., et al.
2004 Inefficient degradation of truncated polyglutamine proteins by the proteasome. EMBO J 23(21):4307-18.

Holmberg, M., et al.
1998 Spinocerebellar ataxia type 7 (SCA7): a neurodegenerative disorder with neuronal intranuclear inclusions. Hum Mol Genet 7(5):913-8.

Humbert, S., et al.
2002 The IGF-1/Akt pathway is neuroprotective in Huntington's disease and involves Huntingtin phosphorylation by Akt. Dev Cell 2(6):831-7.

Huynh, D. P., et al.
2000 Nuclear localization or inclusion body formation of ataxin-2 are not necessary for SCA2 pathogenesis in mouse or human. Nat Genet 26(1):44-50.

Igarashi, S., et al.
1998 Suppression of aggregate formation and apoptosis by transglutaminase inhibitors in cells expressing truncated DRPLA protein with an expanded polyglutamine stretch. Nat Genet 18(2):111-7.

Ignatova, Z., and L. M. Gierasch
2004 Monitoring protein stability and aggregation in vivo by real-time fluorescent labeling. Proc Natl Acad Sci U S A 101(2):523-8.

—
2005 Aggregation of a slow-folding mutant of a beta-clam protein proceeds through a monomeric nucleus. Biochemistry 44(19):7266-74.

—
2006 Extended polyglutamine tracts cause aggregation and structural perturbation of an adjacent beta barrel protein. J Biol Chem 281(18):12959-67.

Ignatova, Z., et al.
2007 In-cell aggregation of a polyglutamine-containing chimera is a multistep process initiated by the flanking sequence. J Biol Chem 282(50):36736-43.

Ikeda, H., et al.
1996 Expanded polyglutamine in the Machado-Joseph disease protein induces cell death in vitro and in vivo. Nat Genet 13(2):196-202.

Ikeuchi, T., et al.

1995 Dentatorubral-pallidoluysian atrophy (DRPLA). Molecular basis for wide clinical features of DRPLA. Clin Neurosci 3(1):23-7.

Iwahashi, C. K., et al.
2006 Protein composition of the intranuclear inclusions of FXTAS. Brain 129(Pt 1):256-71.

Iwata, A., et al.
2005 Increased susceptibility of cytoplasmic over nuclear polyglutamine aggregates to autophagic degradation. Proc Natl Acad Sci U S A 102(37):13135-40.

Jana, N. R., et al.
2000 Polyglutamine length-dependent interaction of Hsp40 and Hsp70 family chaperones with truncated N-terminal huntingtin: their role in suppression of aggregation and cellular toxicity. Hum Mol Genet 9(13):2009-18.

—
2001 Altered proteasomal function due to the expression of polyglutamine-expanded truncated N-terminal huntingtin induces apoptosis by caspase activation through mitochondrial cytochrome c release. Hum Mol Genet 10(10):1049-59.

Jayaraman, M., R. Kodali, and R. Wetzel
2009 The impact of ataxin-1-like histidine insertions on polyglutamine aggregation. Protein Eng Des Sel 22(8):469-78.

Kad, N. M., et al.
2001 Beta(2)-microglobulin and its deamidated variant, N17D form amyloid fibrils with a range of morphologies in vitro. J Mol Biol 313(3):559-71.

Kaganovich, D., R. Kopito, and J. Frydman
2008 Misfolded proteins partition between two distinct quality control compartments. Nature 454(7208):1088-95.

Kalchman, M. A., et al.
1997 HIP1, a human homologue of S. cerevisiae Sla2p, interacts with membrane-associated huntingtin in the brain. Nat Genet 16(1):44-53.

Kanazawa, I.
1999 Molecular pathology of dentatorubral-pallidoluysian atrophy. Philos Trans R Soc Lond B Biol Sci 354(1386):1069-74.

Kar, K., et al.
2011 Critical nucleus size for disease-related polyglutamine aggregation is repeat-length dependent. Nat Struct Mol Biol 18(3):328-36.

Kariya, S., et al.
2006 Cytoprotective effect of novel histone deacetylase inhibitors against polyglutamine toxicity. Neurosci Lett 392(3):213-5.

Kato, S., et al.
2000 New consensus research on neuropathological aspects of familial amyotrophic lateral sclerosis with superoxide dismutase 1 (SOD1) gene mutations: inclusions containing SOD1 in neurons and astrocytes. Amyotroph Lateral Scler Other Motor Neuron Disord 1(3):163-84.

Kayed, R., et al.
2003 Common structure of soluble amyloid oligomers implies common mechanism of pathogenesis. Science 300(5618):486-9.

Kazantsev, A., et al.
1999 Insoluble detergent-resistant aggregates form between pathological and nonpathological lengths of polyglutamine in mammalian cells. Proc Natl Acad Sci U S A 96(20):11404-9.

Kegel, K. B., et al.
2010 Huntingtin cleavage product A forms in neurons and is reduced by gamma-secretase inhibitors. Mol Neurodegener 5:58.
Khare, S. D., et al.
2005 Molecular origin of polyglutamine aggregation in neurodegenerative diseases. PLoS Comput Biol 1(3):230-5.
Kheterpal, I., et al.
2001 Structural features of the Abeta amyloid fibril elucidated by limited proteolysis. Biochemistry 40(39):11757-67.
Kim, M. W., et al.
2009 Secondary structure of Huntingtin amino-terminal region. Structure 17(9):1205-12.
Kim, S., et al.
2002 Polyglutamine protein aggregates are dynamic. Nat Cell Biol 4(10):826-31.
Klein, W. L., G. A. Krafft, and C. E. Finch
2001 Targeting small Abeta oligomers: the solution to an Alzheimer's disease conundrum? Trends Neurosci 24(4):219-24.
Klement, I. A., et al.
1998 Ataxin-1 nuclear localization and aggregation: role in polyglutamine-induced disease in SCA1 transgenic mice. Cell 95(1):41-53.
Ko, J., S. Ou, and P. H. Patterson
2001 New anti-huntingtin monoclonal antibodies: implications for huntingtin conformation and its binding proteins. Brain Res Bull 56(3-4):319-29.
Komure, O., et al.
1995 DNA analysis in hereditary dentatorubral-pallidoluysian atrophy: correlation between CAG repeat length and phenotypic variation and the molecular basis of anticipation. Neurology 45(1):143-9.
Krebs, M. R., et al.
2004 Observation of sequence specificity in the seeding of protein amyloid fibrils. Protein Sci 13(7):1933-8.
Krol, H. A., et al.
2008 Polyglutamine expansion accelerates the dynamics of ataxin-1 and does not result in aggregate formation. PLoS One 3(1):e1503.
Lai, A., and W. H. Frishman
2005 Rho-kinase inhibition in the therapy of cardiovascular disease. Cardiol Rev 13(6):285-92.
Lam, Y. C., et al.
2006 ATAXIN-1 interacts with the repressor Capicua in its native complex to cause SCA1 neuropathology. Cell 127(7):1335-47.
Lambert, M. P., et al.
1998 Diffusible, nonfibrillar ligands derived from Abeta1-42 are potent central nervous system neurotoxins. Proc Natl Acad Sci U S A 95(11):6448-53.
Lammerding, J., et al.
2006 Lamins A and C but not lamin B1 regulate nuclear mechanics. J Biol Chem 281(35):25768-80.
Lamond, A. I., and W. C. Earnshaw
1998 Structure and function in the nucleus. Science 280(5363):547-53.
Laporte, D., et al.
2011 Assembly and architecture of precursor nodes during fission yeast cytokinesis. J Cell Biol 192(6):1005-21.
Lashuel, H. A., et al.

2002 Neurodegenerative disease: amyloid pores from pathogenic mutations. Nature 418(6895):291.

Leavitt, B. R., et al.
2001 Wild-type huntingtin reduces the cellular toxicity of mutant huntingtin in vivo. Am J Hum Genet 68(2):313-24.

Legleiter, J., et al.
2010 Mutant huntingtin fragments form oligomers in a polyglutamine length-dependent manner in vitro and in vivo. J Biol Chem 285(19):14777-90.

Li, X. J., et al.
1995 A huntingtin-associated protein enriched in brain with implications for pathology. Nature 378(6555):398-402.

Liberski, P. P.
2004 Amyloid plaques in transmissible spongiform encephalopathies (prion diseases). Folia Neuropathol 42 Suppl B:109-19.

Licht, D. J., and D. R. Lynch
2002 Juvenile dentatorubral-pallidoluysian atrophy: new clinical features. Pediatr Neurol 26(1):51-4.

Lim, J., et al.
2008 Opposing effects of polyglutamine expansion on native protein complexes contribute to SCA1. Nature 452(7188):713-8.

Lippincott-Schwartz, J., E. Snapp, and A. Kenworthy
2001 Studying protein dynamics in living cells. Nat Rev Mol Cell Biol 2(6):444-56.

Litvinovich, S. V., et al.
1998 Formation of amyloid-like fibrils by self-association of a partially unfolded fibronectin type III module. J Mol Biol 280(2):245-58.

Lomakin, A., et al.
1996 On the nucleation and growth of amyloid beta-protein fibrils: detection of nuclei and quantitation of rate constants. Proc Natl Acad Sci U S A 93(3):1125-9.

Luheshi, L. M., D. C. Crowther, and C. M. Dobson
2008 Protein misfolding and disease: from the test tube to the organism. Curr Opin Chem Biol 12(1):25-31.

Lunkes, A., et al.
2002 Proteases acting on mutant huntingtin generate cleaved products that differentially build up cytoplasmic and nuclear inclusions. Mol Cell 10(2):259-69.

Luthi-Carter, R., et al.
2002 Polyglutamine and transcription: gene expression changes shared by DRPLA and Huntington's disease mouse models reveal context-independent effects. Hum Mol Genet 11(17):1927-37.

Mallik, M., and S. C. Lakhotia
2010 Modifiers and mechanisms of multi-system polyglutamine neurodegenerative disorders: lessons from fly models. J Genet 89(4):497-526.

Mangiarini, L., et al.
1996 Exon 1 of the HD gene with an expanded CAG repeat is sufficient to cause a progressive neurological phenotype in transgenic mice. Cell 87(3):493-506.

Marsh, J. L., et al.
2000 Expanded polyglutamine peptides alone are intrinsically cytotoxic and cause neurodegeneration in Drosophila. Hum Mol Genet 9(1):13-25.

Masino, L., et al.

2004 Characterization of the structure and the amyloidogenic properties of the Josephin domain of the polyglutamine-containing protein ataxin-3. J Mol Biol 344(4):1021-35.

Matsumoto, G., S. Kim, and R. I. Morimoto

2006 Huntingtin and mutant SOD1 form aggregate structures with distinct molecular properties in human cells. J Biol Chem 281(7):4477-85.

Matsumura, R., et al.

1997 Spinocerebellar ataxia type 6. Molecular and clinical features of 35 Japanese patients including one homozygous for the CAG repeat expansion. Neurology 49(5):1238-43.

Matsuyama, Z., et al.

1999 The effect of CAT trinucleotide interruptions on the age at onset of spinocerebellar ataxia type 1 (SCA1). J Med Genet 36(7):546-8.

McCampbell, A., et al.

2000 CREB-binding protein sequestration by expanded polyglutamine. Hum Mol Genet 9(14):2197-202.

Miyashita, T., et al.

1998 Intracellular aggregate formation of dentatorubral-pallidoluysian atrophy (DRPLA) protein with the extended polyglutamine. Biochem Biophys Res Commun 249(1):96-102.

—

1997 Dentatorubral pallidoluysian atrophy (DRPLA) protein is cleaved by caspase-3 during apoptosis. J Biol Chem 272(46):29238-42.

Mohan, A., et al.

2006 Analysis of molecular recognition features (MoRFs). J Mol Biol 362(5):1043-59.

Morfini, G., G. Pigino, and S. T. Brady

2005 Polyglutamine expansion diseases: failing to deliver. Trends Mol Med 11(2):64-70.

Mukai, H., et al.

2005 Formation of morphologically similar globular aggregates from diverse aggregation-prone proteins in mammalian cells. Proc Natl Acad Sci U S A 102(31):10887-92.

Myers, S. L., et al.

2006 Investigating the structural properties of amyloid-like fibrils formed in vitro from beta2-microglobulin using limited proteolysis and electrospray ionisation mass spectrometry. Rapid Commun Mass Spectrom 20(11):1628-36.

Nagafuchi, S., et al.

1994 Structure and expression of the gene responsible for the triplet repeat disorder, dentatorubral and pallidoluysian atrophy (DRPLA). Nat Genet 8(2):177-82.

Nagai, Y., et al.

2003 Prevention of polyglutamine oligomerization and neurodegeneration by the peptide inhibitor QBP1 in Drosophila. Hum Mol Genet 12(11):1253-9.

Narain, Y., et al.

1999 A molecular investigation of true dominance in Huntington's disease. J Med Genet 36(10):739-46.

Neuhoff, V., et al.

1988 Improved staining of proteins in polyacrylamide gels including isoelectric focusing gels with clear background at nanogram sensitivity using Coomassie Brilliant Blue G-250 and R-250. Electrophoresis 9(6):255-62.

Nilsson, M. R.
2004 Techniques to study amyloid fibril formation in vitro. Methods 34(1):151-60.
Nozaki, K., et al.
2001 Amino acid sequences flanking polyglutamine stretches influence their potential for aggregate formation. Neuroreport 12(15):3357-64.
Nucifora, F. C., Jr., et al.
2003 Nuclear localization of a non-caspase truncation product of atrophin-1, with an expanded polyglutamine repeat, increases cellular toxicity. J Biol Chem 278(15):13047-55.
—
2001 Interference by huntingtin and atrophin-1 with cbp-mediated transcription leading to cellular toxicity. Science 291(5512):2423-8.
O'Nuallain, B., et al.
2004 Seeding specificity in amyloid growth induced by heterologous fibrils. J Biol Chem 279(17):17490-9.
Okamura-Oho, Y., et al.
2003 Dentatorubral-pallidoluysian atrophy protein is phosphorylated by c-Jun NH2-terminal kinase. Hum Mol Genet 12(13):1535-42.
—
1999 Dentatorubral-pallidoluysian atrophy protein interacts through a proline-rich region near polyglutamine with the SH3 domain of an insulin receptor tyrosine kinase substrate. Hum Mol Genet 8(6):947-57.
Olzscha, H., et al.
2011 Amyloid-like aggregates sequester numerous metastable proteins with essential cellular functions. Cell 144(1):67-78.
Onodera, O., et al.
1995 Molecular cloning of a full-length cDNA for dentatorubral-pallidoluysian atrophy and regional expressions of the expanded alleles in the CNS. Am J Hum Genet 57(5):1050-60.
Ordway, J. M., et al.
1997 Ectopically expressed CAG repeats cause intranuclear inclusions and a progressive late onset neurological phenotype in the mouse. Cell 91(6):753-63.
Orr, H. T., and H. Y. Zoghbi
2007 Trinucleotide repeat disorders. Annu Rev Neurosci 30:575-621.
Paravastu, A. K., A. T. Petkova, and R. Tycko
2006 Polymorphic fibril formation by residues 10-40 of the Alzheimer's beta-amyloid peptide. Biophys J 90(12):4618-29.
Pardo, R., et al.
2006 Inhibition of calcineurin by FK506 protects against polyglutamine-huntingtin toxicity through an increase of huntingtin phosphorylation at S421. J Neurosci 26(5):1635-45.
Pedersen, J. S., et al.
2006 The changing face of glucagon fibrillation: structural polymorphism and conformational imprinting. J Mol Biol 355(3):501-23.
Perutz, M. F., et al.
2002 Amyloid fibers are water-filled nanotubes. Proc Natl Acad Sci U S A 99(8):5591-5.
Peters, M. F., et al.
1999 Nuclear targeting of mutant Huntingtin increases toxicity. Mol Cell Neurosci 14(2):121-8.
Petkova, A. T., et al.

2005 Self-propagating, molecular-level polymorphism in Alzheimer's beta-amyloid fibrils. Science 307(5707):262-5.

Poirier, M. A., et al.
2002 Huntingtin spheroids and protofibrils as precursors in polyglutamine fibrilization. J Biol Chem 277(43):41032-7.

Pratt, W. B., et al.
2006 Chaperoning of glucocorticoid receptors. Handb Exp Pharmacol (172):111-38.

Preisinger, E., et al.
1999 Evidence for a recruitment and sequestration mechanism in Huntington's disease. Philos Trans R Soc Lond B Biol Sci 354(1386):1029-34.

Rajan, R. S., et al.
2001 Specificity in intracellular protein aggregation and inclusion body formation. Proc Natl Acad Sci U S A 98(23):13060-5.

Robertson, A. L., et al.
2008 The structural impact of a polyglutamine tract is location-dependent. Biophys J 95(12):5922-30.

Rochet, J. C., and P. T. Lansbury, Jr.
2000 Amyloid fibrillogenesis: themes and variations. Curr Opin Struct Biol 10(1):60-8.

Rockabrand, E., et al.
2007 The first 17 amino acids of Huntingtin modulate its sub-cellular localization, aggregation and effects on calcium homeostasis. Hum Mol Genet 16(1):61-77.

Romero, P., Z. Obradovic, and A. K. Dunker
2004 Natively disordered proteins: functions and predictions. Appl Bioinformatics 3(2-3):105-13.

Ross, C. A., and M. A. Poirier
2004 Protein aggregation and neurodegenerative disease. Nat Med 10 Suppl:S10-7.

—
2005 Opinion: What is the role of protein aggregation in neurodegeneration? Nat Rev Mol Cell Biol 6(11):891-8.

Ross, C. A., et al.
2003 Polyglutamine fibrillogenesis: the pathway unfolds. Proc Natl Acad Sci U S A 100(1):1-3.

Rousseau, F., et al.
2006 Domain swapping in p13suc1 results in formation of native-like, cytotoxic aggregates. J Mol Biol 363(2):496-505.

Sakahira, H., et al.
2002 Molecular chaperones as modulators of polyglutamine protein aggregation and toxicity. Proc Natl Acad Sci U S A 99 Suppl 4:16412-8.

Sarkar, S., et al.
2007a Trehalose, a novel mTOR-independent autophagy enhancer, accelerates the clearance of mutant huntingtin and alpha-synuclein. J Biol Chem 282(8):5641-52.

—
2007b Small molecules enhance autophagy and reduce toxicity in Huntington's disease models. Nat Chem Biol 3(6):331-8.

Sathasivam, K., et al.

2010 Identical oligomeric and fibrillar structures captured from the brains of R6/2 and knock-in mouse models of Huntington's disease. Hum Mol Genet 19(1):65-78.

Sato, K., et al.
1995 Does homozygosity advance the onset of dentatorubral-pallidoluysian atrophy? Neurology 45(10):1934-6.

Saudou, F., et al.
1998 Huntingtin acts in the nucleus to induce apoptosis but death does not correlate with the formation of intranuclear inclusions. Cell 95(1):55-66.

Saunders, H. M., and S. P. Bottomley
2009 Multi-domain misfolding: understanding the aggregation pathway of polyglutamine proteins. Protein Eng Des Sel 22(8):447-51.

Scherzinger, E., et al.
1997 Huntingtin-encoded polyglutamine expansions form amyloid-like protein aggregates in vitro and in vivo. Cell 90(3):549-58.

—
1999 Self-assembly of polyglutamine-containing huntingtin fragments into amyloid-like fibrils: implications for Huntington's disease pathology. Proc Natl Acad Sci U S A 96(8):4604-9.

Schilling, G., et al.
2004 Nuclear-targeting of mutant huntingtin fragments produces Huntington's disease-like phenotypes in transgenic mice. Hum Mol Genet 13(15):1599-610.

—
1999 Nuclear accumulation of truncated atrophin-1 fragments in a transgenic mouse model of DRPLA. Neuron 24(1):275-86.

Schneider, R., et al.
2011 Structural characterization of polyglutamine fibrils by solid-state NMR spectroscopy. J Mol Biol 412(1):121-36.

Schubert, U., et al.
2000 Rapid degradation of a large fraction of newly synthesized proteins by proteasomes. Nature 404(6779):770-4.

Seeler, J. S., and A. Dejean
1999 The PML nuclear bodies: actors or extras? Curr Opin Genet Dev 9(3):362-7.

Selkoe, D. J.
2003 Folding proteins in fatal ways. Nature 426(6968):900-4.

Sen, S., et al.
2003 Role of histidine interruption in mitigating the pathological effects of long polyglutamine stretches in SCA1: A molecular approach. Protein Sci 12(5):953-62.

Serio, T. R., et al.
2000 Nucleated conformational conversion and the replication of conformational information by a prion determinant. Science 289(5483):1317-21.

Serpell, L. C., et al.
2000 The protofilament substructure of amyloid fibrils. J Mol Biol 300(5):1033-9.

Sharma, D., et al.
1999 Peptide models for inherited neurodegenerative disorders: conformation and aggregation properties of long polyglutamine peptides with and without interruptions. FEBS Lett 456(1):181-5.

Shen, Y., et al.
2007 Functional architecture of atrophins. J Biol Chem 282(7):5037-44.

Shen, Y., and A. S. Peterson
2009 Atrophins' emerging roles in development and neurodegenerative disease. Cell Mol Life Sci 66(3):437-46.
Shimohata, T., et al.
2000a Expanded polyglutamine stretches interact with TAFII130, interfering with CREB-dependent transcription. Nat Genet 26(1):29-36.
Shimohata, T., O. Onodera, and S. Tsuji
2000b Interaction of expanded polyglutamine stretches with nuclear transcription factors leads to aberrant transcriptional regulation in polyglutamine diseases. Neuropathology 20(4):326-33.
Sikorski, P., and E. Atkins
2005 New model for crystalline polyglutamine assemblies and their connection with amyloid fibrils. Biomacromolecules 6(1):425-32.
Sipe, J. D., and A. S. Cohen
2000 Review: history of the amyloid fibril. J Struct Biol 130(2-3):88-98.
Slepko, N., et al.
2006 Normal-repeat-length polyglutamine peptides accelerate aggregation nucleation and cytotoxicity of expanded polyglutamine proteins. Proc Natl Acad Sci U S A 103(39):14367-72.
Sobue, G., et al.
1996 Homozygosity for Machado-Joseph disease gene enhances phenotypic severity. J Neurol Neurosurg Psychiatry 60(3):354-6.
Soto, C.
2003 Unfolding the role of protein misfolding in neurodegenerative diseases. Nat Rev Neurosci 4(1):49-60.
Srivastava, M., and H. B. Pollard
1999 Molecular dissection of nucleolin's role in growth and cell proliferation: new insights. FASEB J 13(14):1911-22.
Steffan, J. S., et al.
2004 SUMO modification of Huntingtin and Huntington's disease pathology. Science 304(5667):100-4.
—
2000 The Huntington's disease protein interacts with p53 and CREB-binding protein and represses transcription. Proc Natl Acad Sci U S A 97(12):6763-8.
Stenoien, D. L., M. Mielke, and M. A. Mancini
2002 Intranuclear ataxin1 inclusions contain both fast- and slow-exchanging components. Nat Cell Biol 4(10):806-10.
Strom, L., and C. Sjogren
2005 DNA damage-induced cohesion. Cell Cycle 4(4):536-9.
Sunde, M., and C. Blake
1997 The structure of amyloid fibrils by electron microscopy and X-ray diffraction. Adv Protein Chem 50:123-59.
Takahashi, T., et al.
2008 Soluble polyglutamine oligomers formed prior to inclusion body formation are cytotoxic. Hum Mol Genet 17(3):345-56.
Tam, S., et al.
2009 The chaperonin TRiC blocks a huntingtin sequence element that promotes the conformational switch to aggregation. Nat Struct Mol Biol 16(12):1279-85.
Tartaglia, G. G., et al.
2008 Prediction of aggregation-prone regions in structured proteins. J Mol Biol 380(2):425-36.

Terashima, T., et al.
2002 SUMO-1 co-localized with mutant atrophin-1 with expanded polyglutamines accelerates intranuclear aggregation and cell death. Neuroreport 13(17):2359-64.
Thakur, A. K., et al.
2009 Polyglutamine disruption of the huntingtin exon 1 N terminus triggers a complex aggregation mechanism. Nat Struct Mol Biol 16(4):380-9.
Thakur, A. K., and R. Wetzel
2002 Mutational analysis of the structural organization of polyglutamine aggregates. Proc Natl Acad Sci U S A 99(26):17014-9.
Thompson, L. M., et al.
2009 IKK phosphorylates Huntingtin and targets it for degradation by the proteasome and lysosome. J Cell Biol 187(7):1083-99.
Toombs, J. A., B. R. McCarty, and E. D. Ross
2010 Compositional determinants of prion formation in yeast. Mol Cell Biol 30(1):319-32.
Venkatraman, P., et al.
2004 Eukaryotic proteasomes cannot digest polyglutamine sequences and release them during degradation of polyglutamine-containing proteins. Mol Cell 14(1):95-104.
Volles, M. J., et al.
2001 Vesicle permeabilization by protofibrillar alpha-synuclein: implications for the pathogenesis and treatment of Parkinson's disease. Biochemistry 40(26):7812-9.
von Bergen, M., et al.
2006 The core of tau-paired helical filaments studied by scanning transmission electron microscopy and limited proteolysis. Biochemistry 45(20):6446-57.
Wacker, J. L., et al.
2004 Hsp70 and Hsp40 attenuate formation of spherical and annular polyglutamine oligomers by partitioning monomer. Nat Struct Mol Biol 11(12):1215-22.
Waelter, S., et al.
2001 Accumulation of mutant huntingtin fragments in aggresome-like inclusion bodies as a result of insufficient protein degradation. Mol Biol Cell 12(5):1393-407.
Walsh, D. M., et al.
2002 Naturally secreted oligomers of amyloid beta protein potently inhibit hippocampal long-term potentiation in vivo. Nature 416(6880):535-9.
Walsh, D. M., and D. J. Selkoe
2004 Oligomers on the brain: the emerging role of soluble protein aggregates in neurodegeneration. Protein Pept Lett 11(3):213-28.
Walsh, R., et al.
2005 The roles of proteolysis and nuclear localisation in the toxicity of the polyglutamine diseases. A review. Neurotox Res 7(1-2):43-57.
Walter, G. M., et al.
2011 Ordered assembly of heat shock proteins, Hsp26, Hsp70, Hsp90, and Hsp104, on expanded polyglutamine fragments revealed by chemical probes. J Biol Chem 286(47):40486-93.
Wandinger, S. K., K. Richter, and J. Buchner
2008 The Hsp90 chaperone machinery. J Biol Chem 283(27):18473-7.
Wang, L., et al.

2008 Atrophin recruits HDAC1/2 and G9a to modify histone H3K9 and to determine cell fates. EMBO Rep 9(6):555-62.

Wanker, E. E., et al.
1999 Membrane filter assay for detection of amyloid-like polyglutamine-containing protein aggregates. Methods Enzymol 309:375-86.

Warby, S. C., et al.
2009 Phosphorylation of huntingtin reduces the accumulation of its nuclear fragments. Mol Cell Neurosci 40(2):121-7.

Weis, K.
2003 Regulating access to the genome: nucleocytoplasmic transport throughout the cell cycle. Cell 112(4):441-51.

Wellington, C. L., et al.
1998 Caspase cleavage of gene products associated with triplet expansion disorders generates truncated fragments containing the polyglutamine tract. J Biol Chem 273(15):9158-67.

Wood, J. D., et al.
2000 Atrophin-1, the dentato-rubral and pallido-luysian atrophy gene product, interacts with ETO/MTG8 in the nuclear matrix and represses transcription. J Cell Biol 150(5):939-48.

Wood, S. J., et al.
1999 alpha-synuclein fibrillogenesis is nucleation-dependent. Implications for the pathogenesis of Parkinson's disease. J Biol Chem 274(28):19509-12.

Yamada, M., et al.
2001 Interaction between neuronal intranuclear inclusions and promyelocytic leukemia protein nuclear and coiled bodies in CAG repeat diseases. Am J Pathol 159(5):1785-95.

—
2008 CAG repeat disorder models and human neuropathology: similarities and differences. Acta Neuropathol 115(1):71-86.

Yamada, M., S. Tsuji, and H. Takahashi
2000 Pathology of CAG repeat diseases. Neuropathology 20(4):319-25.

Yamamoto, A., M. L. Cremona, and J. E. Rothman
2006 Autophagy-mediated clearance of huntingtin aggregates triggered by the insulin-signaling pathway. J Cell Biol 172(5):719-31.

Yamamoto, A., J. J. Lucas, and R. Hen
2000 Reversal of neuropathology and motor dysfunction in a conditional model of Huntington's disease. Cell 101(1):57-66.

Yanagisawa, H., et al.
2000 Protein binding of a DRPLA family through arginine-glutamic acid dipeptide repeats is enhanced by extended polyglutamine. Hum Mol Genet 9(9):1433-42.

Ying, M., et al.
2006 Sodium butyrate ameliorates histone hypoacetylation and neurodegenerative phenotypes in a mouse model for DRPLA. J Biol Chem 281(18):12580-6.

Zoghbi, H. Y., and H. T. Orr
1995 Spinocerebellar ataxia type 1. Semin Cell Biol 6(1):29-35.

—
2000 Glutamine repeats and neurodegeneration. Annu Rev Neurosci 23:217-47.

6. Appendix

6.1 Amino acid sequences of the polyQ proteins used

GFP-FL19Q/71Q:

M V S K G E E L F T G V V P I L V E L D G D V N G H K F S V S G E G E G D A T Y
G K L T L K F I C T T G K L P V P W P T L V T T L T Y G V Q C F S R Y P D H M K
Q H D F F K S A M P E G Y V Q E R T I F F K D D G N Y K T R A E V K F E G D T L
V N R I E L K G I D F K E D G N I L G H K L E Y N Y N S H N V Y I M A D K Q K N
G I K V N F K I R H N I E D G S V Q L A D H Y Q Q N T P I G D G P V L L P D N H
Y L S T Q S A L S K D P N E K R D H M V L L E F V T A A G I T L G M D E L Y K S
G R T Q I L K T R Q N K D S M S M R S G R K K E A P G P R E E L R S R G R A S
P G G V S T S S S D G K A E K S R Q T A K K A R V E E A S T P K V N K Q G R S
E E I S E S E S E E T N A P K K T K T E Q E L P R P Q S P S D L D S L D G R S L
N D D G S S D P R D I D Q D N R S T S P S I Y S P G S V E N D S D S S S G L S
Q G P A R P Y H P P P L F P P S P Q P P D S T P R Q P E A S F E P H P S V T P
T G Y H A P M E P P T S R M F Q A P P G A P P P H P Q L Y P G G T G G V L S G
P P M G P K G G G A A S S V G G P N G G K Q H P P P T T P I S V S S S G A S G
A P P T K P P T T P V G G G N L P S A P P P A N F P H V T P N L P P P P A L R P
L N N A S A S P P G L G A Q P L P G H L P S P Y A M G Q G M G G L P P G P E K
G P T L A P S P H S L P P A S S S A P A P P M R F P Y S S S S S S S A A A S S S
S S S S S S S A S P F P A S Q A L P S Y P H S F P P P T S L S V S N Q P P K Y T
Q P S L P S Q A V W S Q G P P P P P P Y G R L L A N S N A H P G P F P P S T G
A Q S T A H P P V S T H H H H H **(Q)$_{19/71}$** H H G N S G P P P P G A F P H P L E G
G S S H H A H P Y A M S P S L G S L R P Y P P G P A H L P P P H S Q V S Y S Q
A G P N G P P V S S S S N S S S S T S Q G S Y P C S H P S P S Q G P Q G A P Y
P F P P V P T V T T S S A T L S T V I A T V A S S P A G Y K T A S P P G P P P Y
G K R A P S P G A Y K T A T P P G Y K P G S P P S F R T G T P P G Y R G T S P
P A G P G T F K P G S P T V G P G P L P P A G P S G L P S L P P P P A A P A S
G P P L S A T Q I K Q E P A E E Y E T P E S P V P P A R S P S P P P K V V D V P
S H A S Q S A R F N K H L D R G F N S C A R S D L Y F V P L E G S K L A K K R
A D L V E K V R R E A E Q R A R E E K E R E R E R E R E K E R E R E K E R E L
E R S V K L A Q E G R A P V E C P S L G P V P H R P P F E P G S A V A T V P P
Y L G P D T P A L R T L S E Y A R P H V M S P G N R N H P F Y V P L G A V D P
G L L G Y N V P A L Y S S D P A A R E R E R E A R E R D L R D R L K P G F E V
K P S E L E P L H G V P G P G L D P F P R H G G L A L Q P G P P G L H P F P F
H P S L G P L E R E R L A L A A G P A L R P D M S Y A E R L A A E R Q H A E R
V A G L G N D P L A R L Q M L N V T P H H H Q H S H I H S H L H L H Q Q D A I H
A A S A S V H P L I D P L A S G S H L T R I P Y P A G T L P N P L L P H P L H E N
E V L R H Q L F A A P Y R D L P A S L S A P M S A A H Q L Q A M H A Q S A E L
Q R L A L E Q Q Q W L H A H H P L H S V P L P A Q E D Y Y S H L K K E S D K P L

GFP-ΔN19Q/71Q

M V S K G E E L F T G V V P I L V E L D G D V N G H K F S V S G E G E G D A T Y
G K L T L K F I C T T G K L P V P W P T L V T T L T Y G V Q C F S R Y P D H M K
Q H D F F K S A M P E G Y V Q E R T I F F K D D G N Y K T R A E V K F E G D T L
V N R I E L K G I D F K E D G N I L G H K L E Y N Y N S H N V Y I M A D K Q K N
G I K V N F K I R H N I E D G S V Q L A D H Y Q Q N T P I G D G P V L L P D N H
Y L S T Q S A L S K D P N E K R D H M V L L E F V T A A G I T L G M D E L Y K S
G R T Q I S E S E S E E T N A P K K T K T E Q E L P R P Q S P S D L D S L D G R
S L N D D G S S D P R D I D Q D N R S T S P S I Y S P G S V E N D S D S S S G L
S Q G P A R P Y H P P P L F P P S P Q P P D S T P R Q P E A S F E P H P S V T
P T G Y H A P M E P P T S R M F Q A P P G A P P P H P Q L Y P G G T G G V L S
G P P M G P K G G G A A S S V G G P N G G K Q H P P P T T P I S V S S S G A S
G A P P T K P P T T P V G G G N L P S A P P P A N F P H V T P N L P P P P A L R
P L N N A S A S P P G L G A Q P L P G H L P S P Y A M G Q G M G G L P P G P E
K G P T L A P S P H S L P P A S S S A P A P P M R F P Y S S S S S S S S A A A S S
S S S S S S S S S A S P F P A S Q A L P S Y P H S F P P P T S L S V S N Q P P K Y
T Q P S L P S Q A V W S Q G P P P P P P Y G R L L A N S N A H P G P F P P S T
G A Q S T A H P P V S T H H H H H H **(Q)$_{19/71}$** H H G N S G P P P P G A F P H P L E
G G S S H H A H P Y A M S P S L G S L R P Y P P G P A H L P P P H S Q V S Y S
Q A G P N G P P V S S S S N S S S S T S Q G S Y P C S H P S P S Q G P Q G A P
Y P F P P V P T V T T S S A T L S T V I A T V A S S P A G Y K T A S P P G P P P Y
G K R A P S P G A Y K T A T P P G Y K P G S P P S F R T G T P P G Y R G T S P
P A G P G T F K P G S P T V G P G P L P P A G P S G L P S L P P P P A A P A S
G P P L S A T Q I K Q E P A E E Y E T P E S P V P P A R S P S P P P K V V D V P
S H A S Q S A R F N K H L D R G F N S C A R S D L Y F V P L E G S K L A K K R
A D L V E K V R R E A E Q R A R E E K E R E R E R E R E K E R E R E K E R E L
E R S V K L A Q E G R A P V E C P S L G P V P H R P P F E P G S A V A T V P P
Y L G P D T P A L R T L S E Y A R P H V M S P G N R N H P F Y V P L G A V D P
G L L G Y N V P A L Y S S D P A A R E R E R E A R E R D L R D R L K P G F E V
K P S E L E P L H G V P G P G L D P F P R H G G L A L Q P G P P G L H P F P F
H P S L G P L E R E R L A L A A G P A L R P D M S Y A E R L A A E R Q H A E R
V A G L G N D P L A R L Q M L N V T P H H H Q H S H I H S H L H L H Q Q D A I H
A A S A S V H P L I D P L A S G S H L T R I P Y P A G T L P N P L L P H P L H E N
E V L R H Q L F A A P Y R D L P A S L S A P M S A A H Q L Q A M H A Q S A E L
Q R L A L E Q Q Q W L H A H H P L H S V P L P A Q E D Y Y S H L K K E S D K P L

DsRed-F_N:

M A S S E D V I K E F M R F K V R M E G S V N G H E F E I E G E G E G R P Y E
G T Q T A K L K V T K G G P L P F A W D I L S P Q F Q Y G S K V Y V K H P A D I
P D Y K K L S F P E G F K W E R V M N F E D G G V V T V T Q D S S L Q D G S F
I Y K V K F I G V N F P S D G P V M Q K K T M G W E A S T E R L Y P R D G V L K
G E I H K A L K L K D G G H Y L V E F K S I Y M A K K P V Q L P G Y Y Y V D S K
L D I T S H N E D Y T I V E Q Y E R A E G R H H L F L R S I S E S E S E E T N A P
K K T K T E Q E L P R P Q S P S D L DS L D G R S L N D D G S S D P R D I D Q D
N R S T S P S I Y S P G S V E N D S D S S S G L S Q G P A R P Y H P P P L F P P
S P Q P P D S T P R Q P E A S F E P H P S V T P T G Y H A P M E P P T S R M F
Q A P P G A P P P H P Q L Y P G G T G G V L S G P P M G P K G G G A A S S V
G G P N G G K Q H P P P T T P I S V S S S G A S G A P P T K P P T T P V G G G
N L P S A P P P A N F P H V T P N L P P P P A L R P L N N A S A S P P G L G A Q
P L P G H L P S P Y A M G Q G M G G L P P G P E K G P T L A P S P H S L P P A
S S S A P A P P M R F P Y S S S S S S S A A A S S S S S S S S S S A S P F P A S
Q A L P S Y P H SF

DsRed-F_C:

M A S S E D V I K E F M R F K V R M E G S V N G H E F E I E G E G E G R P Y E
G T Q T A K L K V T K G G P L P F A W D I L S P Q F Q Y G S K V Y V K H P A D I
P D Y K K L S F P E G F K W E R V M N F E D G G V V T V T Q D S S L Q D G S F
I Y K V K F I G V N F P S D G P V M Q K K T M G W E A S T E R L Y P R D G V L K
G E I H K A L K L K D G G H Y L V E F K S I Y M A K K P V Q L P G Y Y Y V D S K
L D I T S H N E D Y T I V E Q Y E R A E G R H H L F L R S Q H H G N S G P P P P
G A F P H P L E G G S S H H A H P Y A M S P S L G S L R P Y P P G P A H L P P
P H S Q V S Y S Q A G P N G P P V S S S S N S S S S T S Q G S Y P C S H P S P
S Q G P Q G A P Y P F P P V P T V T T S S A T L S T V I A T V A S S P A G Y K T
A S P P G P P P Y G K R A P S P G A Y K T A T P P G Y K P G S P P S F R T G T
P P G Y R G T S P P A G P G T F K P G S P T V G P G P L P P A G P S G L P S L
P P P P A A P A S G P P L S A T Q I K Q E P A E E Y E T P E S P V P P A R S P S
P P P K V V D V P S H A S Q S A R F N K H L D R G F N S C A R S D L Y F V P L
E G S K L A K K R A D L V E K V R R E A E Q R A R E E K E R E R E R E R E K E
R E R E K E R E L E R S V K L A Q E G R A P V E C P S L G P V P H R P P F E P
G S A V A T V P P Y L G P D T P A L R T L S E Y A R P H V M S P G N R N H P F
Y V P L G A V D P G L L G Y N V P A L Y S S D P A A R E R E R E A R E R D L R
D R L K P G F E V K P S E L E P L H G V P G P G L D P F P R H G G L A L Q P G
P P G L H P F P F H P S L G P L E R E R L A L A A G P A L R P D M S Y A E R L A
A E R Q H A E R V A G L G N D P L A R L Q M L N V T P H H H Q H S H I H S H L
H L H Q Q D A I H A A S A S V H P L I D P L A S G S H L T R I P Y P A G T L P N P
L L P H P L H E N E V L R H Q L F A A P Y R D L P A S L S A P M S A A H Q L Q A
M H A Q S A E L Q R L A L E Q Q Q W L H A H H P L H S V P L P A Q E D Y Y S H
L K K E S D K P L

DsRed-$F_{Q19/Q71}$:

M A S S E D V I K E F M R F K V R M E G S V N G H E F E I E G E G E G R P Y E
G T Q T A K L K V T K G G P L P F A W D I L S P Q F Q Y G S K V Y V K H P A D I
P D Y K K L S F P E G F K W E R V M N F E D G G V V T V T Q D S S L Q D G S F
I Y K V K F I G V N F P S D G P V M Q K K T M G W E A S T E R L Y P R D G V L K
G E I H K A L K L K D G G H Y L V E F K S I Y M A K K P V Q L P G Y Y Y V D S K
L D I T S H N E D Y T I V E Q Y E R A E G R H H L F L R S P P V S T H H H H H H
$(Q)_{19/71}$ H H G N S G P P P P G A F P H P L E G G S

CRABP-Htt53Q:

M G H H H H H H H H H H S S G H I E G R H M P N F A G T W K M R S S E N F D
E L L K A L G V N A M L R K V A V A A A S K P H V E I R Q D G D Q F Y I K T S T
T V R T T E I N F K V G E G F E E E T V D G R K C R S L P T W E N E N K I H C T
Q T L L E C C G P C C K T Y W T R E L A N D E L I L T F G A D D V V C T Q I Y V
R E L E M A T L E K L M K A F E S L K S F **$(Q)_{53}$** P P P P P P P P P P P P Q L P Q P
P P Q A Q P L L P Q P Q P P P P P P P P P P P G S A V A E E P L H R P

HA-Htt20Q:

M Y P Y D V P D Y A M A T L E K L M K A F E S L K S F **$(Q)_{20}$** P P P P P P P P P
P P Q L P Q P P P Q A Q P L L P Q P Q P P P P P P P P P P P G S A V A E E P L H
R P

P39A CRABP:

M G H H H H H H H H H H S S G H I E G R H M P N F A G T W K M R S S E N F D
E L L K A L G V N A M L R K V A V A A A S K A H V E I R Q D G D Q F Y I K T S T
T V R T T E I N F K V G E G F E E E T V D G R K C R S L P T W E N E N K I H C T
Q T L L E C C G P C C K T Y W T R E L A N D E L I L T F G A D D V V C T Q I Y V
R E

P39A CRABP-myc:

M G H H H H H H H H H H S S G H I E G R H M P N F A G T W K M R S S E N F D
E L L K A L G V N A M L R K V A V A A A S K A H V E I R Q D G D Q F Y I K T S T
T V R T T E I N F K V G E G F E E E T V D G R K C R S L P T W E N E N K I H C T
Q T L L E C C G P C C K T Y W T R E L A N D E L I L T F G A D D V V C T Q I Y V
R E E Q K L I S E E D L

GST-Htt53Q:

M S P I L G Y W K I K G L V Q P T R L L L E Y L E E K Y E E H L Y E R D E G
D K W R N K K F E L G L E F P N L P Y Y I D G D V K L T Q S M A I I R Y I A D
K H N M L G G C P K E R A E I S M L E G A V L D I R Y G V S R I A Y S K D F
E T L K V D F L S K L P E M L K M F E D R L C H K T Y L N G D H V T H P D F
M L Y D A L D V V L Y M D P M C L D A F P K L V C F K K R I E A I P Q I D K Y
L K S S K Y I A W P L Q G W Q A T F G G G D H P P K S D L E V L F Q G P L
G S P E F I M C E Q K L I S E E D L G M Q I R M A T L E K L M K A F E S L K S
F **$(Q)_{53}$** P P P P P P P P P P P Q L P Q P P P Q A Q P L L P Q P Q P P P P P
P P P P P G P A V A E E P L H R P G S S G H H H H H H

6.2 Selection of the positive stably transfected N2a/Tet-Off/LacI clones

After the selection of of N2a/Tet-Off/LacI cells as described in “Materials and methods” (see 2.2.4.1), the positive clones resistant to both G418 and hygromycin B, that should contain stably integrated genes expressing *tTA* expression transactivator (Tet-Off system) and *LacI* (Lac repressor from LacSwitch I system) were grown in a full-DMEM medium with the selection antibiotics. Following that, total cell lysates were prepared from the equal cell numbers of growing N2a/Tet-Off/LacI clones. The clones, most abundantly expressing Lac-repressor were chosen based on western blot analysis of the cell lysates using anti-LacI antibody (Fig. 6-1).

To exclude the false positives the chosen clones were transiently transfected with a pLac-DsRed plasmid, encoding the DsRed protein. Next, the live cells were analysed using confocal imaging microscopy 12h, 24h and 36h post-transfection (not shown). In the absence of IPTG stably integrated *LacI,* constitutively expressed under the control of the *RSV* promoter should efficiently inhibit a synthesis of the DsRed protein. The presence of cells expressing DsRed revealed the false positive clones, consisting of a mixed population of non-transfected cells and those that contained the stably transfected *LacI* gene (not shown). Thus chosen positive clone (clone number 4) was further grown in the suitable conditions (see 2.2.4.1) and used to develop the N2a/Tet-Off/LacI cell line.

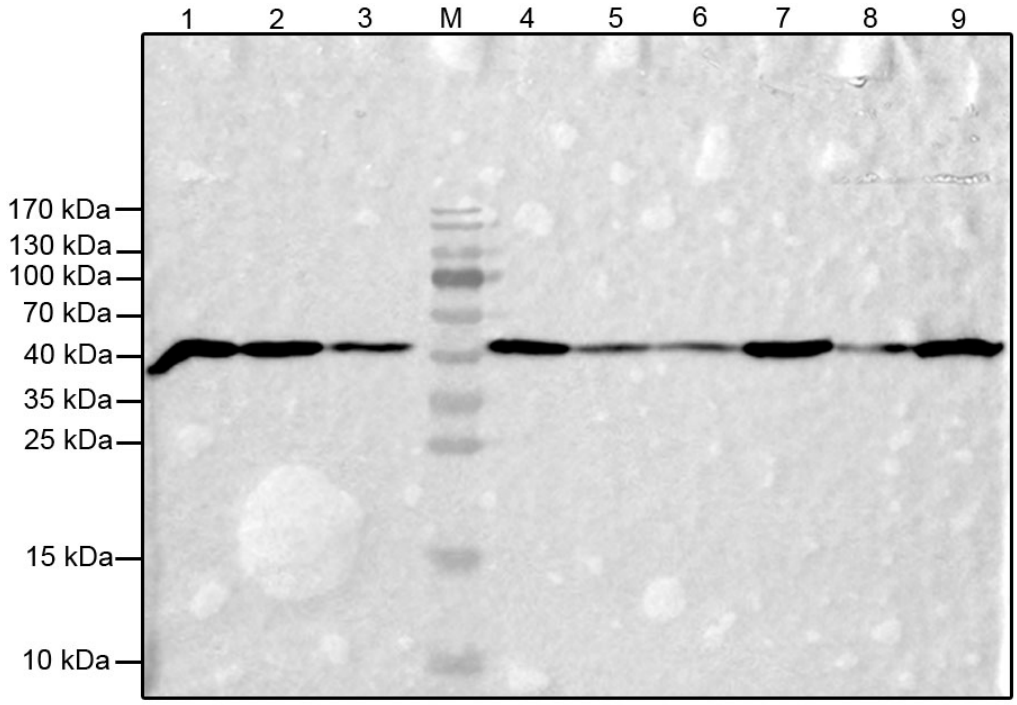

Figure 6-1: Selection of the positive N2a/Tet-Off/LacI clones. *To chose positive clone containing stably integrated tTA and LacI genes the clones selected as described in section 2.2.4.1 were grown in a full DMEM medium supplemented with 0.3 mg/ml of G418 and 0.3 mg/ml of hygromycin B. To chose the clones with the highest level of constitutive LacI gene expression total lysates originating from equal cell numbers were analyzed by immunoblot with anti-LacI antibody. The 38 kDa band corresponds to the monomer of LacI protein. Clones 1, 2, 4, 7, and 9 were chosen for further analysis*.

7. Declaration of authorship/originality

I, Justyna Hinz, declare that this thesis is my own work and has not been submitted in any form for another degree or diploma at any other university.
I also certify that the thesis has been written by me and any help that I have received in my research work and the preparation of the thesis itself has been acknowledged.
In addition, I certify that all information sources have been acknowledged in the text and a list of references is given in the bibliography.

Potsdam, 15.02.2012

……

Justyna Hinz